1-29-2015

Modeling the Effects of Vertically Variable Soil Parameters and Hillslope Shape on Runoff

Benjamin L. Smith
statler75@gmail.com

Modeling the Effects of Vertically Variable Soil Parameters and Hillslope Shape on Runoff

Benjamin Leo Smith

B.S., University of Connecticut, 1998

A Thesis

Submitted in Partial Fulfillment of the

Requirements for the Degree of

Master of Science

At the University of Connecticut

2015

Approval Page

Masters of Science Thesis

Modeling the Effects of Vertically Variable Soil Parameters and Hillslope Shape on Runoff

Presented by

Benjamin Leo Smith, B.S.

Major Advisor 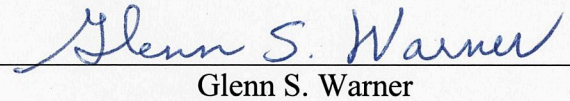
Glenn S. Warner

Associate Advisor 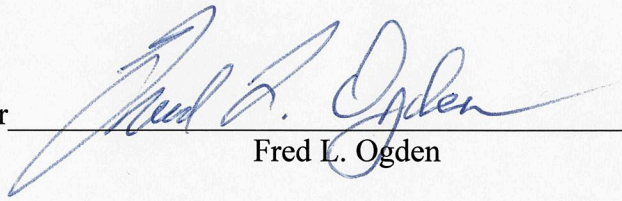
Fred L. Ogden

Associate Advisor 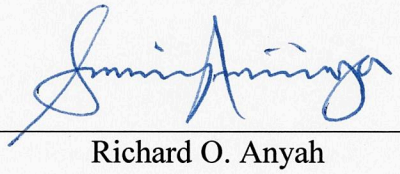
Richard O. Anyah

University of Connecticut

2015

Acknowledgements

I would like to thank my Advisor Glenn Warner for sticking with me on this and other projects throughout the years. Through his advice and encouragement, we were able to explore many what-if's of the science of hydrology.

I would also like to thank my Thesis Committee. First to Dr. Fred Ogden, for staying on after leaving UConn and moving across the country. Also to Dr. Richard Anyah, for joining and bringing a different perspective.

I would like to recognize my coworkers at the Natural Resources Conservation Service for their support, especially Shawn McVey, who provided much of the soil data and assistance, and whose poster inspired the idea to look at the effects of variable soil parameters over depth. Also Wayne Bogovich and Margo Wallace, for allowing me a flexible schedule to assist in my research and writing.

Thanks to my fellow grad students, whether working on projects together, or encouragement and inspiration, especially Scott Bighinatti, who I had the pleasure of working with for several years, and Eric Njuki, for helping me prepare my defense.

Finally I would like to thank my parents, Leo & Patricia Smith, and brother Andrew Smith.

This work is dedicated to Patricia Smith

Table of Contents

Table of Contents (continued)

List of Figures

List of Figures (continued)

List of Tables

Abstract

Soil parameters used in hydrologic modeling, such as porosity (ϕ), volumetric water content (θ), and saturated hydraulic conductivity (K_{sat}) are commonly known to be variable over depth within the soil profile, however these parameters are often modeled as single values, constant over depth. Also, hillslopes found in glacial till features of Connecticut tend to have an S-shaped profile over distance. This study proposes that using variably vertical soil parameters and hillslope shape has effects on runoff modeling results. The effects of vertical soil heterogeneity and hillslope shape on runoff production are evaluated by comparing soil water drainage and runoff production from different vertical distributions of the soil parameters in a hydrologic model of a hillslope. A mass-balance finite-difference hydrologic model of hypothetical hillslopes is developed for use in saturation overland flow modeling. The impacts of changes in physical soil properties such as porosity, volumetric water content, and saturated hydraulic conductivity with depth are evaluated. Timing and amount of runoff for a uniform rainfall are compared for an S-shaped vs. straight hillslope. The dynamic modeling package STELLA® was used to develop the model.

Introduction

Hydrologic Processes

Prediction of the amount and timing of runoff is critical for the design of hydraulic structures, floodplain analysis, flood threats and water availability during times of drought. Runoff is also the critical factor in the transport of nutrients, bacteria, pesticides and other potential non-point pollutants. It is important that processes that create runoff be understood so that the above items can be designed or modeled more accurately, and that we better understand the critical or dominant processes at different scales.

Many factors affect the amount and timing of runoff, most notably generation of runoff by different mechanisms and the path which the water will follow to its point of measurement (surface, subsurface, or some combination thereof). Water flowing on the surface is governed by conditions such as surface roughness, surface slope, and micro topography. Subsurface flow is dependent on soil physical conditions including depth, water content, and hydraulic conductivity. Surface velocities are typically an order or two higher than subsurface velocities and therefore have much shorter travel times.

Conceptually, there are four major processes that contribute to storm runoff, generally divided by the path that water follows. These processes are infiltration excess, shallow subsurface stormflow, return flow, and saturation excess (Dunne & Leopold, 1978). It is possible for all of these processes to occur within a drainage area but some are more common than others and each may represent a different proportion or part of a storm hydrograph. An additional process involving percolation to deep groundwater and

groundwater discharge is much slower and is the major contributor to baseflow on larger streams as opposed to upland hillslopes.

Infiltration excess (Hortonian) runoff is the process in which the infiltration capacity (rate) of a soil is exceeded by the rainfall rate resulting in excess water ponding on the surface, followed by overland flow (Horton, 1933). Infiltration excess runoff has often been the sole runoff producing mechanism in hydrologic models. However in humid regions this type of runoff is typically not observed over large areas, as well-vegetated conditions maintain a high infiltration capacity (Dunne, et al., 1975). Infiltration excess runoff still occurs in humid regions with highly disturbed soil or impervious cover, such as in urban areas with paved surfaces (Dunne et al., 1975).

Shallow subsurface stormflow involves the lateral underground movement of water through the soil matrix and macropores, and typically occurs where shallow soils overlay a more impermeable layer such as dense till or bedrock. Water following this path may reach a surface water body through the soil or re-surface down slope and become overland flow. Shallow subsurface stormflow generally contributes less to peak runoff than infiltration excess and saturation excess runoff. It is more likely to contribute to the tail end of a hydrograph or even to become baseflow (Dunne & Leopold, 1978).

Return flow (Musgrave & Holtan, 1964) is the return of subsurface stormflow from the soil to the surface. This type of runoff may occur as hillslope gradients become less steep, such as at the hillslope toe or in areas where a hillslope turns from convex to concave. It may also be observed where impermeable layers, such as bedrock, intercept the downward flow path of subsurface stormflow causing it to resurface. Deep

groundwater may also return to the surface in valley bottoms where flow paths may be upwards, although this flow is typically considered part of baseflow as the storm that caused the flow cannot be isolated.

Saturation excess runoff (Hewlett, 1961) is produced by rainfall onto areas that are already saturated or become saturated within a storm. Saturation usually occurs from below, when percolating water reaches the water table or an impermeable layer, causing the water table to rise. Hence, saturation excess runoff is also known as "saturation from below" runoff. Once the voids of the soil profile are filled, additional rainfall will pond on the surface and produce runoff. Subsurface stormflow may also contribute to saturated source areas (Dunne et al., 1975).

Runoff calculations in a physics-based model ideally should incorporate as many of the physical processes that occur for a given location as possible. The variation of runoff for different conditions, including the soil type and position in the landscape, is also important since the spatial and temporal variations in runoff are important in assessing management options.

Hillslope Scale

Spatial scale is an important aspect of physics-based hydrologic modeling due to the relative importance of different processes and physical attributes at different scales. Models can be developed for the entire basin, hillslope, and runoff plot scales. Each of these scales offers advantages and disadvantages.

An advantage of modeling an entire basin is that some aspects of runoff production can be simplified. Local soil parameter variations become less important and

modeling regional conditions may still produce accurate results. Some parameters that may be simplified into regional conditions include soil types, soil moisture, and other land conditions.

Disadvantages of a basin model are that some detail must be sacrificed in order to manage the amount of data and calculations potentially causing some desirable local attributes to be lost. An example of where this occurs is the commonly used TOPMODEL (Beven & Kirkby, 1979). In TOPMODEL the $\ln(a/\tan\beta)$ index is used to group areas of topographic hydrologic similarity into areas of similar drainage class (Beven et al., 1995). This method is still distributed and physics-based, but the original location of each cell is lost in the indexing process and the model becomes statistical-dynamical rather than explicit. Other models such as GSSHA (Downer & Ogden, 2003) attempt to keep track of detailed cell by cell calculations but are extremely computationally intensive and may take a long time to run.

At the runoff plot scale, more local information can be generated than in the basin-wide model. Examples include point groundwater levels, soil moisture, infiltration capacity, runoff depth, runoff velocity, etc. However, the level of detail necessary for accurate calculations of these parameters increases, and it is difficult to apply over large areas, as noted above. Also the plot scale does not provide information regarding the influence of position in the landscape such as lateral surface and subsurface flows into, or out from, the plot.

A balance between modeling an entire basin or a single plot is to use a hillslope model. Analyses at the hillslope scale provide a somewhat detailed level of local

calculations while still allowing area dependent processes to develop. Processes that become apparent at the hillslope scale (e.g. 10 to 500 meters in length) include the accumulation of surface and subsurface flow along the slope, and the delay (travel time) of accumulated runoff over the land surface to the channel system.

The hillslope scale is especially important because it is where the saturated source area and return flow runoff processes begin to appear. Many of the parameters that are important at the plot scale, such as hydraulic conductivity and soil water content, can be applied at the hillslope scale but possibly include variation by position on the hillslope. Hillslope investigations and modeling are usually applied using a two-dimensional (2-D) approach in order to simplify the calculations and to isolate the horizontal convergence effects. A drawback of (2-D) hillslope models is that they lack the ability to handle convergent flow from outside the linear path of the hillslope. Hence, saturated source areas may be underestimated as they are not represented by variable-width 3-dimensional areas but only by distances along the hillslope.

Hydrologic Soil Parameters in Runoff Modeling

Hydrologic parameters of soil can have a major role in a physics-based hydrologic modeling, especially concerning infiltration rate, available water holding capacity and transmissivity. Parameters such as porosity (ϕ), volumetric water content (θ), and saturated hydraulic conductivity (K_{sat}) are important descriptors of the volume and flow rates of sub-surface water. Relationships based on these parameters are a valuable tool in developing an accurate hydrologic model.

Physical laboratory models of hillslope soil water movement and runoff production have historically used soil with homogeneous porosity and saturated hydrologic conductivity throughout the profile (Hewlett & Hibbert, 1963; Nieber & Walter, 1981). Note that Nieber & Walter claimed to have sampled significant variations in bulk density (and hence porosity) throughout the model but the variation is less disparate than found in nature and did not occur in an observably consistent pattern.

Recent modeling research has reinforced the understanding that K_{sat} may vary with depth on natural hillslopes. A recent in-field hillslope study shows that the variation of lateral K_{sat} with depth could be represented by a double-exponential function (Brooks, Boll, & McDaniel, 2004). The double-exponent was needed to fit the slow exponential decline in K_{sat} with depth observed below 0.1 m and rapid decline observed above 0.1 m.

Hydrologic modeling utilizing the variation of K_{sat} with depth has been applied by several researchers using the TOPMODEL concepts (Beven et al., 1995). The TOPMODEL methods allowed a constant or exponentially decreasing K_{sat} related to saturation deficit however this is applied to the statistical-dynamical $\ln(a/\tan\beta)$ index as described above, not actual locations on the hillslope. Saturation deficit acts as a substitute for depth when using a single porosity value for the entire soil column.

In the late 1990's several researchers expanded on the TOPMODEL capabilities and experimented with generalized power functions to represent K_{sat} as a function of saturation deficit. An analysis of the recession curves of the Ringelbach catchment (Ambroise et al., 1996b) showed that the power function may be a better representation of K_{sat} than the exponential equation when used in TOPMODEL. Further research

(Iorgulescu & Musy, 1997) used the depth to water table as the input parameter rather than the saturation deficit.

Other researchers have dealt with vertically variable soil parameters by using layered models. For example the SWAT model (Arnold et al., 1998) can address vertical heterogeneity using multiple soil layers that can be correlated to pedologic soil horizons. This method was also used by Boll et al., (1998) in a three soil layer Soil Moisture Recharge (SMR) model, developed from the methods of Steenhuis & Van der Molen (1986).

Models utilizing highly detailed soil data require large amounts of input data and can be computationally intensive, making the isolation of the desired relationships extremely difficult, if not impossible. The additional accuracy may not justify the extra effort. However, estimating the vertical profiles by fitting equations to observed patterns and known relationships is a convenient compromise that is not as intensive and may give more accurate results than using single parameters.

While it is becoming more common to include vertically heterogeneous soil parameters such as K_{sat} in hillslope runoff modeling, little research has been found analyzing the effects of doing so. Ambroise et al., (1996a, & 1996b) showed that the shape of the transmissivity profile in TOPMODEL can have a significant effect on the prediction of runoff and saturated areas. They showed how the use of parabolic and linear transmissivity functions lead to second order hyperbolic and exponential recession curves, which they say are more frequently observed.

Two other papers, (Duan & Miller, 1997; and Iorgulescu & Musy, 1997) expanded on the work of Ambroise et al., (1996a & 1996b) by modifying TOPMODEL with a generalized power function of the subsurface transmissivity profile. The power function form is flexible and can recreate linear or exponential functions used by Ambroise et al., as the limits by changing the exponent to 1 or infinity respectively. Duan & Miller (1997) showed that the linear extreme of the power curve resulted in rapid decay or normalized flow over time while the exponential extreme had the slowest decay.

The DHSVM hydrology-vegetation basin model (Wigmosta, et al., 1994) also uses an exponential decay function to represent variable K_{sat} with depth. This model uses the same explicit saturated flow function used in this thesis project except that it is applied in three dimensions instead of one, and is based on the surface slopes rather than the water table slope.

Further research compared water table profiles and hillslope outflow for a simple linear hillslope model configuration of DHSVM and TOPMODEL to analytical kinematic wave equation results for both linear (n=1) and power function (n=3) K_{sat}/depth equations. (Wigmosta & Lettenmaier, 1999) They found that the explicit DHSVM results using both the linear and power functions were in good agreement with the kinematic wave results. The statistical-dynamical TOPMODEL results tended to over simulate discharge on the rising limb of the hydrograph, slowly decay to steady state with constant rainfall, and underestimate runoff on the falling limb. These effects were most pronounced when using the linear K_{sat} function and were in better agreement when using the power equation.

More recently, Rupp and Selker (2005& 2006) applied a power function of K_{sat} vs. depth to the 1-D Boussinesq equation for the recession curve of flat (2005) and sloping (2006) aquifers. Their power function is different than applied in this study, in that it was started at 0 conductivity at the bottom of the soil profile and was not fit to real data. In both studies, they found that the recession curve is not affected much by the power function early in the drainage period but it is after longer periods of time.

No research was found analyzing the effects of using vertically variable porosity (ϕ) and volumetric water content (θ) on hydrologic hillslope modeling although it is commonly observed that both can be variable with depth. This is not to say that these parameters are not used in this manner, but such model configuration details are not always published or the focus of such modeling research.

Hillslope Shape

No studies have been found that directly compare runoff production from straight vs. S-shaped hillslopes for single rainfall events. Hilberts et al. (2004) studied the use of the Boussinesq, Kinematic Wave, and Richards Equation to model drainage on 2-D hillslopes of various bedrock curvature; concave, convex, and linear averaging 5% and 30%. They determined that the both hillslope storage and runoff hydrographs are affected by plan and profile curvature for all 3 models, with better agreement on divergent hillslopes and poorer agreement on convergent hillslopes, due to the high influence of diffusivity. Huang et al. (2001) discussed the hydrologic processes and their effects on erosion by position on a generalized S-shaped hillslope. They measured runoff from 5 hillslope positions for a year and found that each position produced seasonally-

different runoff due to the influence of soil crusting, Soil crusting occurred in different hillslope positions based on erosion, deposition, and vegetated cover.

Goals and Objectives

The goals of this research are to assess the importance of common assumptions regarding soil property variation with depth and of the role of hillslope shape on runoff production. Specific objectives of the study are:

1. To compare effects of using various vertical distributions of soil porosity, saturated hydraulic conductivity, and volumetric water content on initial conditions at the start of rainfall and runoff production in a physics-based conceptual hillslope model.
2. To compare impacts of straight vs. S-shaped hillslopes on the variation of initial conditions by hillslope position and on the timing and amount of runoff and drainage in a physics-based conceptual hillslope model.

Methods

Approach

The effects of vertically distributed parameters (ϕ, θ, and K_{sat}) and different slope shapes are examined in a 2-D, physics-based, finite-difference model of hypothetical hillslopes. The model is developed in the dynamic modeling environment STELLA (Systems Thinking, Experiential Learning Laboratory, with Animation) version 8 (isee systems) to implement the different distributions of the above parameters and different hillslope forms as further described below. The vertically variation in soil parameter values are compared with an average value for each parameter that is constant with depth. A straight hill slope is compared with an "S" shaped slope to determine the influence of curvature on runoff amount and timing.

Physical Setting

This study is based on hydrologic conditions frequently observed in the northeast region of the United States, specifically the glaciated hills of Connecticut. This region is typified by moderately sloped glacial till, drumlin-like topography in the uplands overlain by shallow permeable soils, and valleys containing glacial drift and alluvial deposits. This study focuses on soils found in the uplands. Regional water tables range from at or near the surface to over 10 meters deep depending on local topography, rainfall history, and time of year. Soils derived from the weathered till are typically less than a meter in depth. Hydraulic conductivities typically are an order of magnitude or two greater in the solum than in the non-weathered till below (Melvin et al., 1992; Pelletier, 1982), which can result in reduced permeability and locally perched water tables. Surface vegetation is

generally plentiful with many hillsides being covered by forests, hayfield/grassland, or agricultural crops.

Connecticut receives an average annual precipitation of approximately 1194 mm (47 inches), with the typical average annual runoff of about 610 mm (24 inches) leaving a typical annual evapotranspiration of about 584 mm (23 inches) (Carr et al., 1990). This humid climate results in shallow water tables and portions of the landscape that are often saturated during some parts of the year. Rainfall types include frontal systems, tropical storms, and convectional thunderstorms; with frontal systems being the most common. Storms of interest to modelers are generally the larger and more intense tropical or convectional storms that can cause the most flood damage and erosion.

The rainfall and soil/land conditions described above determine which flow processes occur in the region. The dominant flow processes that commonly occur in humid, well vegetated areas common to New England are saturation excess flow (from rainfall on a saturated area and return flow) and shallow subsurface flow (or interflow) (Dunne & Leopold, 1978). High regional water tables and locally perched water tables above the compact basal till result in saturated conditions and lateral flow in higher conductivity layers in the near surface weathered till. Areas at or near saturation are known to contribute a major portion of the runoff hydrograph through saturation overland flow (Dunne & Black, 1970). Infiltration excess overland flow is rarely seen in well vegetated, undisturbed soils of the region as they exhibit infiltration capacities that are higher than most observed rainfall rates (Dunne et al., 1975). Areas with compacted soils are an exception and may often exhibit infiltration excess runoff. Frozen soil conditions may also result in infiltration excess runoff but are not typically modeled in Connecticut.

This study uses hypothetical hillslopes typical of eastern Connecticut that are assumed to have permanent grass cover where the runoff mechanisms are saturation excess and shallow subsurface flow. All surface runoff is assumed to be generated from saturated source areas and return flow, i.e. Hortonian (infiltration excess) runoff is assumed to not occur. These assumptions are used in the model development process.

Soil Description

The soil used in the model is the Natural Resources Conservation Service (NRCS) Woodbridge soil series. It is a coarse-loamy, mixed, active, mesic Aquic Dystrudept, consisting of moderately well drained fine sandy loam with varying degrees of stoniness, and generally has compact low permeability sub stratum within one meter of the surface, where the C horizon begins (Soil Survey Staff, 1999). Woodbridge soil is found on the sides of hills and was chosen to represent all of the soils in the catena of which it is a member. All soils in the catena are derived from the same parent material and have similar structure, with the major differences among them being position on the hillslope and the amount of mottling resulting from frequency and duration of saturation.

Development of Soil Profile Data

Depth profiles of hydrologic soil parameters porosity (ϕ), volumetric water content (θ), and saturated hydraulic conductivity (K_{sat}) are required inputs to the hillslope model. For this study, some inputs are derived from field collected data while others are based on commonly accepted principles of hydrology.

Soil parameters are kept horizontally homogeneous in this study to limit the scope to a manageable level, suitable for this analysis, and to better isolate the effects of the

vertical distributions. The model as constructed in STELLA can allow for horizontal heterogeneity among grid cells if desired. Information derived from only one soil type, Woodbridge, is used for the entire hillslope, assuming that the other members of the soil catena possess similar hydrologic parameters.

The soil data set for use in the model is taken from a study done by Natural Resources Conservation Service (NRCS) in 2000, when tests were run for several locations of Woodbridge soil (McVey, 2002). In that study, in-situ K_{sat} measurements of each pedologic soil horizon were taken in the soil borings. Lab tests were conducted on selected soil cores to determine other physical parameters such as moisture content, bulk density (b_d), and mineral and organic fractions.

Saturated Hydraulic Conductivity

Saturated hydraulic conductivity is used to determine the rates of sub surface flow. Values of K_{sat} are taken from the NRCS study in which in-situ measurements were taken for several soil horizons at each pedon (sample site). Measurements were taken from 0.07-1.68 meters below the surface for the following horizons, in order of increasing depth; Ap, BW1, BC, and Cd3. Measurements in the relatively undisturbed, non-compacted soil surrounding each test hole are expected to give more accurate values than those obtained from disturbed samples in laboratory tests which destroy soil structure and macropores.

K_{sat} was measured using a portable compact constant head permeameter made by *Ksat Inc.*, known as an Amoozemeter. The unit can take measurements at discreet 15cm segments up to 2 meters deep. The Amoozemeter delivers water to a 6 cm diameter hole augured into the soil for incremental depths of approximately 15 cm (*Ksat Inc.*, 1994).

The edges of the auger holes were scraped with a planer auger to loosen any smearing due to the auguring process.

The K_{sat} data obtained in the NRCS 2000 study were originally presented in a poster by McVey (2002). Observations of this poster showed that a curve may fit the data fairly well and sparked interest in the idea of using the concept in a hydrologic model. The use of a general equation to represent vertically heterogeneous K_{sat} permits greater flexibility in a model for integration of parameters with depth and simplifies data input into a single function. This method is not meant for the prediction of values outside of this study but is a simplification of observed data for a particular site and is appropriate for the general comparisons in this study. Both the power and exponential functions are fit to a plot of the K_{sat} data vs. depth below ground surface in Microsoft Excel and tested. Figure 1 shows the resulting K_{sat} curve with fitted equations.

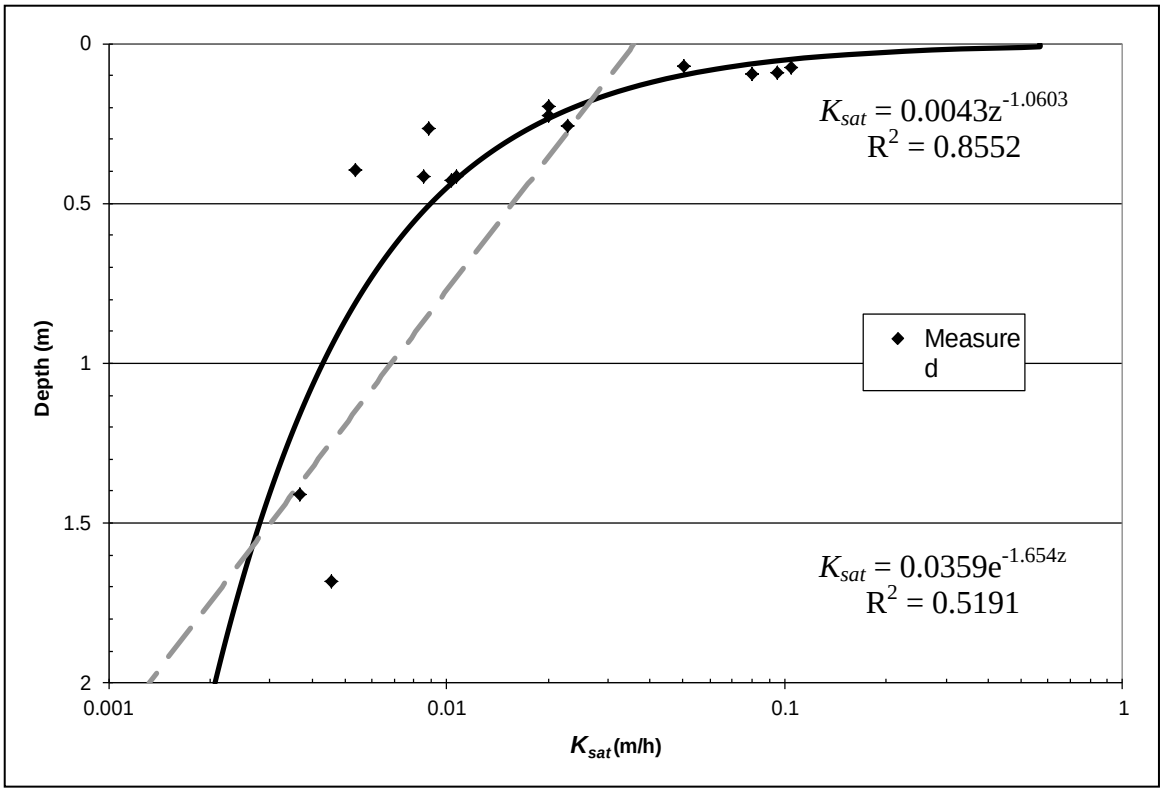

Figure 1: K_{sat} curve fitting for Woodbridge soil. Data from McVey (2002).

The power function for K_{sat} vs. depth has a better R^2 value (0.8552) than that of the exponential function (0.5191) and a better fit at the ends of the soil profile. The exponential function underestimates K_{sat} near the surface. Only the K_{sat} power function is used in the STELLA model.

The K_{sat} power function is allowed to increase above the measured values near the surface in order to represent flow through mesopores and macropores that may not be well represented by using the Amoozemeter over the 15cm range. Such a large increase in K_{sat} near the surface is not uncommon. For example, Elsenbeer, et al., (1992) found a 2 to 3 log increase in K_{sat} in the top 0.1 m compared to the next 0.1 m below for a tropical soil in Amazonia. Beven (1984) analyzed 38 soils where porosity and K_{sat} data as a function of depth were given. Values of K_{sat} varied by about three orders of magnitude,

from 0.02 to 91.2 m/hr for 24 *in-situ* soils, but only from 0.01 to 0.81 m/hr for soils from Holtan et al., (1968). The later values are presumed to be from laboratory studies involving disturbed samples. Researchers at the University of Connecticut have measured near surface K_{sat} values for several Connecticut soils, one of which is Woodbridge taken from the same property as the NRCS data used in this study (Dest, 2006). Table 1 shows the results of this research. These values were not used in the initial analysis when calculating the K_{sat} fitted equations as they were obtained after the analysis and through different measurement techniques, but provide an independent check of the near-surface values. These K_{sat} measurements are somewhat higher near the surface than predicted by the power function used. The fitted power equation is concluded to be reasonable.

Table 1: Ksat values from Bill Dest (2006).

depth (cm)	K_{sat}*(m/hr)*
0 - 2.99	1.1
5.1 - 11	0.41

Porosity

Porosity data are needed in this study in order to determine the depth of the water table and available pore space for a given amount of water in the profile as later described in the model processes section. Samples were lab tested from one of the test holes in the NRCS study. Porosity is calculated here using the measured values for bulk density (ρ_d), and percent carbon (*%C*) in the NRCS lab report based on the Equation 1 (Jury, 1991).

$$\phi = 1 - \rho_b / \rho_p \qquad [1]$$

Particle density (ρ_p) is calculated from the equation below based on the values of 2.65 g/cm^3 for the percent inorganic and 0.80 g/cm3 for the *%C* (Warner 2005).

$$\rho_p = \%C * 0.80 g/cm^3 + (1 - \%C) * 2.65 g/cm^3 \quad [2]$$

Similar to the K_{sat} data, power and exponential curves are tested for fitting the ϕ data. Six values were used for the range of 0.58 to 1.15 meters for the Ap, BW1, BW2, BC Cd1, and Cd2 horizons. One available ϕ value from a lower horizon (Cd3) is not included in the fitted curves because it is below one meter in depth, has a higher porosity than the layer above it, and causes a poorer curve fit to the data in the upper meter of soil. This deeper range of the soil profile is not used in the model. Figure 2 shows the ϕ curve fitting results.

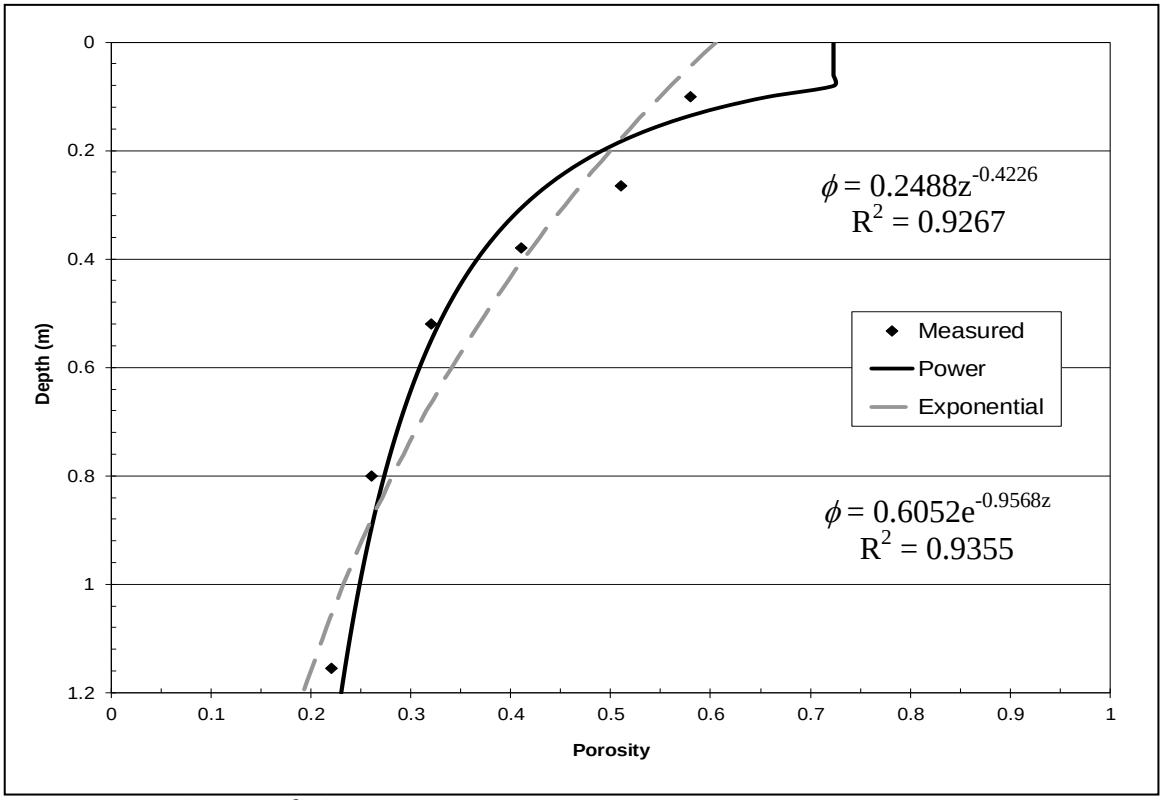

Figure 2: Porosity curve fitting.

Of the two equations, the power function has a slightly worse but comparable R^2 value (0.9267) vs. that of the exponential function (0.9355). Even though the exponential

function has a slightly higher R^2, it predicts values that are low near the bottom of the profile and lower than expected near the surface. The power function is again chosen based on these observations and for consistency.

The use of the power equation requires limits to be set for both K_{sat} and ϕ near the surface of the soil. As the depth approaches zero, the power function approaches infinity and extremely overestimates both K_{sat} and ϕ. Consequently, the minimum depth limits $z_{fmin(\phi)}$ (0.1m) and $z_{fmin(Ksat)}$ (0.08m) are used as shown in Figure 1 and Figure 2. The limits are set closer to the surface than sample depths in an effort to represent increased pore space and increased flow due to mesopores and macropores found in the field. Typically the top few centimeters of an undisturbed, vegetated soil have high porosity and very high K_{sat} values due to the presence of root systems and biotic activity as seen in the Dest (2006) data. These features are not always accounted for when sampled as they may be destroyed or too sparse to show up in laboratory samples. The Amoozemeter data, while considered relatively undisturbed, did not isolate the upper part of the Ap horizon, where K_{sat} would be expected to be highest. A rapidly increasing K_{sat} at the surface permits the model to address the impacts from rapid lateral movement of water near the surface as the soil approaches saturation.

Unsaturated Volumetric Water Content

An estimate of the total unsaturated volumetric water content (θ_t) is needed in conjunction with the porosity data to determine the available pore space (ϕ_a) of the soil profile. A theoretical equilibrium profile (where the pressure head is equal to the matric potential) is developed based on the work of Clapp & Hornberger (1978), who

approximated the upper portion of the θ distribution with the moisture characteristic relation rearranged here to solve for θ, where ψ_{ae} is the absolute value of air entry tension (meters), *b* is the pore size distribution index, and *h* is the pressure head(meters), which is considered equal to the height above the water table in this study.

$$\theta = \phi\left(\frac{\psi_{ae}}{h}\right)^{1/b} \quad [3]$$

The model is simplified by assuming that all points in the unsaturated soil moisture profile are at equilibrium at any given time. Equation 3 is meant to be an approximation of typical field capacity conditions and ignores the effects of hysteresis and evapotranspiration.

Figure 3 below shows the typical relationship of soil moisture to height above the water table. It is based on Clapp & Hornberger (1978) Fig 1. Clapp & Hornberger used the right half of a parabolic curve to represent the relationship near saturated conditions. Their original work included segments 1 and 3. For simplicity, this study only uses the equation representing the upper portion of the curve (segments 1 and 2). Everything below the capillary fringe is considered saturated and treated as part of the saturated zone. Segment 4 is not used in either case and is just the other half of the parabolic curve.

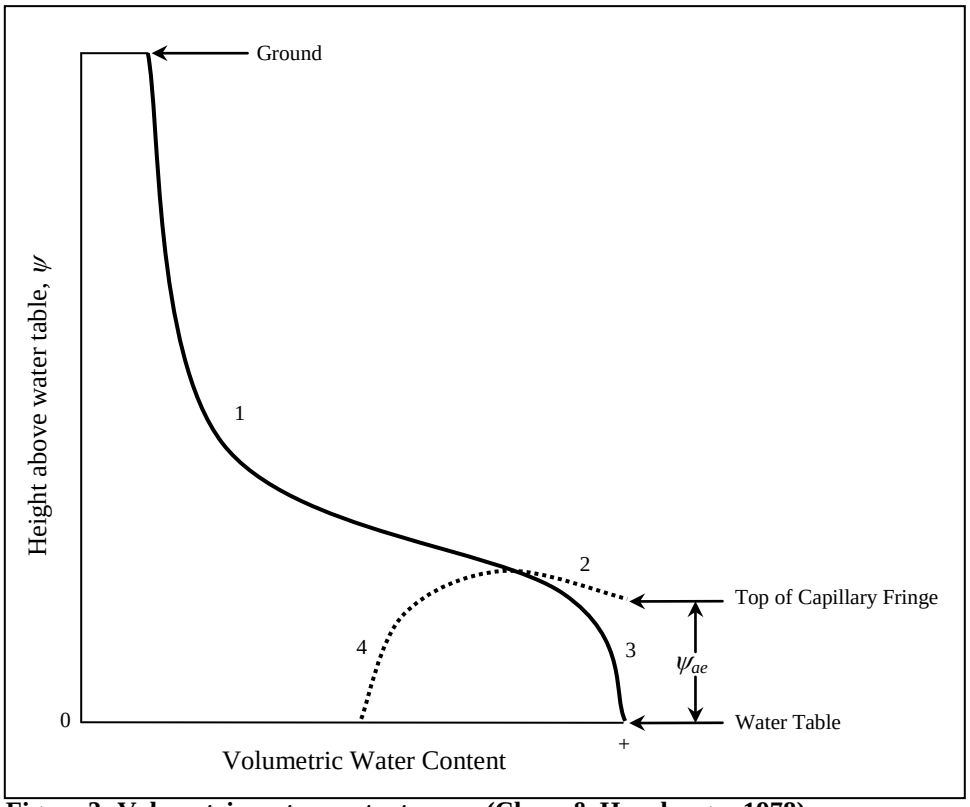

Figure 3: Volumetric water content curve (Clapp & Hornberger 1978).

Other Parameters

The ψ_{ae} and b (pore size distribution index) soil parameters used in Equation 3 may vary in different soil layers, and thus also be distributed over depth, however single values are used to simplify the study and focus on the three main parameters described above. Representative values of ψ_{ae} (0.200 m*) and b (4.90) for a sandy loam (Clapp & Hornberger, 1978) are used for the experiment.

*The mean value of ψ_{ae} from Clapp and Hornberger (1978) for the sandy loam is 0.218 m but 0.200 m is used due to rounding by a STELLA model component. There should be minimal differences caused by using the different value, which is within the range provided in the source table.

Summary of Profile Data

Table 2: Summary of soil parameter equations.

Parameter	General Equation	Equation with Values	eq #
Porosity (ϕ) from 0.1m-1m deep	$\phi = W_{\phi} \times z^{n_{\phi}}$	$\phi = 0.2488z^{-0.4226}$	[eq 4]
K_{sat} from 0.08m-1m deep	$K_{sat} = W_{K_{sat}} \times z^{n_{K_{sat}}}$	$K_{sat} = 0.0043z^{-1.0603}$	[eq 5]
Theta (θ)	$\theta = \phi\left(\frac{\psi_{ae}}{h}\right)^{1/b}$	$\theta = \phi\left(\frac{0.20}{h}\right)^{1/4.9}$	[eq 3]

The Model in STELLA

Introduction

The hillslope model designed for this study is a conceptual model based on physical characteristics of a theoretical hillslope, including soil structure, size, and shape, which are similar to those conditions found in the glaciated uplands of Connecticut as previously described. It is a mass-balanced finite-difference model where physics-based equations govern water movement throughout the hillslope.

Surface runoff is produced in the model via the variable source area concept (Hewlett 1961). The dominant process producing peak flows is typically rain falling on saturated areas (saturation excess runoff) over a portion of the hillslope, which may vary within an event or between events. Surface runoff may also be produced by return flow (also referred to as exfiltration). Surface runoff velocities are calculated using Manning's equation for sheet flow which substitutes water depth for the hydraulic radius. Shallow subsurface flow is modeled using Darcy's law for groundwater flow in an unconfined shallow aquifer.

The model is meant to be run for single events or for short term continuous studies. Long term continuous use is not recommended at this time due to the small time increment used and the fact that some hydrologic processes such as evapotranspiration and deep groundwater flow are not modeled in great detail.

STELLA Modeling Environment

STELLA® (Systems Thinking, Experiential Learning Laboratory, with Animation) version 8 (isee systems), is used to create and run the hillslope model. STELLA is modeling software that lets users create dynamic models of systems in an icon based graphical environment. Users build models through components (Stocks, flows, and converters) which are graphically connected on screen and then assign equations or values to each component. Equations that describe the conservation of mass, energy or momentum are automatically developed within STELLA based on the stock and flow connections in the model diagram and the resulting finite-difference equations are solved by the software. Results are viewed with built in tables or graphs, or can be exported. Some other components\functions of STELLA include graphical inputs, controls, and outputs such as input graphs, sliders, switches, knobs, and output boxes.

The benefits of using STELLA to develop the hillslope model are that it permits a researcher to: a) gain an in-depth knowledge and have control of all model components and their interactions, b) tailor the model for specific conceptual configurations, c) address different hydrologic processes, and add additional components for other hydrologic processes, and d) control spatial and temporal scales.

There are several benefits of using STELLA as opposed to conventional programming languages. The learning curve for STELLA is much quicker than for other languages so non-programmers should have an easier time learning how to use STELLA models. Equations can be input in familiar forms and many built in mathematical functions are designed to save time. It is fairly easy to make changes to the model and connections are seen on screen to help the modeler visualize the structure much easier than if everything was buried in code only. STELLA also keeps track of stocks and flows automatically so the volumetric budget of the model should be correct and small programming errors, or rounding will not lead to unexplained losses or gains.

Basic Array Unit (Cell)

The basic unit of the model described here is called a cell. Each cell represents a horizontally uniform area including the surface, and the soil profile below, as well as interactions with the atmosphere above. The cells are each made of identical model elements: stocks, flows, and converters, and sets of identical equations. By using the array function in STELLA a cell is converted into a 2 dimensional hillslope in the x and z directions. The model could be expanded to a 3 dimensional drainage basin if array connections were made in the y direction, but that would greatly complicate the model in its current STELLA form and is not done in this study.

Once turned into an array, each cell could have different dimensions and hydrologic parameters. For this study the only differences among cells are the surface and bottom elevations of each uphill and downhill edge, the boundary conditions, and flow calculations at the hillslopes' most uphill and downhill boundaries.

The structure of stocks shown in Figure 4 is adapted from the commonly used concept of hydrologic horizons, as described by Dingman (1994). Similar "saturated zone" concepts are also used by other researchers, example: Beven (1982).

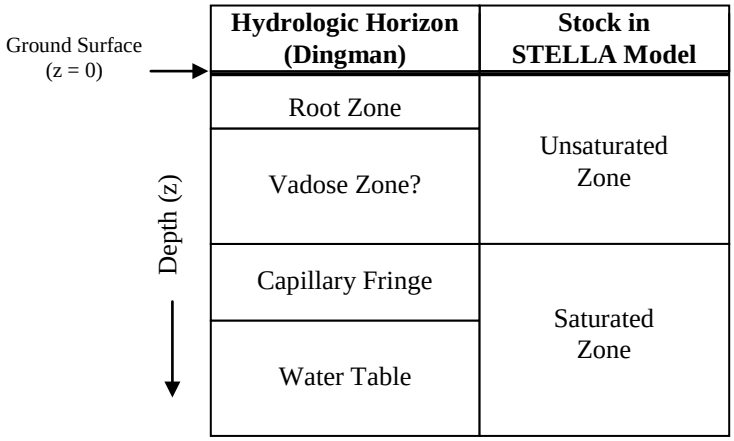

Figure 4: Hydrologic horizons.

These hydrologic horizons are based on the depth ranges of different water contents in the profile which may vary over time, unlike soil pedologic horizons which remain fixed. Hydrologic horizons are combined into zones of similar conditions to simplify implementation in STELLA™. Soil water below the water table and the capillary fringe are combined into a single saturated zone as they are assumed to both contribute to lateral groundwater flow. Dingman's intermediate zone and root zone are combined into a single unsaturated zone.

In STELLA a stock is used for each of the surface water, unsaturated zone, and saturated zone. Water is then given vertical flow paths into, among, and out of the stocks of the profile to represent precipitation, infiltration, return flow, percolation, and changes due to residual water exchange as the depth of the saturated/unsaturated boundary changes over time. Horizontal flows used to connect array elements through surface

runoff and saturated flow. The unsaturated zone does not have horizontal flows in this model.

Figure 5 shows the basic stocks and flows in STELLA. In order to keep the main model orderly, most calculations are done in other sectors with outputs and inputs to the main model handled with ghosts (copies of other model elements). These ghosts and connections (arrows connecting dependent variables) are not shown here for clarity.

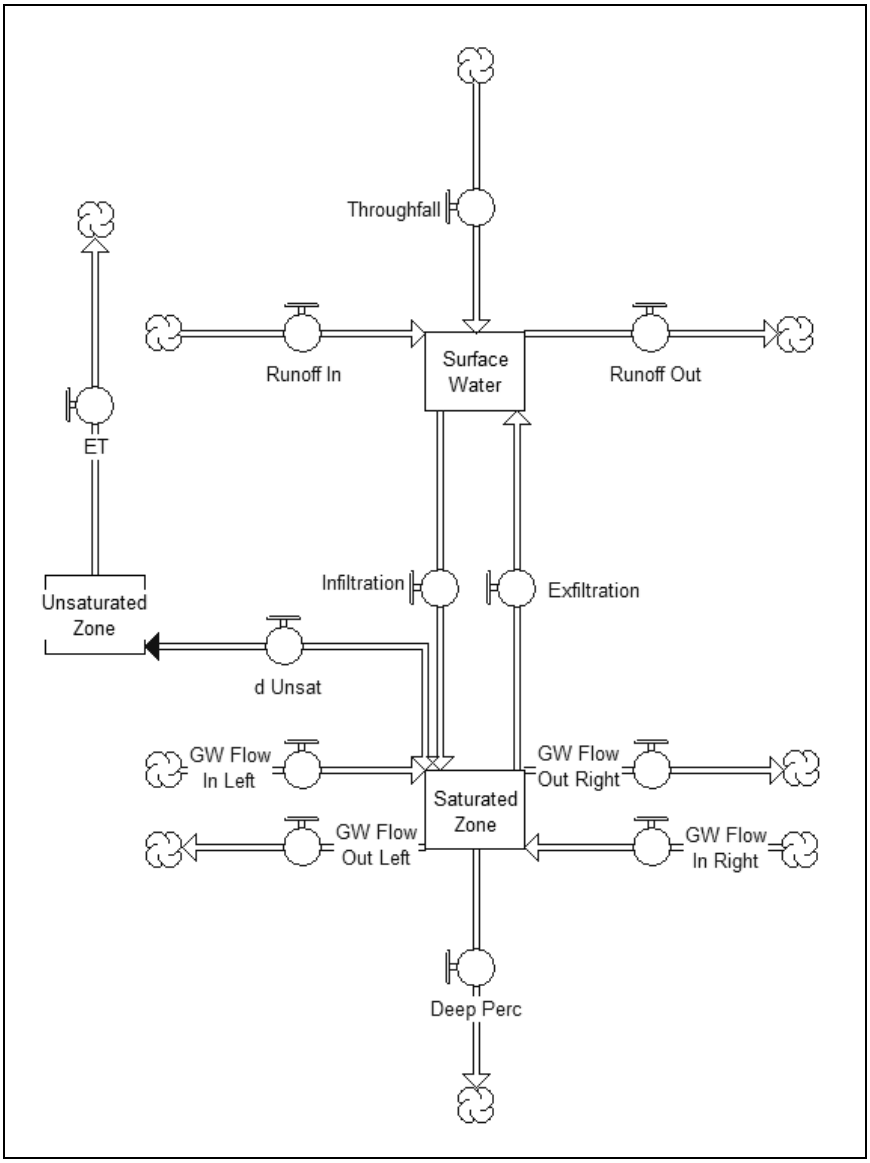

Figure 5: Hillslope model basic unit in STELLA

Model Control

Model run control is handled using the Run Specs and Sensi Specs control boxes. The Run Specs are used to control time settings while the Sensi Specs are used to set initial parameters for multiple model runs.

Run Specs

Model Run Specs include such parameters as run length, delta time (*dt*), and time integration method. Run length and *dt* are discussed further under experiment design. The time integration method is chosen from either Euler's, Runge-Kutta second-order, or Runge-Kutta fourth-order methods from radio buttons on the time specs control box. The Euler's method is the default but can lead to oscillation problems. The Runge-Kutta fourth-order method is chosen to maximize accuracy and avoid the oscillation problems. Runge-Kutta fourth-order uses 4 calculations within a given *dt* to create an estimate for the change in a stock over the *dt*. A weighted average of these calculations is used as the estimate for the change in the stock (STELLA Help File).

Sensi Specs

The Sensi Specs window is used to set initial conditions and change model controls. The switches that govern the parameter profile shapes are turned on and off here making eight different soil parameter scenarios that can be run in a row with no additional user input required.

Complete Model

The following figures show the complete model as it appears in STELLA. Figure 6 is the Component View, where the model is constructed. It is here that stocks, flows, and connectors are created, connected, and assigned equations. Figure 7 is the Interface View, where users make choices and set parameters for individual model runs. The third view is the Equation View, included in the Appendices.

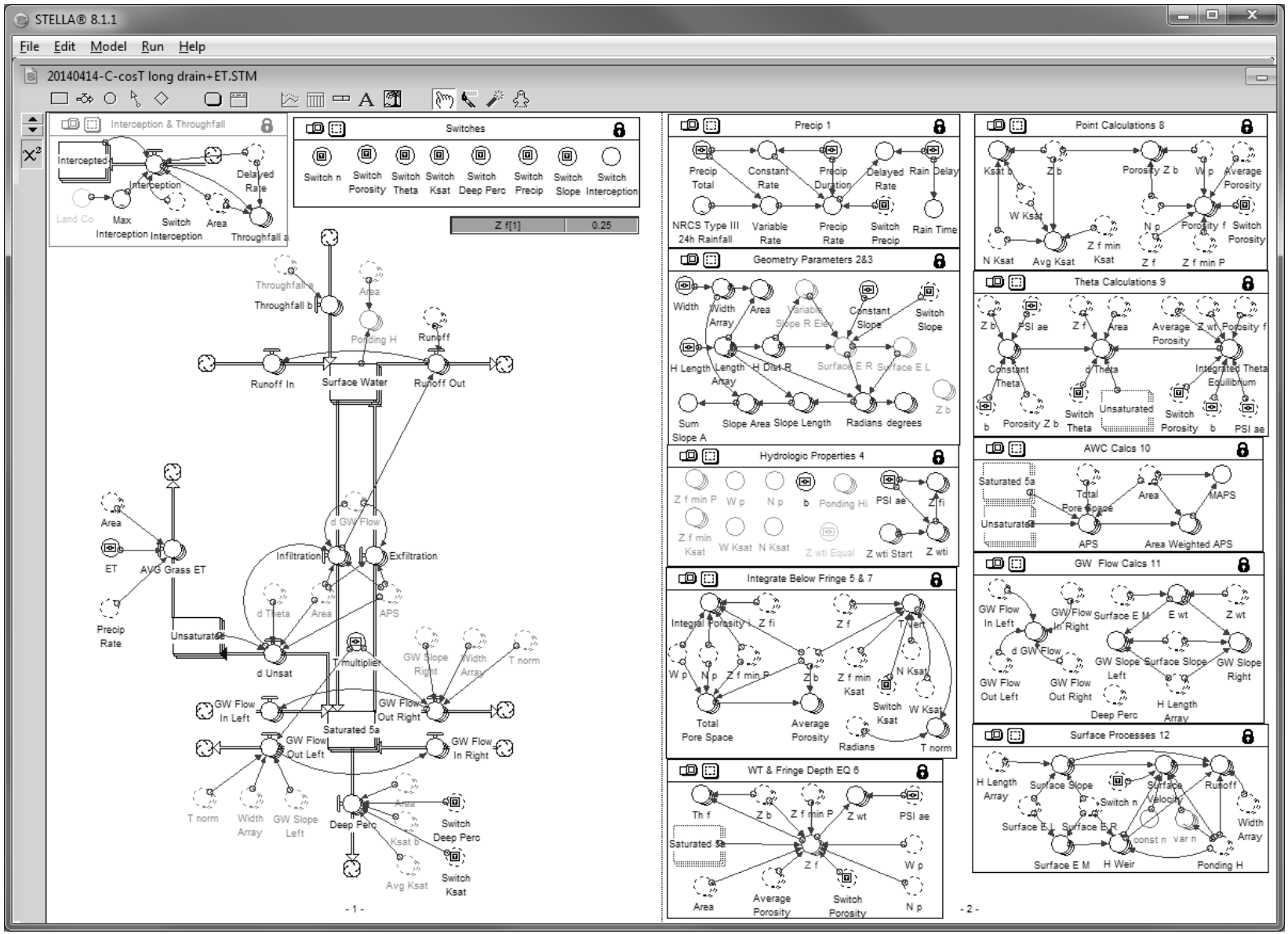

Figure 6: Complete Model, STELLA Map\Model View

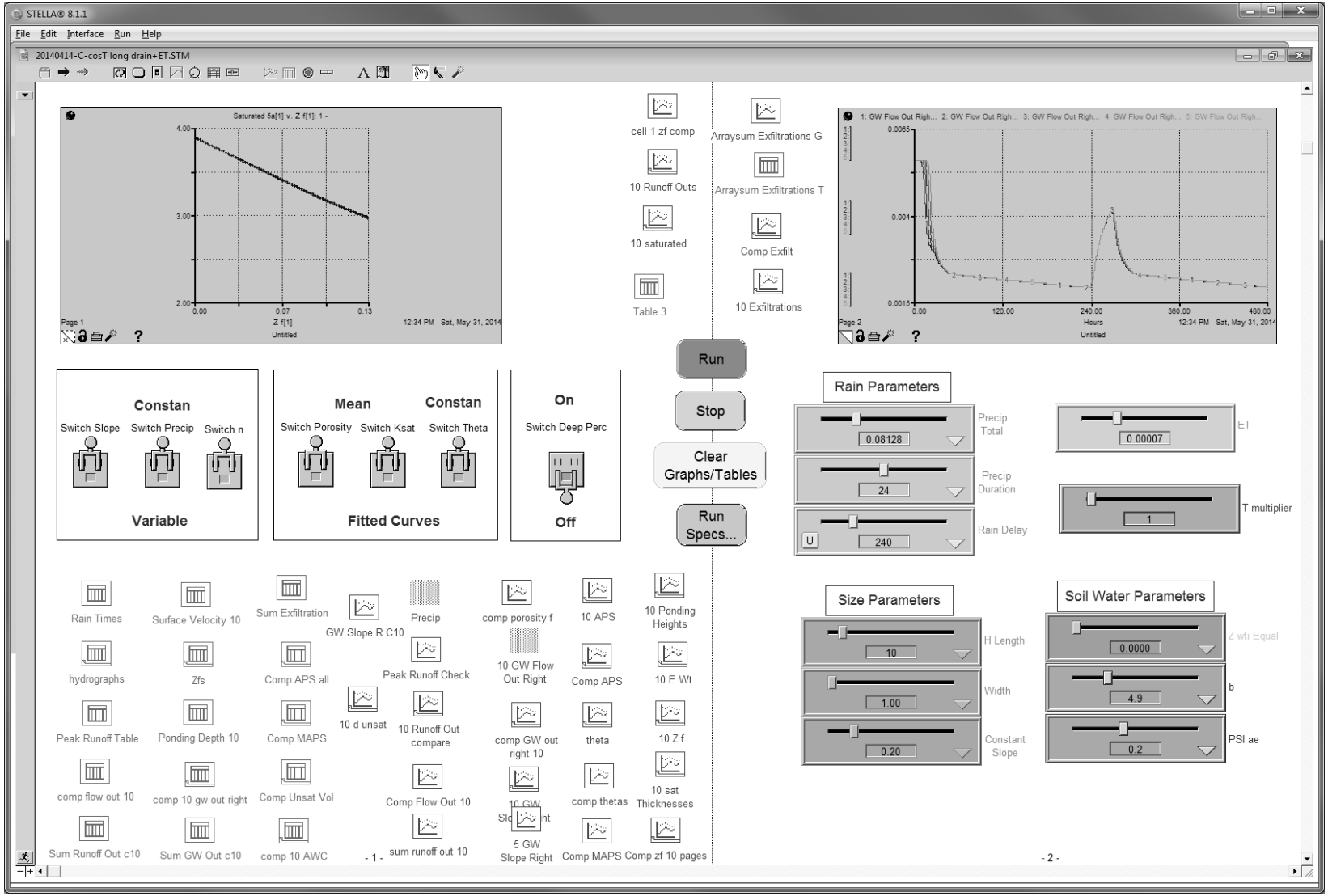

Figure 7: Complete Model, STELLA Interface View

Model Processes and Calculations

Some inputs are required from the user before the model is run, such as each soil parameter's equation multiplier and exponent, the rainfall depth and duration, and thickness of capillary fringe (ψ_{ae}). The equations below are shown for a unit area of $1m^2$ in the horizontal plane and will take true horizontal area into account when used in the model. All depths (z) are measured downward from the ground surface while all heights (h) are measured upward from the water table. See Figure 8 as a guide to the relative locations of selected model variables.

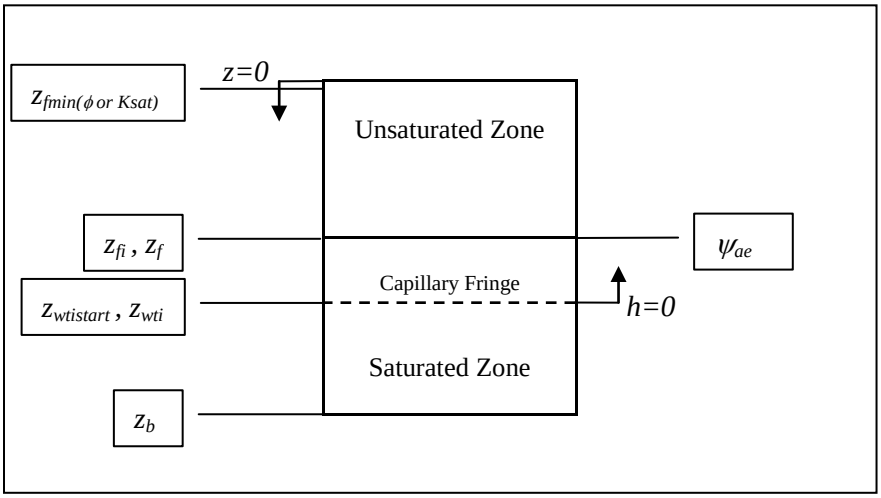

Figure 8: Relative locations of select model variables.

Model Initialization

Saturated Zone

The model is designed so that the volume of water in the saturated zone is determined by stocks and flows in STELLA via the conservation of mass. Other calculations are then based on this volume of water, the boundaries of the soil cell, and the vertical soil profile equations described above.

Once the user sets all the input parameters, the model is run and certain initialization steps are performed. The first step is to check to see if $z_{wtistart} < \psi_{ae}$ which would mean that the capillary fringe elevation would be above the ground surface, an impossible condition. If $z_{wtistart} < \psi_{ae}$ then z_{wti} is set to equal ψ_{ae}. If $z_{wtistart} > \psi_{ae}$ then z_{wti} is set to equal $z_{wtistart}$. After this check the initial depth to the saturated zone/unsaturated zone interface (z_{fi}) is calculated by adding ψ_{ae} to z_{wti}.

The next step is to fill the saturated zone stock based on the depth z_{fi}. The power function representing porosity vs. depth (Equation 4) is integrated in Equation 6 below from z_{fi} to the depth of bottom of the soil profile (z_b) as long as the depth z_{fi} is below $z_{fmin(\phi)}$. The $z_{fmin(\phi)}$ parameter is needed to limit the power function of ϕ near the surface to a reasonable value.

$$\int_{z_{fi}}^{z_b} W_\phi z^{N_\phi} dz = \left(\frac{W_\phi}{N_\phi + 1} \right) \left(z_b^{(N_\phi + 1)} - z_f^{(N_\phi + 1)} \right) \quad [6]$$

If the level of z_{fi} is above $z_{fmin(\phi)}$ the model only integrates Equation 6 from $z_{fmin(\phi)}$ to z_b. Then the pore space above $z_{fmin(\phi)}$ is added in Equation 7 by multiplying the porosity value at $z_{fmin(\phi)}$, ($\phi(z_{fmin(\phi)})$), by the height above $z_{fmin(\phi)}$.

$$\left(W_\phi z_{f\min(\phi)}^{N_\phi} \right) * \left(z_{f\min(\phi)} - z_{fi} \right) \quad [7]$$

Figure 9 shows the total pore space resulting from integrating ϕ for both the depth varied and constant porosity relationships. This is the vertical pore space in meters and is multiplied by the cell area to get a volume. Note that the pore space is less when integrating the power curve than for integrating the constant ϕ except at the end values.

They are equal at the ends because average porosity is calculated from total pore space (from power curve integration) divided by the total depth of the soil profile (z_b).

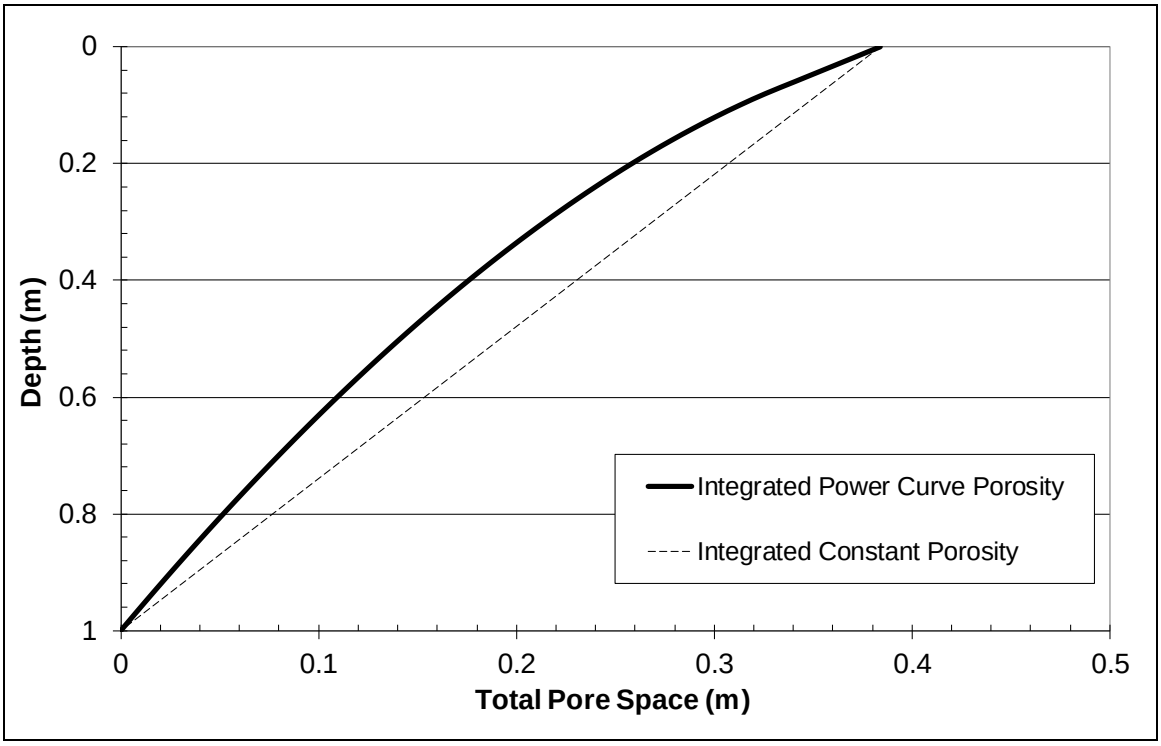

Figure 9: Integrated porosity curves.

Unsaturated Zone

At this point z_{wt} has been calculated (see *Volumetric Calculations* below) but is still equal to z_{wti} as flow calculations have not started. The amount of water in the unsaturated zone (θ_t) is calculated in a similar manner to that of the saturated zone and then set as the initial volume in the unsaturated zone stock. Equation 3 is integrated from the height of the capillary fringe above the water table (ψ_{ae}) to the surface height above the water table giving Equation 8. Since height of the ground surface above the water table happens to equal to z_{wt} no new parameter is needed.

$$\theta_t = \int_{\psi_{ae}}^{z_{wti}} \phi \left(\frac{\psi_{ae}}{h} \right)^{1/b} dh = \phi \left(\frac{{\psi_{ae}}^{(1/b)}}{1-1/b} \right) \left({z_{wt}}^{(1-1/b)} - {\psi_{ae}}^{(1-1/b)} \right) \quad [8]$$

In order to use the moisture characteristic curve with a vertical ϕ distribution in this model, ϕ is calculated at the capillary fringe. By using this method, the value for θ is never more than ϕ at any given point. Figure 10 shows how the θ curve is applied for two water table depths. The area below where each θ curve meets the ϕ line is considered saturated while the area above is unsaturated.

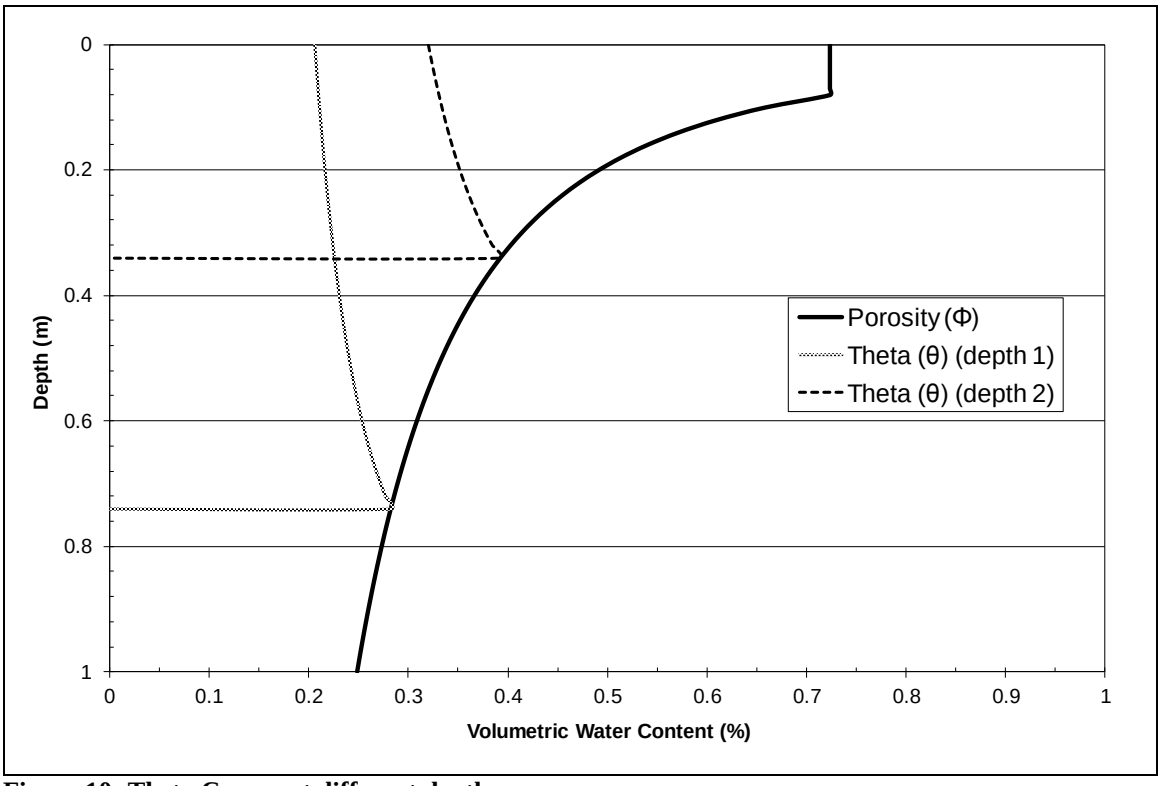

Figure 10: Theta Curves at different depths.

To calculate a constant (average) θ, Equation 8 is applied using ϕ at z_b and setting z_f equal to z_b. The resulting θ_t is divided by the depth z_b to get an average θ for each cell. This is necessary to prevent θ from exceeding ϕ for certain parameter combination scenarios but underestimates true θ_{eq} for shallower water tables. It in fact could be raised slightly to ϕ at $z_b + \psi_{ae}$ but would have minimal effects due to ϕ not changing much near the bottom of the soil profile.

Volumetric Calculations

Saturated Zone

After initialization STELLA keeps track of the amount of water in the saturated zone automatically by use of the stocks and flows. In order to determine the depth to saturation, Equation 6 is rearranged to solve the upper limit (z_f) based on the amount of water in the saturated zone stock using Equation 9.

$$z_f = \left[z_b{}^{(N_\phi + 1)} - \left(\int_{z_f}^{z_b} W_\phi z^{N_\phi} dz \right) \frac{(N_\phi + 1)}{W_\phi} \right]^{1/(N_\phi + 1)} \quad [9]$$

If the new z_f is above $z_{fmin(\phi)}$, then the above equation must be treated similarly to how the saturated zone was initially filled using a constant ϕ value for the soil above $z_{fmin(\phi)}$.

Unsaturated Zone

The last of the soil profile volumetric calculations is used to determine vertical flow between the saturated and unsaturated zones. θ_t is recalculated in Equation 8 above using the current z_{wt}. If the new amount differs from the amount actually in the stock, that difference is induced as flow between the saturated and unsaturated zones. See Figure 10 for an exaggerated example of the differences at 2 depths. This method corrects for either water table rise or fall, assuming that the profile is at equilibrium for each time step. Note that hysteresis is not accounted for and that this method is not designed for extremely large changes between time steps.

Flow Calculations

Rainfall/Infiltration

Rainfall is input as either a constant rate or a sketchable user-defined graph or input table. It flows into the surface water stock and then is given an opportunity to infiltrate before becoming runoff. As this is a saturation excess model and not an infiltration excess model, infiltration is only limited by the available pore space of the soil profile ϕ_a and the net change in groundwater flow ($d\theta$) between each time step.

θ_a is calculated by subtracting the total amount of water (in both the unsaturated zone and saturated zone) from the total pore space in the soil column (ϕ_t). To calculate ϕ_t, the ϕ power function is integrated from the minimum depth that the power equation can be applied ($z_{fmin(\phi)}$) to the bottom of the profile z_b, and the pore space from the uppermost portion of the profile is added. See equation 10 below. Note that $\phi_{zfmin(\phi)}$ is the ϕ value at that depth.

$$\phi_t = \int_{z_{f\min}(\phi)}^{z_f} W_\phi z^{N_\phi} dz = \left(\frac{W_\phi}{N_\phi + 1}\right)\left(z_f{}^{(N_\phi+1)} - z_{f\min(\phi)}{}^{(N_\phi+1)}\right) + \left(z_{f\min(\phi)}\right)\left(\phi_{z_{f\min}(\phi)}\right) \qquad [10]$$

$$\underbrace{\qquad\qquad\qquad}_{\theta \text{ below } z_{fmin(\phi)}} \qquad \underbrace{\qquad\qquad}_{\theta \text{ above } z_{fmin(\phi)}}$$

The net groundwater change is needed in conjunction with Equation 10 to prevent overfilling the unsaturated zone stock and to see if there is room for infiltration into the soil profile. The infiltration rate has no limit but it is assumed that large amounts of surface water will not accumulate over unsaturated soil within the small time step used. θ_a varies among cells along the hillslope based on the different water table and unsaturated zone conditions.

Percolation

Percolation of the infiltrated water within the soil profile is not delayed by a rate in this model, i.e. infiltrating water bypasses the unsaturated zone and reaches the saturated zone within a single time step as described above. Preferential flow paths such as saturated fingering below a wetting front or flow through macropores can account for some of this rapid water movement but in reality some flow would be delayed in the unsaturated soil matrix as percolation.

Shallow Subsurface Groundwater Flow

Shallow lateral groundwater movement in this model only occurs in the saturated zone. Unsaturated water only flows vertically between the saturated and unsaturated zones. Lateral velocity is calculated by Darcy's law for saturated flow,

$$v = -K_{sat} \frac{dz}{dl} \qquad [11]$$

where *dz/dl* is the hydraulic gradient of the water table between cells. The hydraulic gradient is calculated in the center of each cell and if negative, will allow groundwater to flow into an uphill cell (for very flat slopes only).

Unlike the previous studies mentioned in this paper (e.g. Beven 1982), this model does not assume that the groundwater surface is parallel to the surface or impermeable layer slope. The model takes advantage of the STELLA array form and *dz/dl* based on the difference between water table elevations from the midpoint of one cell to the next downslope cell.

To calculate transmissivity (T) the K_{sat} power function (Equation 5) is integrated downward from z_f to the bottom of the profile z_b using the equation:

$$T = \int_{z_f}^{z_b} W_{K_{sat}} z^{N_{K_{sat}}} dz = \left(\frac{W_{K_{sat}}}{N_{K_{sat}} + 1} \right) \left(z_b^{(N_{K_{sat}}+1)} - z_f^{(N_{k\,sat}+1)} \right) \quad [12]$$

When the value of z_f is smaller than $z_{fmin(Ksat)}$ the lower limit of the above formula becomes $z_{fmin(Ksat)}$ and the transmissivity of the uppermost portion of the profile is added from the equation. Actual transmissivity is calculated normal to the surface slope by multiplying Equation 12 by the cosine of the surface slope,

$$(z_{fmin(Ksat)} - z_f) * K_{sat}(z_{fmin(Ksat)}) \quad [13]$$

where $z_{fmin(Ksat)}$ is the minimum depth that the power equation can be applied and $K_{sat}(z_{zfmin(Ksat)})$ is the K_{sat} value at that point.

Average K_{sat} is calculated by dividing T (from the K_{sat} power curve integration over the whole soil profile) by total depth. Figure 11 shows the transmissivity resulting from integrating K_{sat} for both the power curve and constant value. Like the pore space graph (Figure 9), T is always less using the power curve K_{sat} than the constant K_{sat} except when at the end values z_b and z_{fmin} where it when equal.

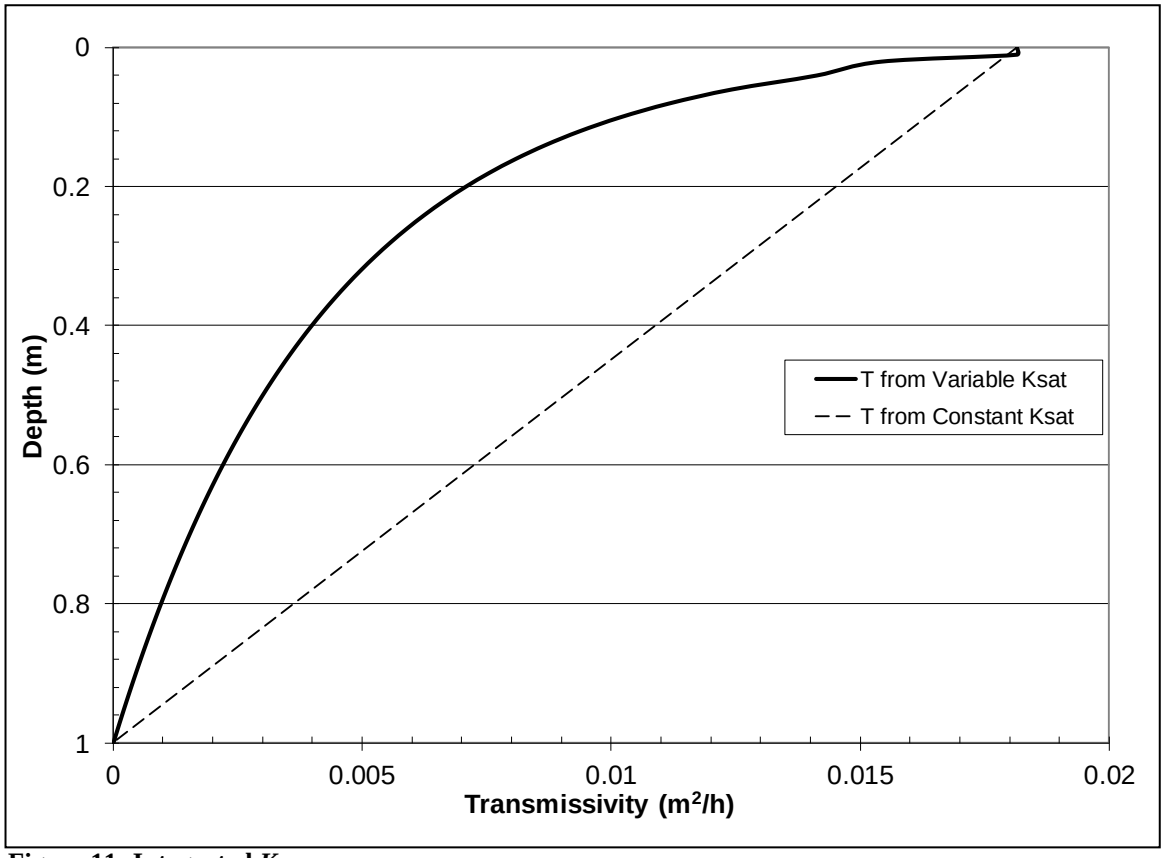

Figure 11: Integrated K_{sat} curves.

This graph shows that the relative difference in transmissivity between using the power curve vs. a single averaged value appears greater when applied to K_{sat} than for ϕ seen in Figure 9. This indicates that using the power curve for K_{sat} may have greater effects on the model.

The hydraulic gradient is calculated by the difference from the water table elevation (e_{wt}) of the middle of one cell to the middle of the next downslope cell. This approach may misestimate the slope since the model does not allow the water table to rise above the depth ψ_{ae} below the ground surface. For example, over estimation of the gradient may occur between two cells when a downslope cell should have a true water table above ψ_{ae} and the water table in the upslope cell is not at the same relative depth,

resulting in too much groundwater flowing between the cells. The effect will be most pronounced in areas with water table slopes much flatter than the surface slope.

One alternative would be to use saturation elevation (e_f) rather than the elevation of the water table (e_{wt}) to calculate groundwater slope. It is currently assumed that capillary forces in the fringe negate the pressure that would be exerted by that water and the net gradient would be the same since e_f and e_{wt} are always separated by constant ψ_{ae}. This alternate form would be more useful with horizontally heterogeneous soil parameters rather than the current horizontally homogeneous experiment. There would be additional problems in STELLA having water tables closer to the surface than ψ_{ae}.

Other alternatives would be to move the capillary fringe to the unsaturated zone by redefining the boundary of the saturated and unsaturated zones as z_{wt} rather than z_f , or to include another stock for the capillary fringe. These forms would be more flexible but also more difficult to implement in STELLA™. Their use was not explored but could be in future research.

Return Flow

Return flow (Q_r) occurs when the inputs to a saturated or near saturated cell are greater than θ_a plus the space made available by water leaving the stock, which includes lateral groundwater flow (*GW out*) and deep percolation. Return flow is simply the mass balance

$$Q_r = GW_{in} - \theta_a - GW_{out} - Deep\ Perc \qquad [14]$$

Equation 14 does not include ET flux, however, if ET is occurring, it is accounted for in the next time step by the updated θ_a. This way, return flow is given a priority over ET. No infiltration is allowed in a cell when a soil water stock is filled and return flow is occurring.

Surface Runoff

Surface water arriving from any of the processes mentioned above becomes overland flow if it is not able to infiltrate into the soil. Surface runoff velocities are calculated using the Manning's equation for shallow laminar flow with the water depth (H_p) substituted for hydraulic radius as is typical for shallow wide flows,

$$V = \frac{H_p^{(2/3)} * S^{(1/2)}}{n} \quad [15]$$

where S is the surface slope, H_p is the height of surface ponding, and n is Manning's roughness coefficient. There can be no backwater effect from downslope cells and surface water can never flow uphill because surface runoff is based on slope of the cell's ground surface, not the water surface.

If a single cell of the model is positively sloped so that water will pond, the broad crested weir equation (Equation 16) below is used to control surface runoff out instead of Manning's equation. The model cannot handle multiple adjacent positively sloped cells at this time.

$$Q(m/s^2) = g^{1/2}\left(\frac{2}{3}H_{weir}\right)^{3/2} \times width \quad [16]$$

H_{weir} is the height of the water over the ground surface (m), *width* is the width of the array (m) and g is the acceleration due to gravity (9.8 m/s^2),

Manning's *n* is set at a constant 0.45 in this model run, which is the value recommended by Engman (1986) for routing surface flows. The model has the ability to vary Manning's *n* with ponding depth for use in future research. A variable Manning's *n* was not used at this time but could improve surface velocity calculations.

Boundary Conditions

External model boundary conditions include flows through both the top and bottom of each cell and through the uphill wall of the uppermost cell and the downhill wall of the lowermost cell. Surface water is allowed to infiltrate with an unlimited rate, assuming that only very shallow ponding depths will form from rain in any given time step. Large amounts of surface runoff onto an unsaturated cell from an upslope cell may infiltrate at an unrealistic rate due to this limitation. A simple constant rate of evapotranspiration (*ET*) is included in to assist with the model initiation, described in more detail further on. The model contains a switch to turn off *ET* during periods of rain.

Lateral groundwater and surface water flows do not occur through the most uphill boundary. These flows do occur out of the most downhill cell's outer wall and will vary based on saturated zone depth and slope, and surface water depth and surface slope respectively. Sub-surface flow out is calculated the same as for the other model cells except the water table slope is the same as the next uphill cell since there is no downhill water table. Surface runoff is always based on the surface slope of the cell it is leaving.

There are currently no methods to account for backwater due to downhill water elevations such as a river or pond.

Model Validation

No suitable empirical hydrologic data sets were found in the literature to compare with the results of the theoretical hillslopes of this study. In order to validate that the model produces reasonable results, it is configured to simulate the Coweeta Hydrologic Laboratory sloping soil mass experiment (Hewlett & Hibbert, 1963) and compared to subsequent modeling research (Sloan & Moore, 1984).

The Hewlett & Hibbert experiment was a physical model of a hillslope, a 0.92m x 0.92m x 13.72m concrete trough at a 40% slope containing well mixed soil at a bulk density of 1.3 ±0.1 ($\phi \approx 50\%$). Sand, gravel, and rock were put at the toe of the slope to allow full drainage out of the soil profile and a hole was put in the downslope wall below the surface to control water level. Simulated rainfall was applied until the runoff reached equilibrium, and then the model was covered with plastic film so that no evaporation could occur. Several piezometers and tensiometers were installed in the trough to measure water table and soil moisture as it drained for 145 days.

For this validation, physical parameters are taken from Sloan and Moore (1984), who received additional verbal and published information that was not available in the Hewlett and Hibbert (1963) study, for their examination of five mathematical subsurface models. This included K_{sat} (0.168m/hr) and outflow results given in m^3/day/m.

Other soil parameters used by Hewlett and Hibbert (1963) are unknown so are estimated from Table 2 of Clapp & Hornberger (1978). Hewlett and Hibbert's (1963)

source soil was the C-horizon of a Halewood sandy loam. However, when their published textures are plotted on a USDA soil texture triangle for the current study the soil is classified as a sandy clay loam. Therefore, values of ψ_{ae} (29.9 cm) and b (7.12) for a sandy clay loam are used. This change gives results that slightly better matched the Hewlett and Hibbert (1963) outflow results than when using the sandy loam representative values.

Note, the Hewlett & Hibbert (1963) K_{sat} used is similar to the Clapp and Hornberger (1978) sandy loam K_{sat} value (0.125 m/hr) but over seven times higher than the Clapp and Hornberger (1978) value for sandy clay loam (0.0227 m/hr).

To simulate the Hewlett & Hibbert (1963) experiment in STELLA, the straight hillslope model is configured to 10 cells at 1.273 m long (horizontally at 40% slope) each. The outlet elevation is set by having groundwater flow out of cell 10 equal 0 m^3/hr when z_f is deeper than 0.46 m and equal to the groundwater inflow from cell 9 plus precipitation onto cell 10 when above that elevation. Precipitation is applied at a rate of 0.0021 m/hr normal to the slope, as in the Sloan and Moore (1984) models, by multiplying the rainfall rate by the slope plane area instead of the horizontal plane area.

K_{sat} and ϕ are still represented by power equations but given an exponent (n) of 0 (see Equation 17) so they would be constant throughout the profile. The values above were used for the multiplier (W).

$$W \cdot z^n = W \cdot z^0 = W \cdot z \qquad [17]$$

Experimental Design

For the experimental part of this study, several scenarios are run in order to evaluate possible effects on hillslope runoff production from using distributed hydrologic soil parameters vs. single values. The first set of runs is for a straight sloped hillslope as described below. The second set of runs is for an S-shaped hillslope that has the same overall length and elevation change as the straight hillslope.

Hillslope Form

The model allows for different hillslope shapes in the horizontal (x) direction. The straight slope is input as a slope and top elevation while the variable hillslope uses a graphical or tabular input of the cell edge surface elevations. The length of each model cell as discussed below is 10 meters in the x direction so that a group of 10 cells will form the 100 meter long hillslope. For this study the variable hillslope is a symmetric S-shape based on a sin wave from $\pi/2$ to $3\pi/2$. The overall slope of both the straight and S-shaped slopes is 20%, i.e., they have a 20 meter change in elevation over the 100 meter horizontal distance.

The soil profile accounts for a user-defined depth in the vertical (z) direction (1 meter was used here). This depth was measured in the vertical direction (McVey, 2002) so some corrections need to be made to adjust for the cell's slope for the K_{sat} formula previously discussed. Below the 1 meter soil profile, a compact basal layer parallel to the surface is assumed to significantly limit percolation. Any water moving into the basal till via deep percolation is considered lost to deep groundwater and removed from the system, as flow rates for deep groundwater are at a much longer time scale than this event

model. The deep groundwater flow was found to be a very sensitive function in preliminary model runs but is turned off for this study.

The hillslope width (y-direction) is constant at 1 meter so that the effects of lateral divergence or convergence are not introduced. Figure 12 and Figure 13 show each hillslope form in the x & z directions.

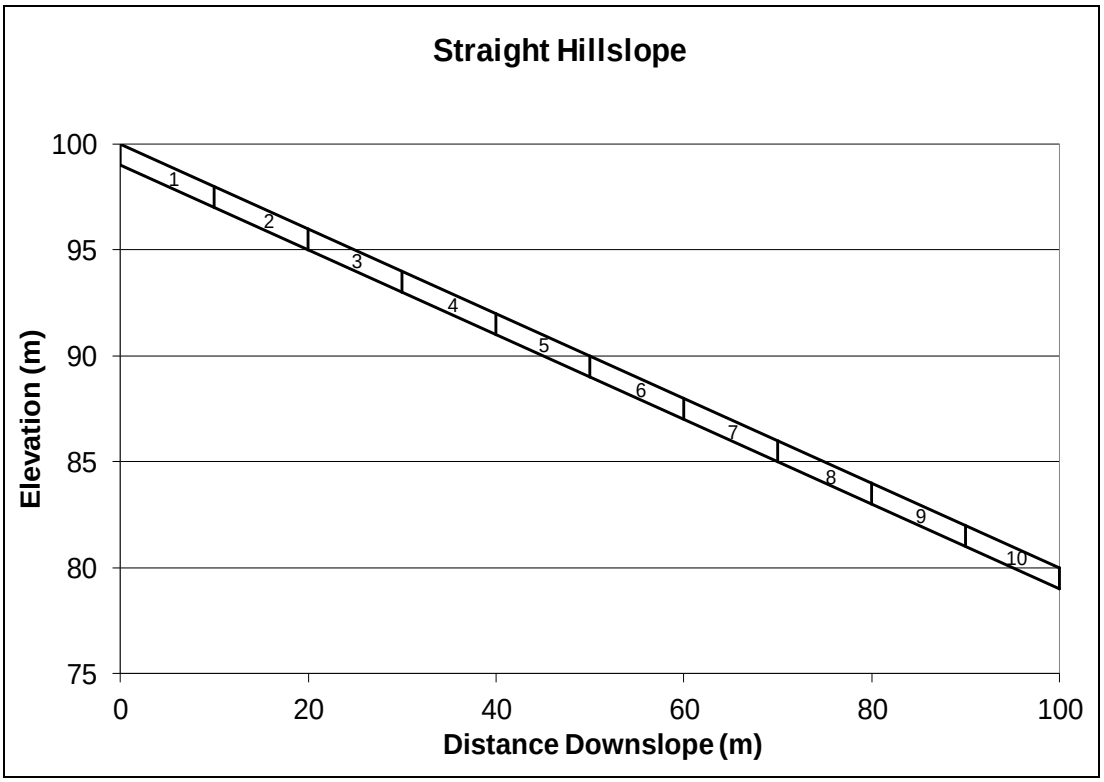

Figure 12: Straight slope model geometry.

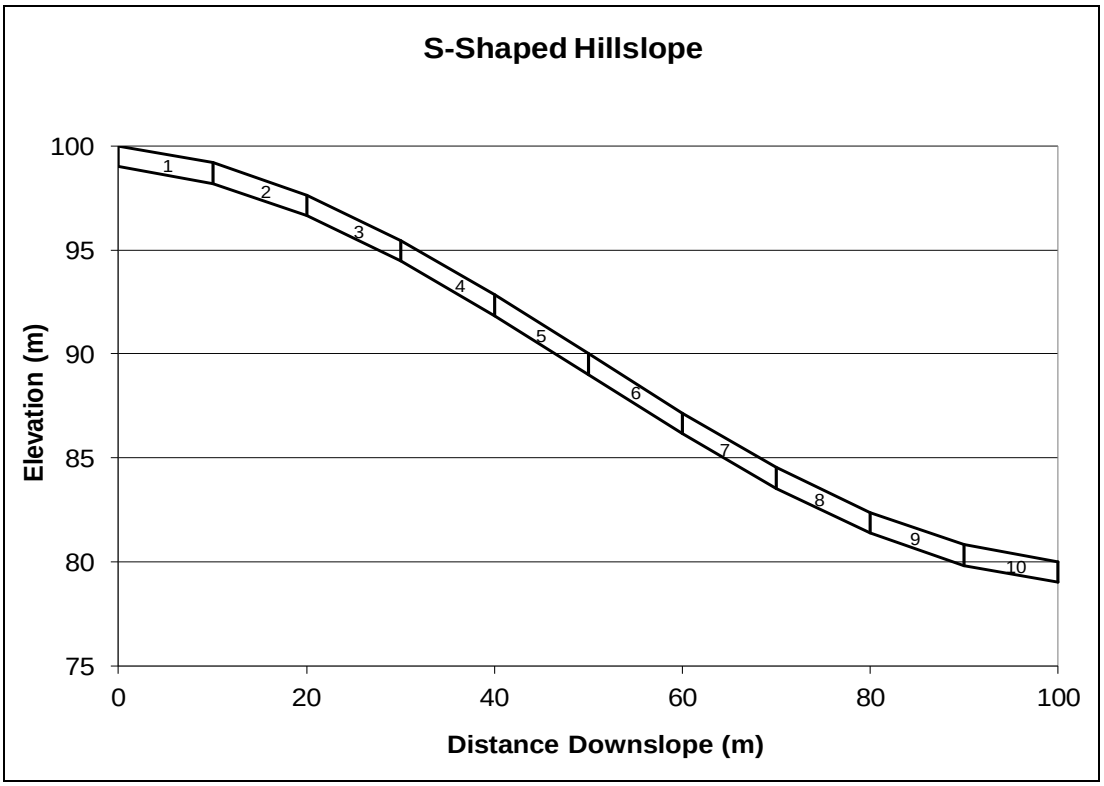

Figure 13: Variable slope model Geometry.

Parameter Profile Forms (Variable vs. Constant Values)

Vertical distributions of K_{sat}, ϕ, and θ are tested in the model based on the data described in the previous *Development of Soil Profile Data* methods section. All possible constant-variable profile combinations are tested as shown in Table 3. In this way the isolated effects of changing the profile form for each variable can be examined as well as the combined effects of changing the form of multiple profiles.

Table 3: Run scenarios based on soil parameter combinations.

Profile Scenario	ϕ	K_{sat}	θ
1	Average	Average	Constant
2	Power Curve	Average	Constant
3	Average	Power Curve	Constant
4	Power Curve	Power Curve	Constant
5	Average	Average	Power Curve
6	Power Curve	Average	Power Curve
7	Average	Power Curve	Power Curve
8	Power Curve	Power Curve	Power Curve

Initial Conditions

In order to reduce the effects of initial condition selection among scenarios, a run-in period is applied as a 'hot-start' (Cloke et al. 2003). While their methods involved applying inputs until a steady-state is achieved, the model runs here are started at full soil saturation, with a delayed rainfall start time of 240 hours (10 days). This allows for a period of drainage so that a starting water table profile based on the drainage properties of the soil can be achieved. This method is a simple way to initialize the model but preliminary results indicated that different scenarios may produce different available storage conditions (total and distribution) at the time when rainfall begins.

Evapotranspiration (*ET*) is included to achieve more realistic drainage over several days during the 'hot-start'. The evapotranspiration rate of 6.7559×10^{-5} m/hr (23.2

in x 0.0254 m/in / 365 days/year / 24 hr/day) is calculated from the mean annual ET of 23.2 in, similar to Carr et al., (1990). (This value is chosen as the *ET* rates are likely to be near the mean two seasons a year, in the spring and fall, two typically stormy seasons, as opposed to the two *ET* extremes of summer and winter. This is a constant rate that does not take into account time of day.

Available storage is possible in the form of the available pore space (ϕ_a) which is the depth in meters of water that could fit in the voids of a single model cell. If the variance for this storage is greatly different among parameter scenarios at the start of rainfall then the differences may interfere with analyzing the runoff results. It was decided to investigate if the differences made a noticeable difference in the model results.

Steady Rainfall

Total rainfall of 0.08128 m (3.2 in) is the NRCS 2-year 24-hour design storm for Tolland County, CT (Renn, 2005), which is based on the National Weather Service TP40 (U.S. Department of Commerce, 1961). This amount is chosen as a reasonably large event that would potentially saturate all of the hillslope cells. Further investigations show that not all cells saturate during the event.

Typically TP40 rainfall amounts are used with a synthetic rainfall distribution, but for this part of the study a constant rainfall is more appropriate. The rainfall total is divided by storm duration to get a constant rate of 0.003387 m/hr.

Unsteady Rainfall

The model is rerun with the same configuration, except unsteady rainfall is applied to observe if it behaves differently. Less analysis is done. The same amount of

rain as the previous runs is applied for both hillslope forms, using the NRCS Type-III, 24-hour synthetic rainfall distribution (Cronshey & Woodward, 1989). This rainfall distribution was formed by nesting regionalized TP-40 rainfall amounts from lesser duration storms uniformly around the 12 hour time and is used as a standard NRCS design distribution for rainfall-runoff modeling in Connecticut.

Summary of Values Used in Evaluation

Table 4: Values used in evaluation.

Parameter	Value	Parameter	Value	Parameter	Value
ϕ	Per horizon	b	4.9	$z_{fmin}(\phi)$	0.08m
ψ_{ae}	0.20	W_{ϕ}	0.2488	$z_{fmin}(K_{sat})$	0.01m
Manning's n	0.45	N_{ϕ}	-0.4226	z_b	1.00m
ρ_b	Per horizon	W_{Ksat}	0.0043	$z_{wtistart}$	Per cell
ρ_p	Per horizon	N_{Ksat}	-1.0603		

Sensitivity Analysis

A limited sensitivity analysis is also conducted. It is impossible to evaluate all parameters possibilities for this study so a few key parameters are chosen. The sensitivity analysis is explained in more detail in the results section of this study.

Results and Discussion

Model Validation

Figure 14, adapted from Sloan & Moore (1984), shows the results of Sloan & Moore's mathematical models and the Hewlett & Hibbert's (1963) observed values for the Coweeta sloping slab drainage experiment with the results from the validation run performed in STELLA overlaid on the original Sloan & Moore figure.

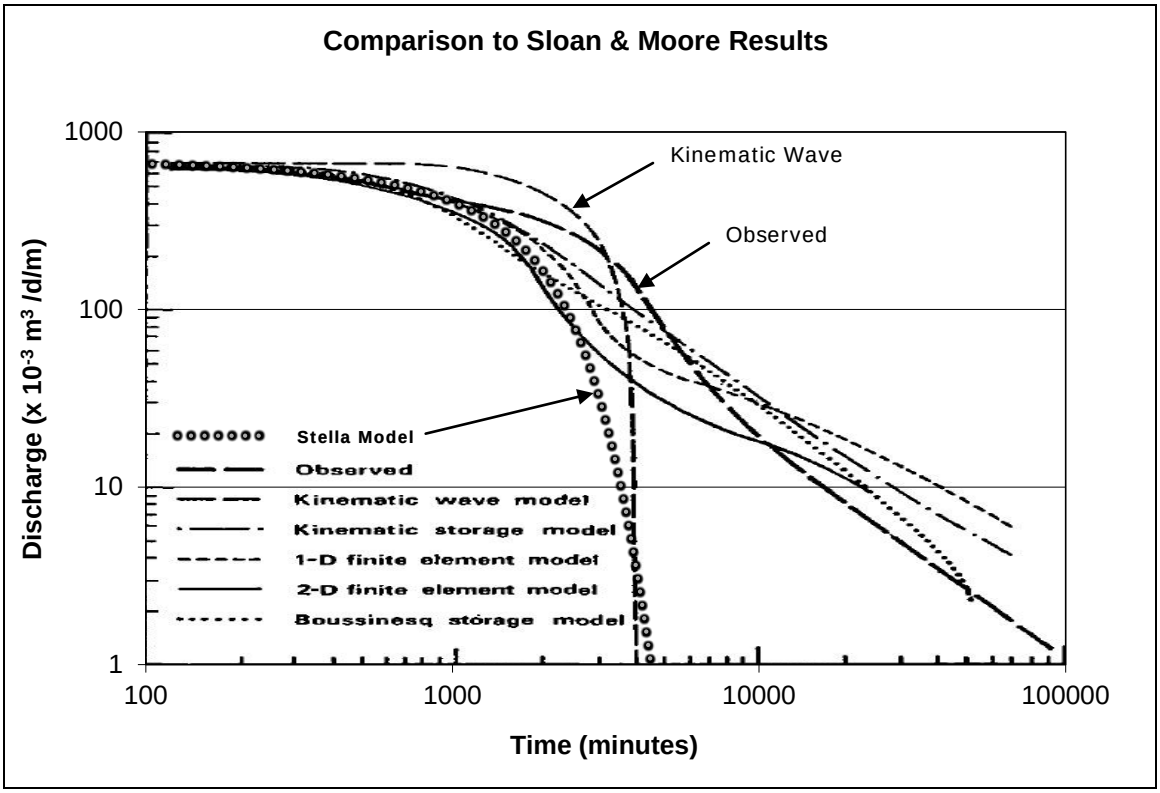

Figure 14: Model validation, discharge. Adapted from Sloan & Moore (1984).

The results of the STELLA hillslope model follow most models favorably for approximately the first 1100 minutes (18 hours), except for the Kinematic Wave model, which has more discharge. After this time separation of the other model results begins and the STELLA model results most closely follow the patterns of the 1-D and 2-D Finite Element models. After about 2000 to 3000 minutes (33 to 50 hours) the Finite Element

results begin to change their patterns while discharge from the STELLA hillslope model quickly slows, similar to the kinematic wave model.

The reasons for the rapid drop in discharge for the STELLA and Kinematic Wave models vs. the Hewlett and Hibbert and Sloan & Moore models are thought to be due to different techniques used to handle unsaturated flow. The hillslope model in STELLA does not allow for unsaturated soil storage above the equilibrium soil moisture profile and has no lateral unsaturated flow or delayed percolation.

Without these delays water in the unsaturated zone above equilibrium tension drains immediately to the saturated zone, causing more saturated water at equilibrium rainfall/runoff but less water overall in the profile than in the other models. With limited water in the unsaturated zone, there is no re-supply to the saturated zone as the water table drops, which then drains more quickly. This is observable as the quick drop off in runoff when rainfall ends. The hydrograph from the Sloan & Moore kinematic wave model is most similar to the hydrograph produced in this study. This method was different from the other models used by Sloan and Moore in that it used a constant percolation rate to the saturated zone.

This validation shows that while the hillslope model used here can predict soil water flow accurately near equilibrium conditions. It is not good at predicting soil water flow long after rainfall application, when lateral unsaturated flow may contribute a greater portion of overall soil/groundwater flow. Even though this discrepancy exists, the primary purpose of this model is to predict stormflow during or close to the rainfall

application. If it is to be used for a longer term water balance, soil moisture accounting should be handled differently.

Modeling Results

Originally equilibrium runoff rate (Q_e) (m^3/hr) and time to equilibrium runoff (T_e) (hours) were to be the model output used to evaluate the different scenarios and hillslope forms in this study. Further investigation showed that these results are highly dependent on initial conditions and rainfall amount/rate and thus are not good indicators for the goals of this study. Instead an evaluation of available pore space, and location of saturation extents are made for both S-shaped and straight hillslopes for all eight of the scenarios described in Table 3. Both initial conditions and conditions at peak runoff are evaluated. These results are more indicative of the differences in saturation excess runoff production than measuring (T_e) and (Q_e).

A period of 240 hours of drainage from saturation is chosen to get a water surface profile at start of rainfall, referred to as a 'hot-start'. Although this approach makes it impossible to get a hillslope with equally distributed storage conditions for each soil parameter scenario, it is easier to apply and thought to be more representative of natural conditions than forcing identical storage conditions for all scenarios. The final results are a combination of the effects of the differences in soil water distributions at the start of rainfall and runoff generated during the rainfall period.

Results for the Straight Hillslope

Available Pore Space

Observations of soil water conditions at the start and end of rainfall are made for each scenario. The mean available pore space over the entire hillslope ($\overline{\phi_a}$) (m) is used to represent the available storage over the entire hillslope. Figure 15 shows that $\overline{\phi_a}$ at the beginning of rainfall (after the 'hot-start' warm-up period) is different for each scenario.

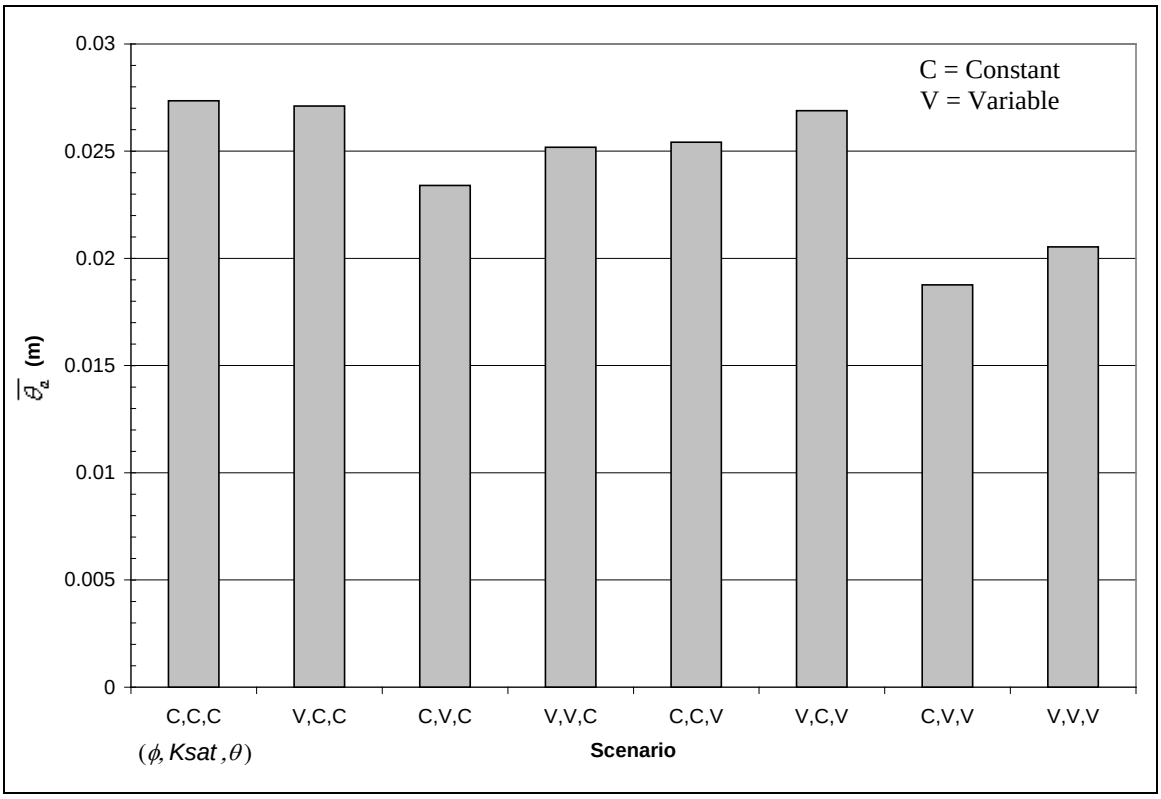

Figure 15: Average available pore space ($\overline{\phi_a}$) at rainfall start on straight hillslope.

The overall mean of $\overline{\phi_a}$ among the scenarios (0.0243 m) is less than the total depth of rainfall that is applied in the analysis indicating that there may be saturation excess flow somewhere on the hillslope. The range of $\overline{\phi_a}$ among scenarios is about 0.0086 m, which is a 33% difference below the maximum value (0.0275 m). This large

range indicates that θ conditions at the start of rain application are likely to have effects on the timing and amount of runoff. There is less $\overline{\phi_a}$ for the variable K_{sat} and variable θ scenarios and more $\overline{\phi_a}$ for variable ϕ scenarios relative to each corresponding constant scenario. Changing K_{sat} seems to have most effect on $\overline{\phi_a}$ and changing ϕ has the least.

The $\overline{\phi_a}$ results do not show the distribution of the available pore space (ϕ_a) (m) for each cell on the hillslope. The ϕ_a distribution over the hillslope at the start of the rain application (as shown in Figure 16) can be used to show which cells are likely to become saturated during the applied rainfall. For clarity, the profiles are divided into gray and black based on the constant or variable θ profile forms, respectively.

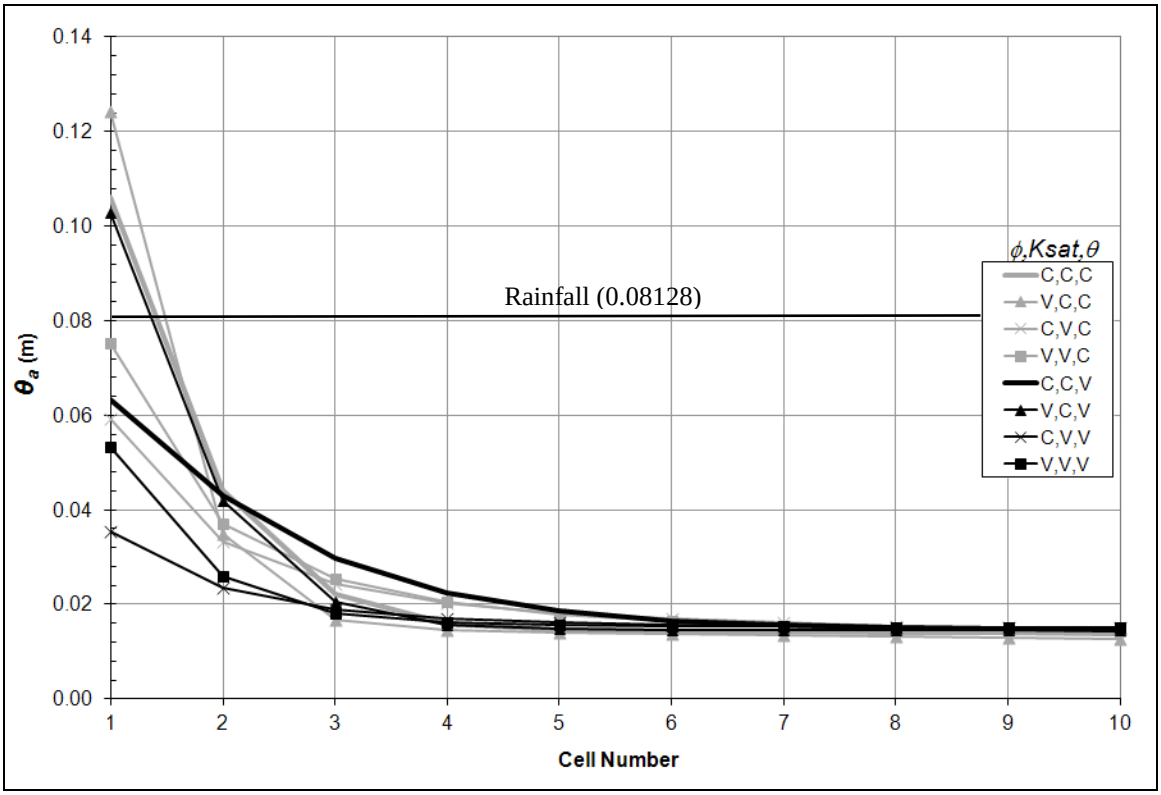

Figure 16: Available pore space (ϕ_a) distribution at rainfall start on straight hillslope.

The most variability among scenarios is in the upper portion of the hillslope for cells 1-5. For three scenarios, ϕ_a in cell 1 is greater than total rainfall depth, indicating that this cell will not saturate. All other cells have less ϕ_a than total rainfall depth and will likely saturate unless lateral subsurface outflow is larger than the inflow of water to those cells.

Table 5 shows selected ϕ_a statistics at the beginning of rainfall. The time to fill the range indicates the difference in time that it would take to fill each cell for the least and most saturated scenarios at the rainfall rate of 0.003387 m/hr and how the different model scenarios may produce different saturated regions on the hillslope.

Table 5: ϕ_a statistics for straight hillslope at rainfall start.

Cell	Mean (m)	Standard Deviation (m)	Range (m)	Time to Fill Range* (hr)
1	0.078	0.031	0.089	26.28
2	0.035	0.008	0.021	6.09
3	0.022	0.004	0.013	3.91
4	0.018	0.003	0.008	2.38
5	0.016	0.002	0.005	1.34
6	0.015	0.001	0.003	0.92
7	0.015	0.001	0.003	0.75
8	0.015	0.001	0.002	0.66
9	0.015	0.001	0.002	0.64
10	0.014	0.001	0.002	0.70

*at 0.003387 m/hr rainfall rate. Total rainfall = 0.08128 m.

The ranges are smaller for the lower portion of the hillslope but become greater for the upper portion. These differences in ranges show that the 'hot-start' method of initialization produces different initial storage conditions, especially in the upper portion of the hillslope.

Saturated Extents

Saturated extents are indicated by the distribution over the hillslope of where ϕ_a equals zero at the end of rainfall. Table 6 shows the results below. A table is used instead of a graph because the range of orders of magnitude of these results do not display well on a graph.

Table 6: Available pore space (ϕ_a) (meters) distribution at end of rainfall for straight hillslope.

	Profile Scenario (ϕ, K_{sat}, θ) C = Constant, V = variable							
Cell	**C,C,C**	**V,C,C**	**C,V,C**	**V,V,C**	**C,C,V**	**V,C,V**	**C,V,V**	**V,V,V**
1	3.52E-02	5.54E-02	5.55E-17	2.64E-03	4.05E-04	3.19E-02	6.86E-05	1.95E-04
2	0	0	0	0	9.56E-05	1.18E-04	4.45E-05	6.70E-05
3	0	0	0	0	5.57E-05	5.78E-05	3.90E-05	5.44E-05
4	0	0	0	0	4.35E-05	5.11E-05	3.69E-05	5.16E-05
5	0	0	0	0	3.86E-05	5.00E-05	3.60E-05	5.08E-05
6	0	0	0	0	3.64E-05	4.97E-05	3.55E-05	5.06E-05
7	0	0	0	0	3.54E-05	4.97E-05	3.52E-05	5.05E-05
8	0	0	0	0	3.49E-05	4.96E-05	3.51E-05	5.04E-05
9	0	0	0	0	3.47E-05	4.96E-05	3.50E-05	5.03E-05
10	0	0	0	0	3.46E-05	4.95E-05	3.49E-05	5.03E-05

In the four constant θ scenarios, all of the cells except for cell 1 are saturated by the end of rainfall. Cell 1 of the *C,V,C* scenario is essentially saturated as ϕ_a is less than the amount of rainfall being applied in a single 0.1 hour (6 minute) time step (3.3387E-03 m) and thus is producing runoff from direct precipitation.

In the four variable θ scenarios, all of the cells are essentially saturated with the exceptions of cells 1 in the *V,C,V* scenario. These results may be due to the way the model handles fluxes and soil water redistribution within each time step as there is enough rainfall per time step to saturate these cells.

Observations of these results are made in relation to the other two soil parameters. Each cell in the constant ϕ scenarios has less ϕ_a (is more saturated) at the end of rainfall

than the corresponding variable ϕ scenario, where K_{sat} and θ are kept the same. Patterns related to constant vs. variable K_{sat} are not as consistent. The constant K_{sat} scenarios have more ϕ_a (are less saturated) than their corresponding variable K_{sat} scenarios near the upper hillslope but the trend reverses lower on the hillslope.

Subsurface Outflow

Lateral subsurface outflow is analyzed for subsurface stormflow and non-storm drainage. Subsurface outflow may be different for each cell of the hillslope, depending on water table slope and depth of water, however analyzing each cell of each scenario would result in 80 hydrographs for each hillslope, too many for this analysis. Instead, subsurface outflow hydrographs are only included for cell 10 as this is the soil water outlet of the model and there is no observed return flow to the surface of the straight hillslope.

Subsurface stormflow is made up of both wetting and drainage periods. Drainage occurs in between rainstorms or when percolation rates are slower than the subsurface outflow rates. Wetting occurs when the percolation rate is higher than the subsurface outflow rates.

Subsurface outflow during the drainage period is important because it is the process which determines the conditions at the start of rainfall such as the ϕ_a distribution, and also affects runoff after each rainfall period. It is during the initial drainage that different behaviors of soil parameter profile scenarios can have a major effect on model results. During the 240 hours of drainage for the 'hot-start' several different patterns are observed, as seen in Figure 17.

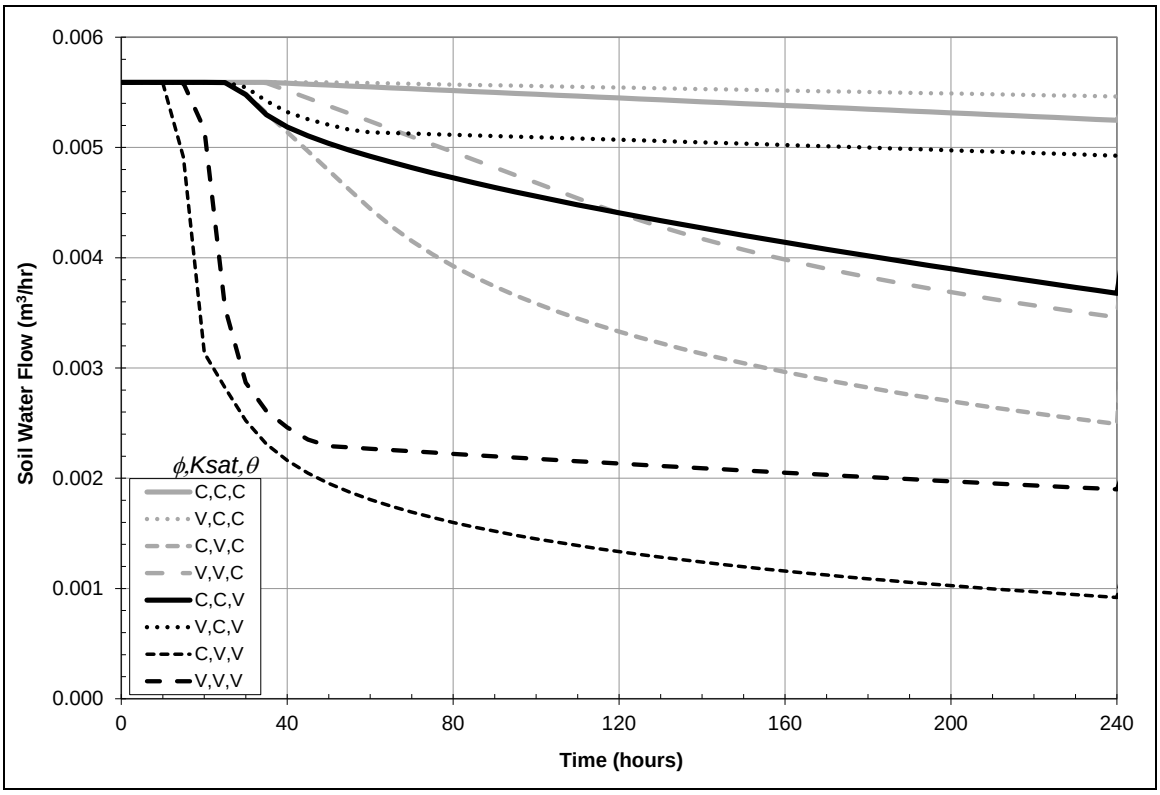

Figure 17: Straight hillslope subsurface outflow during drainage from saturation.

The maximum subsurface outflow is 0.0056 m3/hr, when cell 9 & 10 both start out saturated. During drainage the subsurface outflow for the four constant θ scenarios is higher than for the corresponding variable θ scenarios. Flow for the four constant K_{sat} scenarios is higher than for the corresponding variable K_{sat} scenarios. Flow for the constant ϕ scenarios is lower than the corresponding variable ϕ scenarios. It appears that changing the K_{sat} profile has the greatest effect on drainage since the subsurface outflow after 240 hours has decreased the most in these scenarios.

During the applied-rainfall runoff events, subsurface stormflow is a minor component of overall stormflow, approximately two orders of magnitude less than surface water runoff. Figure 18 shows the patterns of the subsurface stormflow out of cell 10 during the wetting cycle, after the 240 hours of "hot–start" drainage.

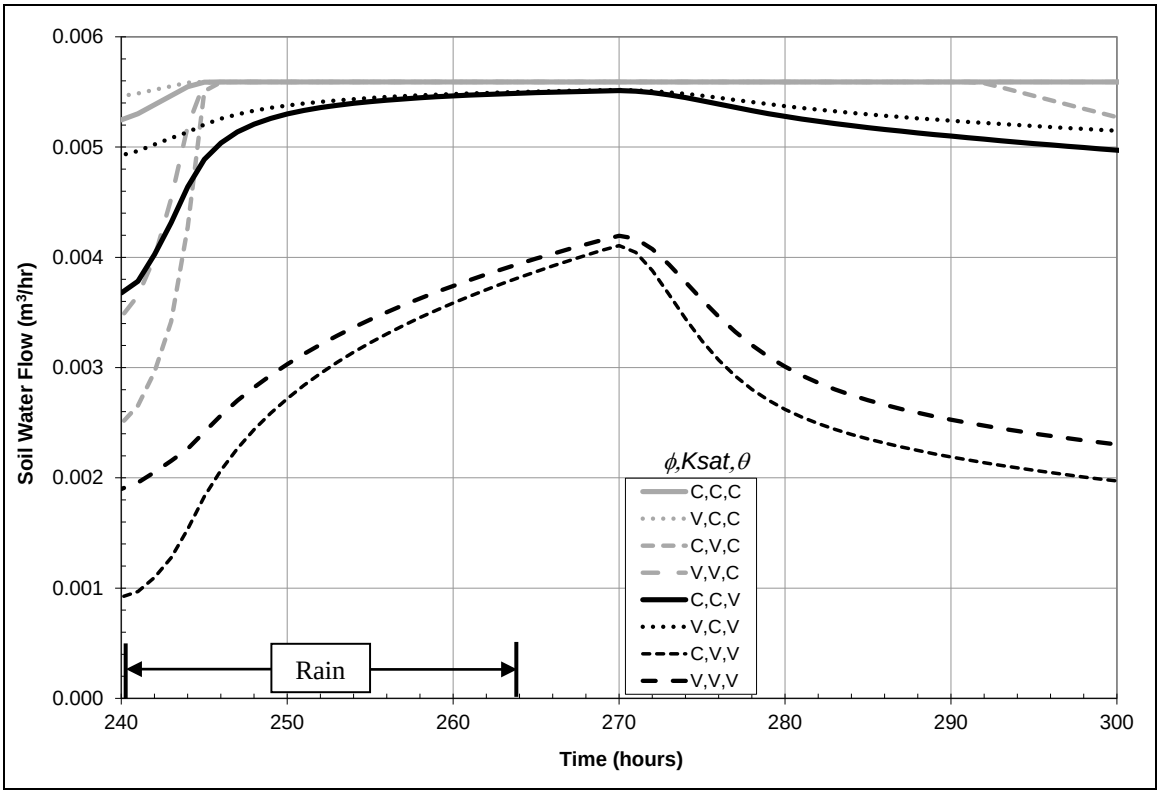

Figure 18: Straight hillslope subsurface outflow during rainfall.

Subsurface flow in all four constant θ scenarios increases the fastest during the first 6 hours of rainfall, then levels off. Flow in all four variable θ scenarios rises more moderately, peaking after approximately 30 hours, and without a long level period.

Of the variable θ scenarios, similar patterns and peak flow amounts are distinguished by K_{sat} scenarios with variable K_{sat} scenarios producing less outflow than the constant K_{sat} scenarios. This is expected as transmissivity is less for variable K_{sat} scenarios at all water table depths until saturation is reached, as shown in Figure 11.

Among the variable θ scenarios, those with variable ϕ have slightly higher flows than their corresponding constant ϕ scenarios but this may only be because these hydrographs were already higher at the beginning of rainfall. After rainfall stops,

drainage continues as in a similar pattern as before (not observable on the graph due to the axis limits).

Return Flow

Return flow (exfiltration) is not observed on the straight hillslope, because the water table slope into a cell is never greater than the water table slope out of the cell given horizontally homogeneous soil parameters, surface slopes, and an evenly applied rainfall after a period of drainage from full saturation.

Surface Runoff

The total cumulative surface runoff that occurs during rainfall is summarized in Figure 19. There is a difference of about 13% between the minimum and maximum of these scenarios. There is no clear correlation between changing any of the three soil variables and more or less total surface runoff. The difference could be in either direction.

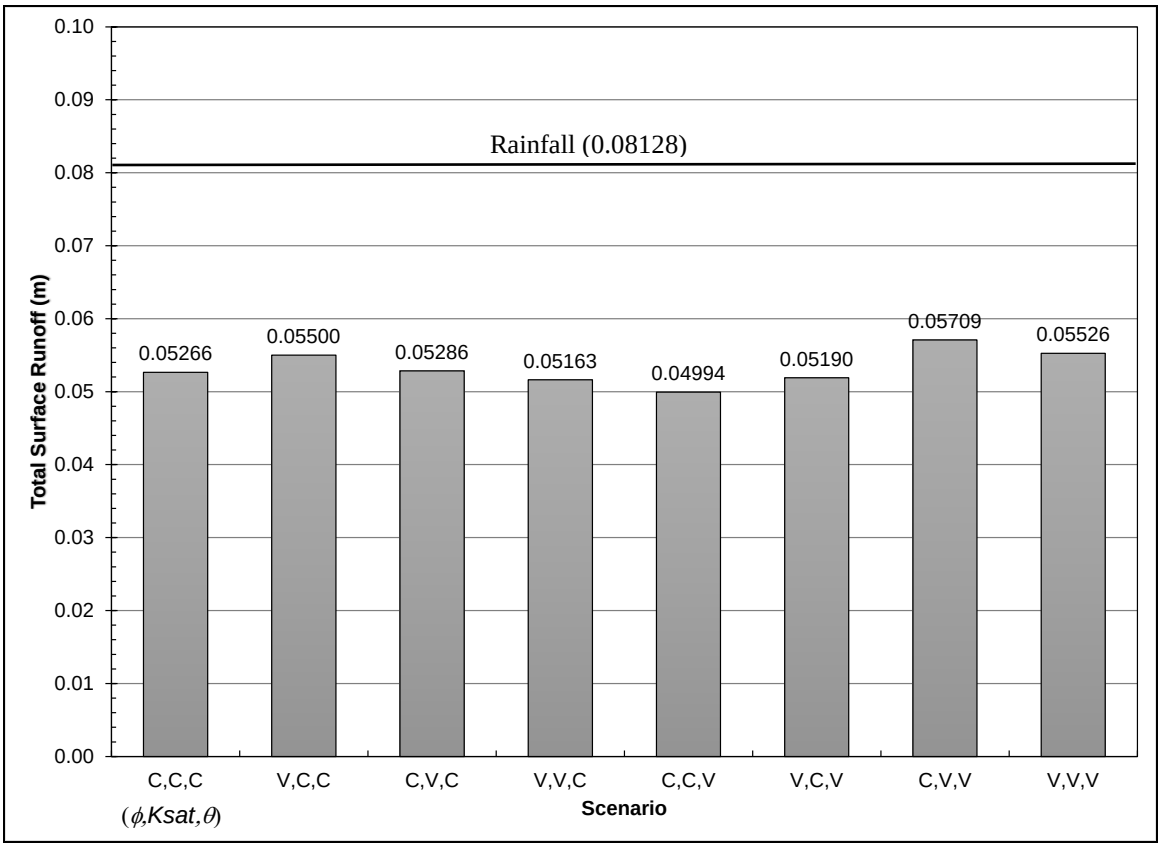

Figure 19: Straight hillslope cumulative surface runoff totals.

Observations of the model output tables (not shown) show that surface runoff does not occur before hour 240 (when rainfall begins). A minor amount of surface runoff does continue after rainfall ends, about 4% of the total surface runoff. It stops between hour 269.4 and hour 341.2, depending on the scenario. All four variable θ scenarios stop in hour 269 (about 5 hours after rainfall ends), while the four constant θ stop producing surface runoff between hour 290.7 and 341.2 (from about 51 to 101 hours after rainfall ends).

Observing the surface runoff hydrographs of these model runs reveals some patterns in the behavior of runoff production for each scenario. The stair step pattern in

Figure 20 shows that there is not a smooth transition from when a downslope cell reaches runoff equilibrium and the next upslope cell starts producing runoff.

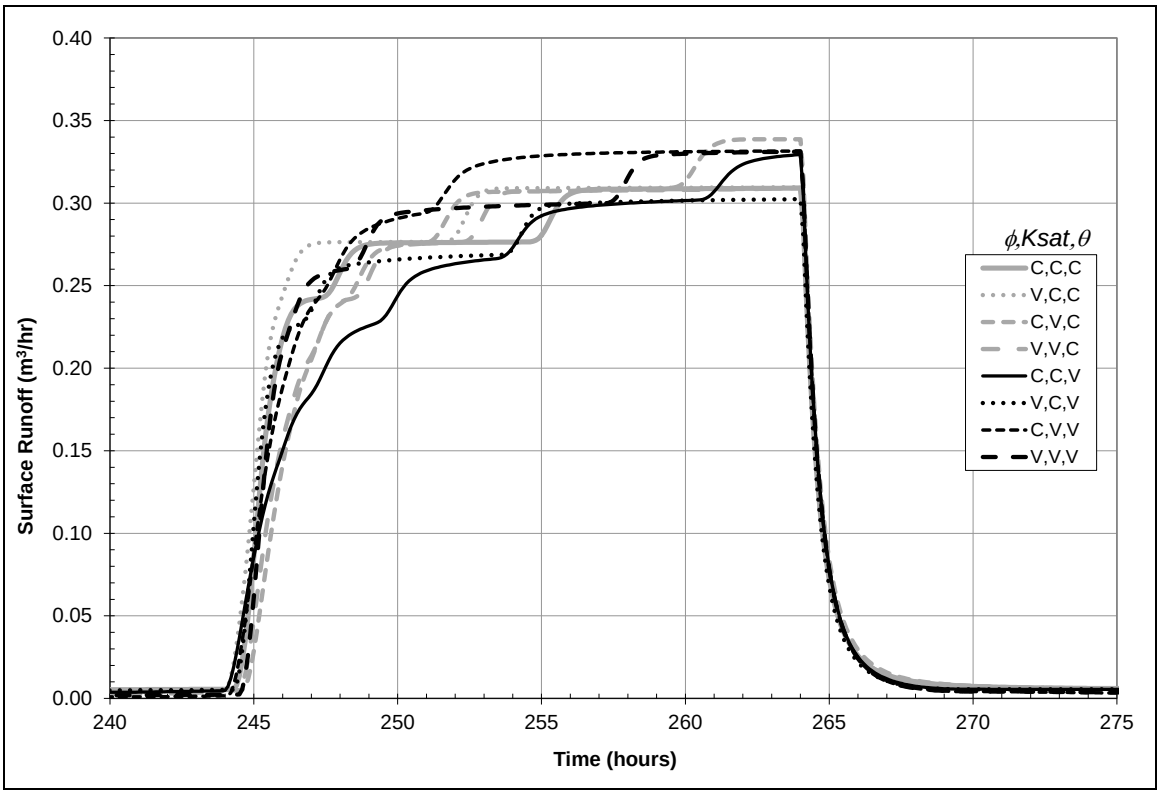

Figure 20: Surface runoff from straight hillslope during rainfall.

Peak runoff rates should be similar as almost all cells become saturated during rainfall, however the timing of saturation excess runoff production is highly variable. Figure 20 shows that the range of peak flow is from approximately 0.30-0.34 m^3/hr. The model outflow never reaches equilibrium with the rainfall so the peak occurs at 240 hours for all scenarios. The sharp drop off in runoff after rainfall ends indicates that direct precipitation onto saturated areas is the dominant component of this hillslope runoff model, with subsurface outflow producing much less. This is discussed in the following section.

It is difficult to isolate individual hydrographs for comparisons in Figure 20 due to the number of data sets. Therefore the following three sets of four figures are created to show the isolated effects on overall hillslope runoff due to changing the soil parameter profiles from constant to variable. Each graph compares the effects of changing only one soil parameter profile form and each set of four graphs shows that same comparison while using other secondary parameter scenarios.

Figure 21 through Figure 24 show the surface runoff from using constant vs. variable K_{sat} profile scenarios. In all four graphs runoff begins to rapidly increase at approximately the same time, with each constant K_{sat} scenarios starting slightly sooner than the relative variable K_{sat} scenario, especially when also using a constant θ profile. Peak runoff, at the end of rainfall is one step higher when using variable K_{sat} for two of the four graphs and approximately equal for the remaining two. One major step increase in outflow indicates that one additional cell is producing surface runoff. Figure 23 shows the most deviation with runoff from variable K_{sat} lagging throughout the hydrograph until the end of rainfall when the peak flows are almost identical. The timing of the stair-steps is different for all four figures.

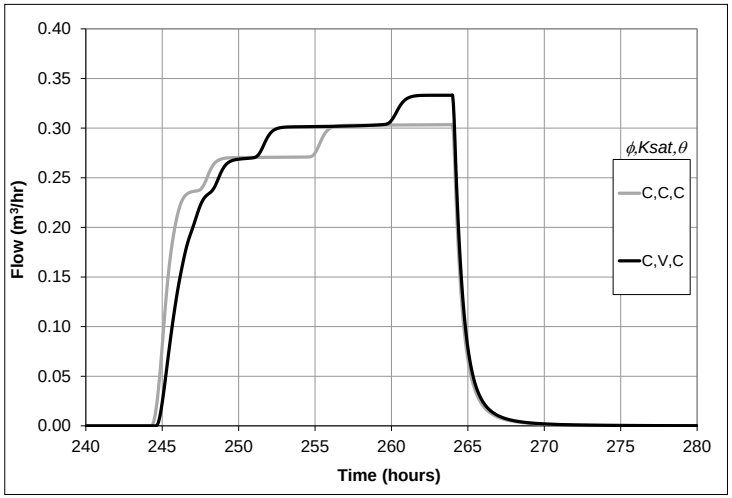

Figure 21: Straight hillslope surface runoff: changing K_{sat}, constant ϕ and θ.

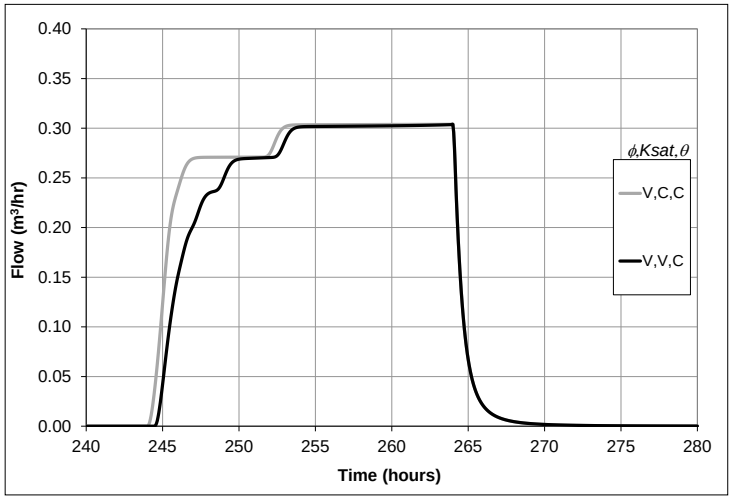

Figure 22: Straight hillslope surface runoff: changing K_{sat}, variable ϕ and constant θ.

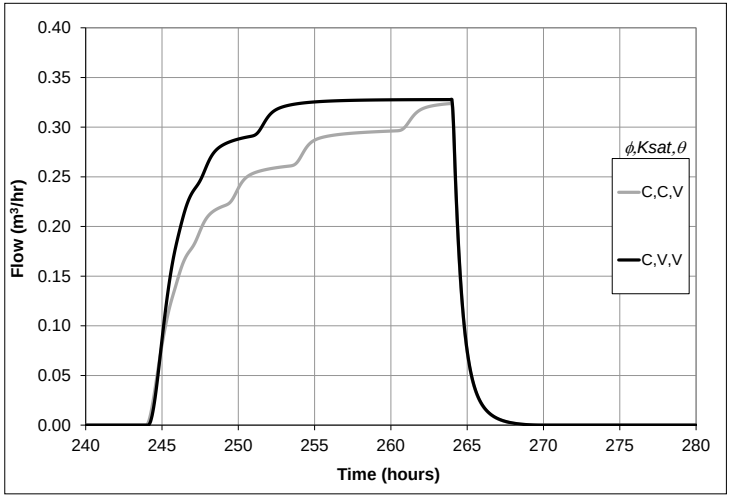

Figure 23: Straight hillslope surface runoff: changing K_{sat}, constant ϕ and variable θ.

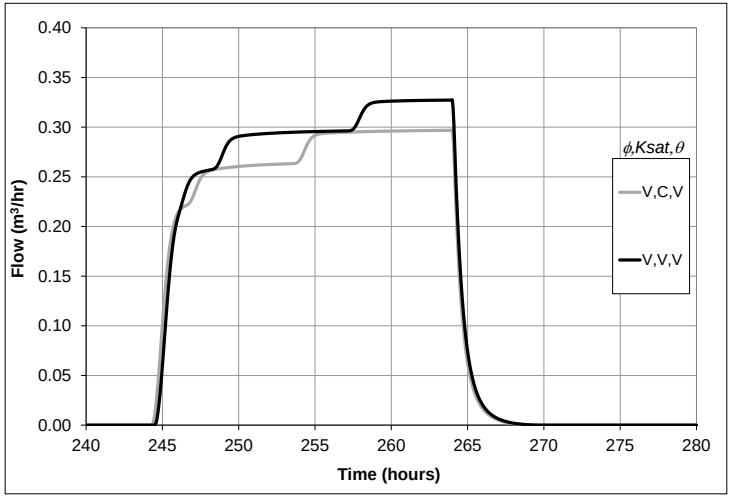

Figure 24: Straight hillslope surface runoff: changing K_{sat}, variable ϕ and θ.

The four figure grouping is repeated to analyze the effects of constant vs. variable ϕ as in Figure 25 through Figure 28. Each of the four figures has different K_{sat} and θ secondary variable profile combinations. There is no observable common trend differentiating the four constant ϕ from the variable ϕ hydrographs.

Among these four graphs, runoff begins to rapidly increase at approximately the same time, with the constant ϕ scenarios starting sooner when coupled with constant θ (Figure 25 and Figure 26) and starting slightly later when coupled with variable θ (Figure 27 and Figure 28). The hydrographs in the last three figures also each cross several times while the variable ϕ hydrograph is always slightly higher in Figure 25. Peak runoff is approximately equal for both ϕ profile scenarios in Figure 25 and Figure 28 and higher for the constant ϕ profile scenarios in Figure 26 and Figure 27. Most of the hydrographs are characterized with long almost constant flows as cells reach equilibrium with rainfall and uphill cells have not saturated yet except for the C,C,V scenario in Figure 27.

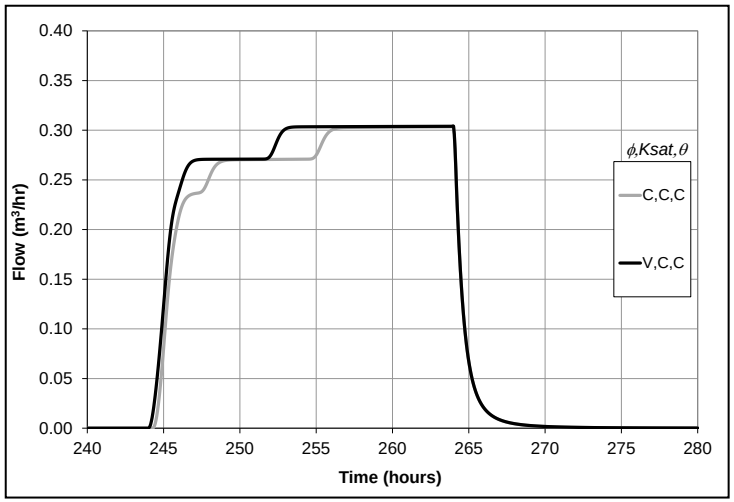

Figure 25: Straight hillslope surface runoff: changing ϕ, constant K_{sat} and θ.

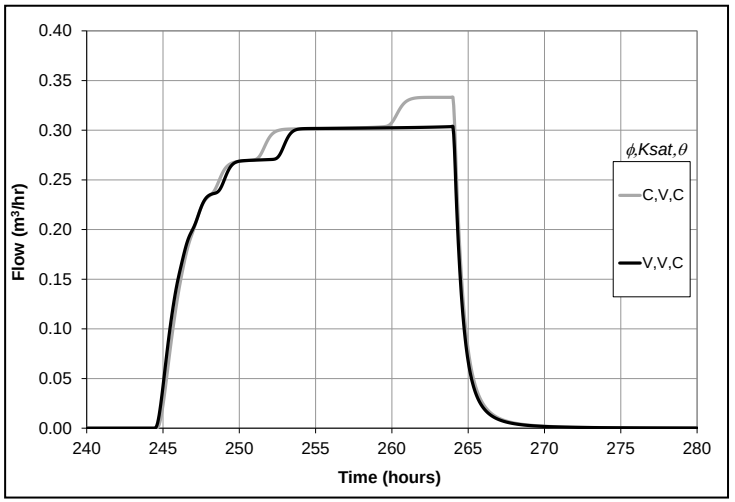

Figure 26: Straight hillslope surface runoff: changing ϕ, variable K_{sat}, and constant θ.

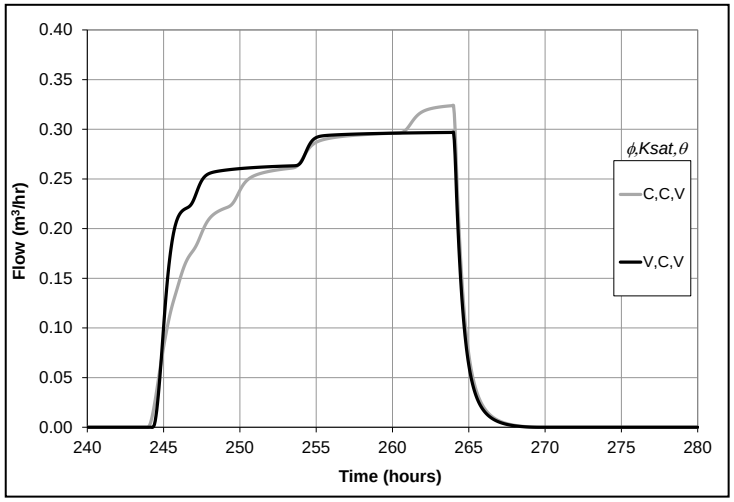

Figure 27: Straight hillslope surface runoff: changing ϕ, constant K_{sat} and variable θ.

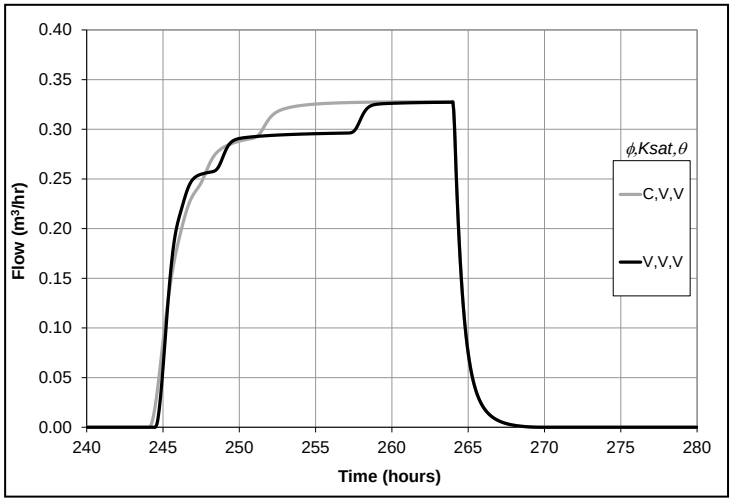

Figure 28: Straight hillslope surface runoff: changing ϕ, variable K_{sat} and θ.

67

Figure 29 through Figure 32 show the effects of constant vs. variable θ on runoff. Each of the four figures has different ϕ and K_{sat} secondary variable profile combinations. There is no observable common trend differentiating the four constant θ hydrographs from the variable θ hydrographs.

The rising limb starts to increase for the constant θ-variable ϕ scenarios in Figure 30 and Figure 32 slightly faster than the other two combinations. All hydrograph pairs cross at least once. The constant θ scenarios in Figure 30 and Figure 31 have slightly higher peaks than their variable θ counterparts. This slight increase is more pronounced here than for the other two hydrograph comparisons indicating that the differences in constant vs. variable θ has a slight effect on runoff when the same number of cells are saturated. The variable θ scenarios in Figure 29 and Figure 32 have higher peaks than their constant θ counterparts indicating that an additional cell is producing runoff.

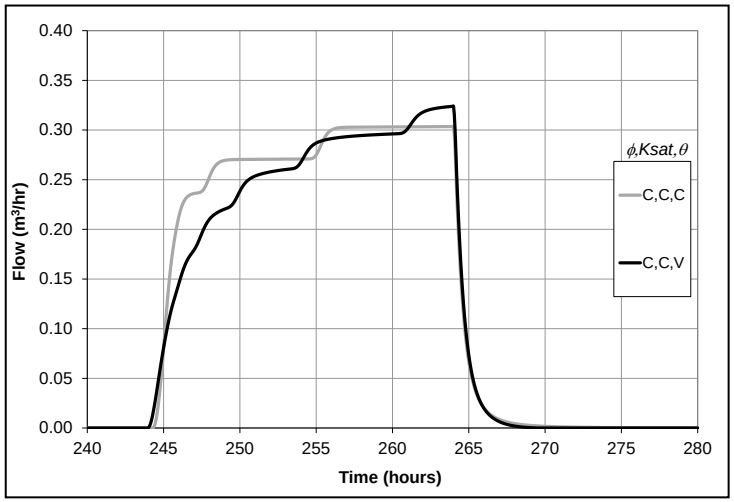

Figure 29: Straight hillslope surface runoff: changing θ, constant ϕ and K_{sat}.

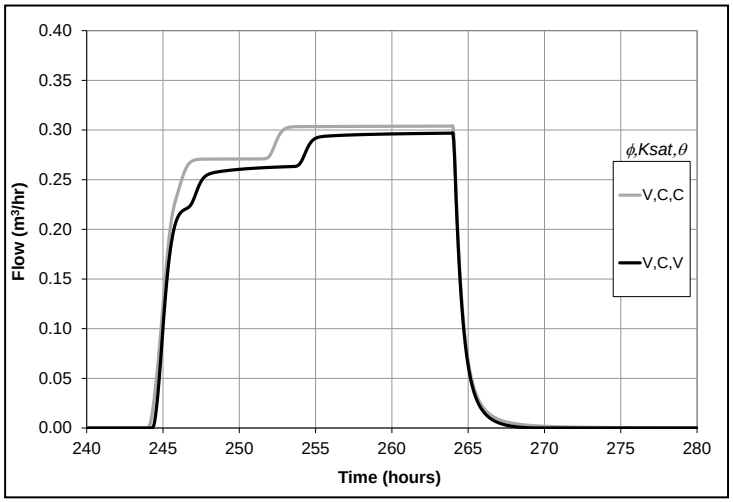

Figure 30: Straight hillslope surface runoff: changing θ, variable ϕ, constant K_{sat}.

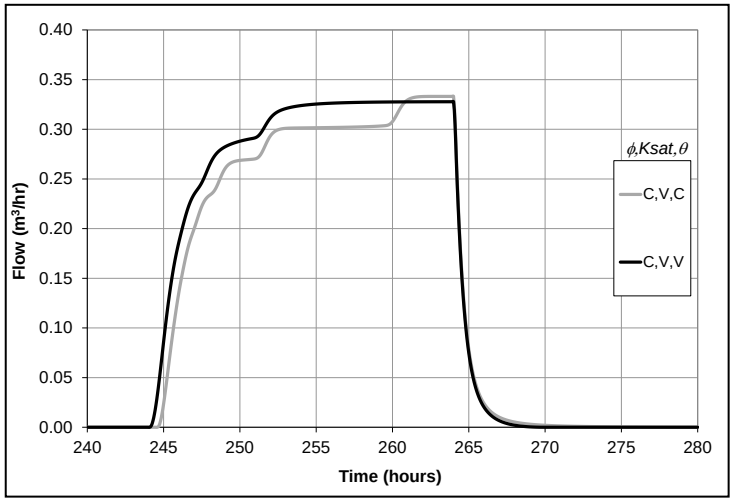

Figure 31: Straight hillslope surface runoff: changing θ, constant ϕ and variable K_{sat}.

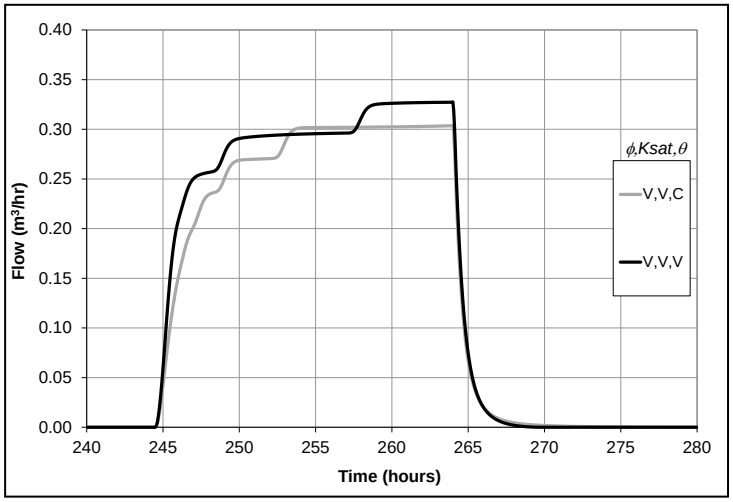

Figure 32: Straight hillslope surface runoff: changing θ, variable ϕ and K_{sat}.

69

Total Hillslope Discharge

The total discharge rate from the straight hillslope includes both surface runoff and groundwater flow out of Cell 10. The peak occurs at the end of rainfall (hour 264.0), coincident with the peak surface runoff time. Peak groundwater discharge out either occurs at that time or afterwards. Table 7 shows the total hillslope discharge and the percent of rainfall rate converted to 0.338667 m^3/hr. 100% equals equilibrium. Only the *C,V,C* scenario total discharge reaches equilibrium with the rainfall rate for the entire hillslope.

Table 7: Total hillslope discharge at end of rainfall for straight hillslope.

Scenario ϕ, K_{sat}, θ	**C,C,C**	**V,C,C**	**C,V,C**	**V,V,C**	**C,C,V**	**V,C,V**	**C,V,V**	**V,V,V**
Total Hillslope Discharge (m^3/hr)	0.309044	0.309529	0.338667	0.309235	0.329357	0.302332	0.331533	0.331146
Percent of Rainfall Rate	91.3%	91.4%	100.0%	91.3%	97.3%	89.3%	97.9%	97.8%

It was expected to be able to graphically represent the components of stormflow; direct precipitation runoff, return flow, and groundwater discharge out of cell 10 as in Dunne & Leopold (1978) Figure 9-1, however saturation overland flow from direct precipitation dominates the hydrograph so much that it is difficult to differentiate the groundwater flow out using a linear scale as they did. Figure 33 and Figure 34 are similar but with a log vertical axis for the *C,C,C* and *V,V,V* scenarios respectively. There is no return flow on the straight hillslope.

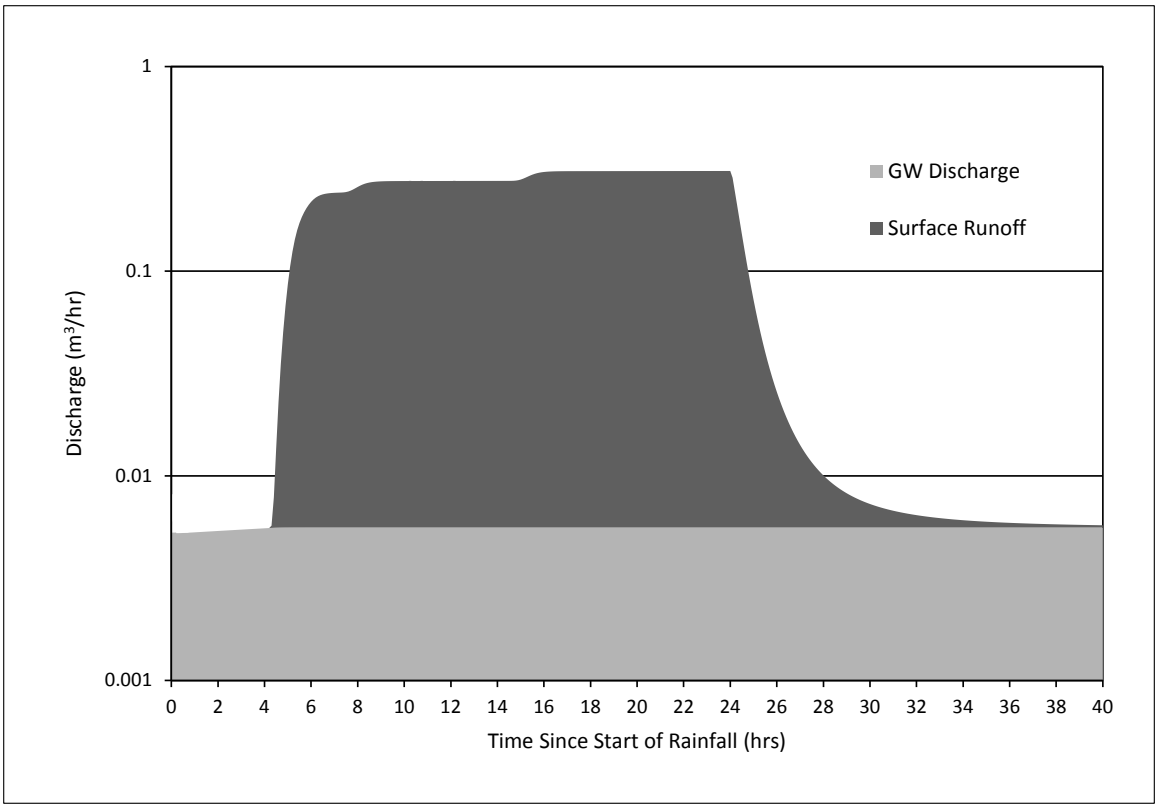

Figure 33: Stormflow components for the Straight Hillslope *C,C,C* Scenario.

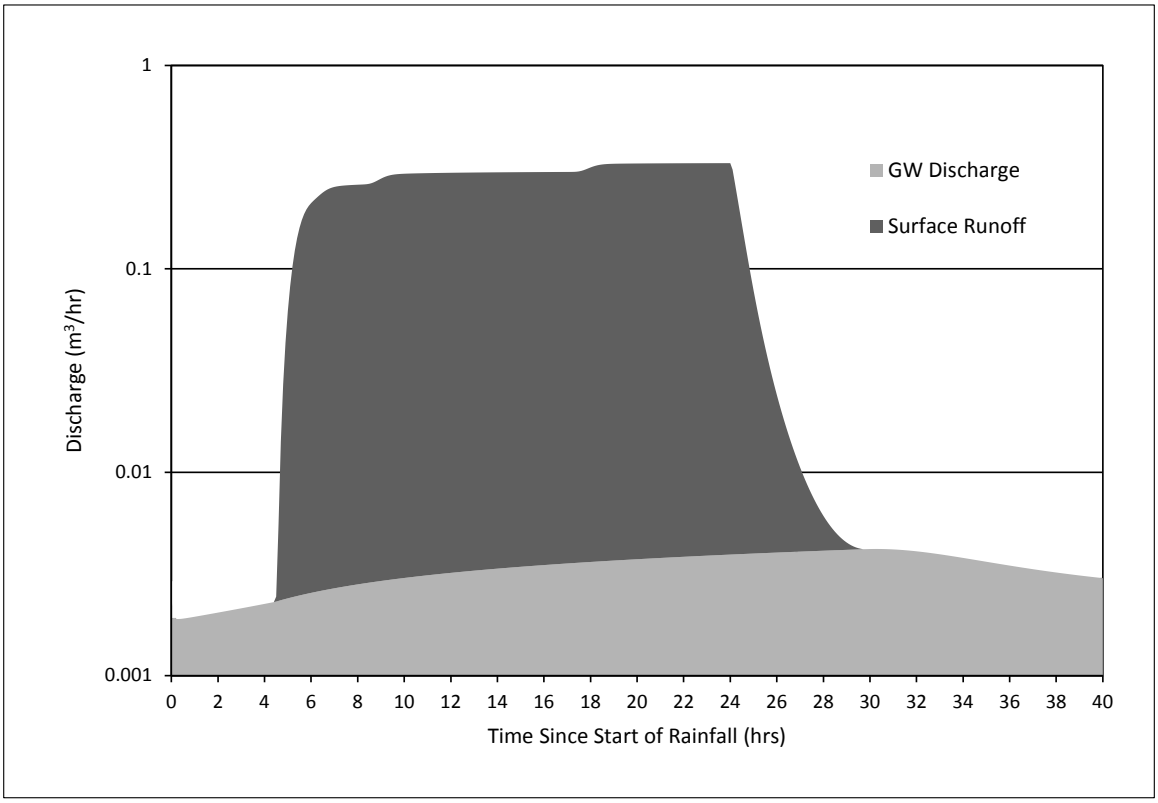

Figure 34: Stormflow components for the Straight Hillslope *V,V,V* Scenario.

Results for S-shaped Hillslope

The model is re-run using an S-shaped hillslope with the same eight scenarios previously described. Similar observations of the results are made.

Available Pore Space

Figure 35 shows that there are different amounts of hillslope average available pore space ($\overline{\phi_a}$) at the time of rainfall start among scenarios for the S-shaped hillslope

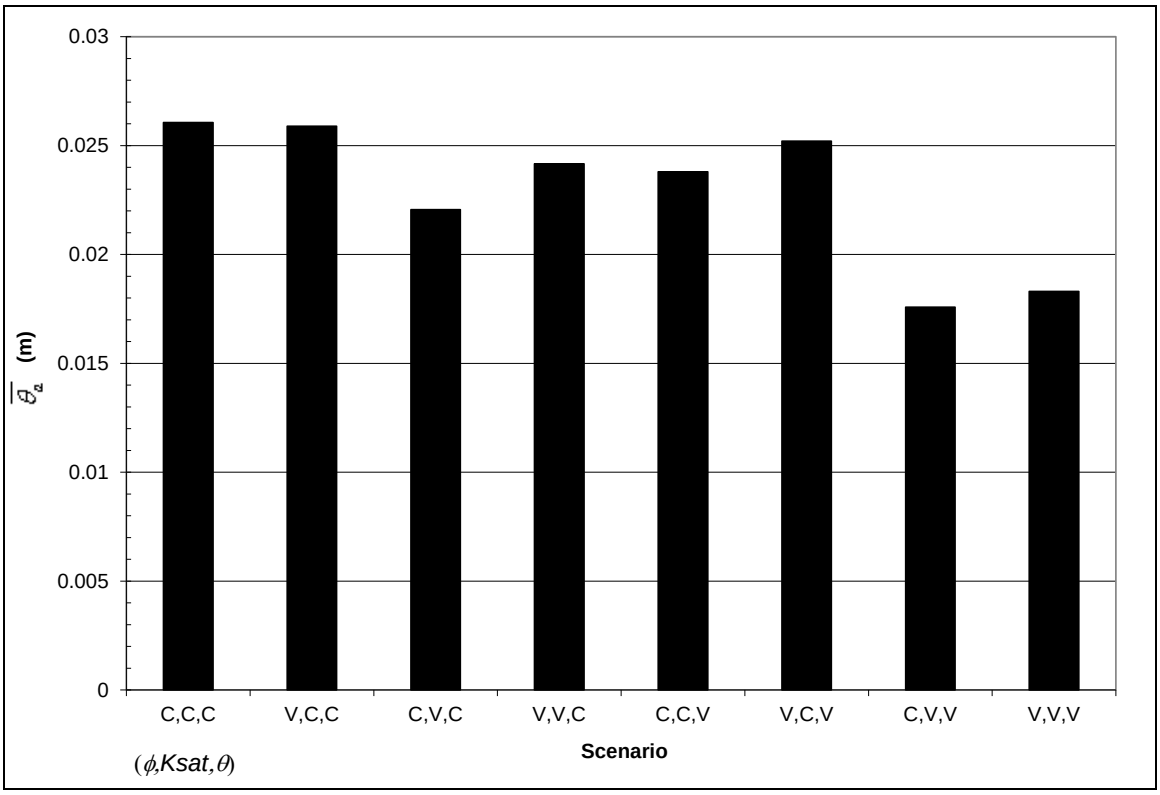

Figure 35: Average available pore space ($\overline{\phi_a}$) at rainfall start on S-shaped hillslope.

The overall mean of $\overline{\phi_a}$ among the scenarios (0.0229 m) is less than the total depth of rainfall that is applied in the analysis indicating that there may be saturation excess flow somewhere on the hillslope. The range of $\overline{\phi_a}$ among scenarios is about 0.0085 m, which is a 33% difference below the maximum value (0.0261 m). This large

range indicates that θ conditions at the start of rain application are likely to have effects on the timing and amount of runoff. There is less $\overline{\phi_a}$ for the variable K_{sat} and variable θ scenarios and more $\overline{\phi_a}$ for variable ϕ scenarios relative to each corresponding constant scenario. Changing K_{sat} seems to have most effect on $\overline{\phi_a}$ and changing ϕ has the least.

The distribution of available pore space (ϕ_a) at the rainfall start time shows a noticeable pattern in Figure 36. The plotted lines of ϕ_a all cross as the hillslope turns from convex to concave and the scenarios with the least ϕ_a in cell 1 have the most in cell 10. The reason for this crossing pattern thought to be the influence of hillslope shape effecting local water table cell-to-cell slopes and thus local drainage. Since the lower cells have less ϕ_a, they are expected to saturate earlier than the upper cells, assuming that rainfall is applied much faster than it can redistribute laterally in the soil.

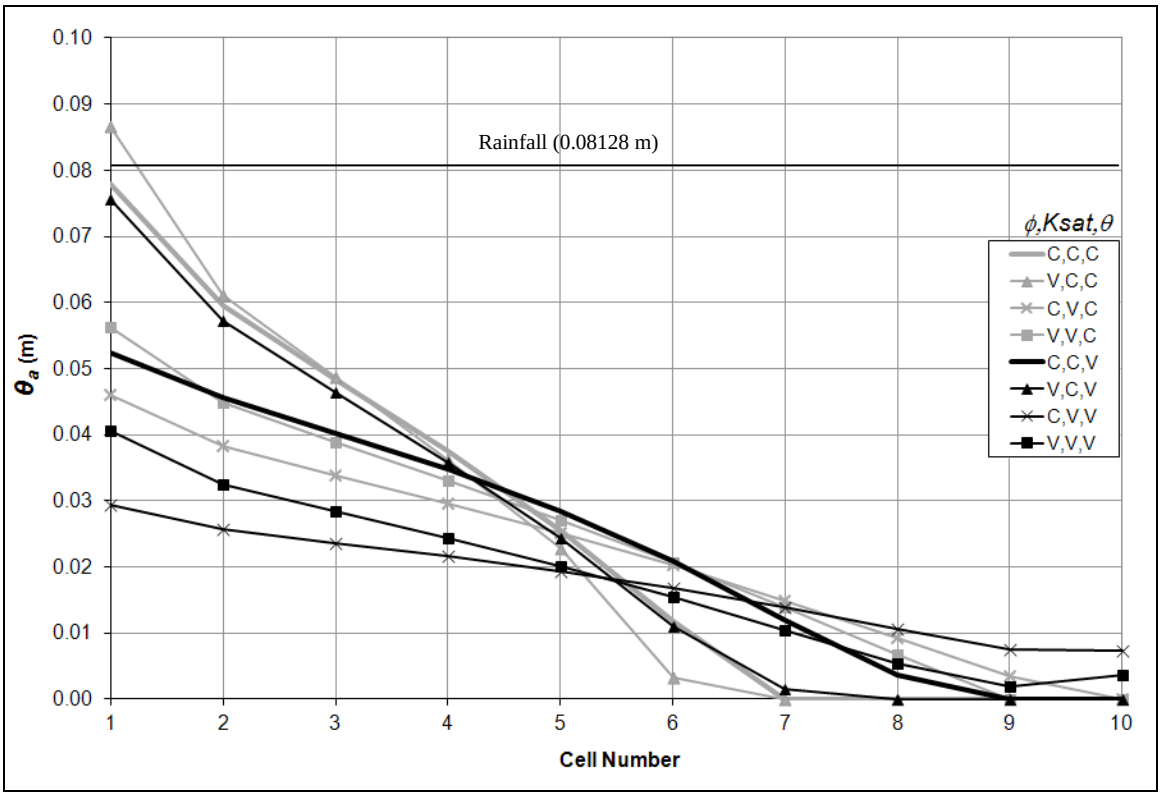

Figure 36: Available pore space (ϕ_a) distribution at rainfall start on S-shaped hillslope.

The same crossing pattern occurs among constant-variable pairs of different scenarios. The four constant K_{sat} scenarios have more ϕ_a in the upper portion of the hillslope and less than or equal amounts of ϕ_a in the lower portions of the hillslope than their corresponding variable K_{sat} scenarios. As before, the lower hillslope is expected to saturate earlier for the constant K_{sat} scenarios and the upper portion of the hillslope is expected to saturate earlier for the variable K_{sat} scenarios. For the four constant θ scenarios, ϕ_a is relatively higher on the upper hillslope cells and relatively lower or equal on the lower hillslope cells than their corresponding variable θ scenarios. For the four constant ϕ scenarios, ϕ_a is relatively lower on the upper hillslope cells and relatively higher or equal on the lower hillslope cells than their corresponding variable ϕ scenarios.

The two variable K_{sat}/variable θ scenarios have some ϕ_a in cell 10, unlike any other scenarios.

Figure 36 is useful for viewing overall patterns but it is difficult to interpret individual differences. Table 8 shows the absolute differences in ϕ_a between each pair of scenarios at the time of rainfall start for cell 1. Cell 1 was chosen because the range of ϕ_a values is the greatest, which will likely cause it to saturate last and control the overall peak surface runoff. The difference between any two scenarios can be found by selecting the column of one scenario and then reading down to the row of the corresponding scenario. Cells with dashes are left blank as they are a repeated inverse pattern of the filled in cells. The largest difference is observed between the *C,C,V* and *V,V,C* scenarios with the smallest difference between *C,V,C* and *V,V,V* scenarios.

Table 8: Relative differences in ϕ_a for cell 1 at rainfall start on S-shaped hillslope.

ϕ, $K_{sat,}$ θ	C,C,C	V,C,C	C,V,C	V,V,C	C,C,V	V,C,V	C,V,V	V,V,V
C,C,C	0.000	-	-	-	-	-	-	-
V,C,C	0.170	0.000	-	-	-	-	-	-
C,V,C	0.141	0.029	0.000	-	-	-	-	-
V,V,C	0.243	0.073	0.102	0.000	-	-	-	-
C,C,V	0.413	0.582	0.554	0.655	0.000	-	-	-
V,C,V	0.021	0.191	0.162	0.264	0.391	0.000	-	-
C,V,V	0.179	0.348	0.320	0.421	0.234	0.158	0.000	-
V,V,V	0.130	0.039	0.011	0.112	0.543	0.151	0.309	0.000

A summary of the average cell 1 ϕ_a differences from is shown in Table 9. This summary shows that among changing single parameter profiles, changing θ has the largest average effect and largest range of ϕ_a in cell 1, while changing $K_{sat,}$ has the least average effect and smallest range. Changing all three parameters has the greatest average effect while changing ϕ and θ together has the greatest range.

Table 9: Average cell 1 ϕ_a differences among scenarios at rainfall start on S-shaped hillslope.

Changed Profiles	Average Difference (m)	Min-Max of differences (m)	Range (m)
Porosity(ϕ)	0.243	0.102-0.391-	0.289
$K_{sat,}$	0.150	0.073-0.234-	0.161
Theta(θ)	0.259	0.112-0.413	0.301
$K_{sat,}$ & ϕ	0.243	0.029-0.543	0.514
ϕ- & θ	0.259	0.011-0.582	0.571
$K_{sat,}$& θ	0.259	0.039-0.554	0.515
All 3	0.324	0.130-0.655	0.525

Saturated Extents

Looking at ϕ_a when peak runoff occurs shows which cells are saturated and thus producing runoff from direct precipitation onto saturated areas. Results are shown in Table 10 as the range is too large to display minor differences in graphical format. This table shows a similar pattern as for the straight hillslope in that the constant θ scenarios are almost fully saturated except for cell 1. Among the variable θ scenarios only cell 1 in the *V,C,V* scenario is not saturated or essentially saturated.

Table 10: ϕ_a distribution (meters) at end of rainfall for S-shaped hillslope.

	Profile Scenario (ϕ, K_{sat}, θ) C = Constant, V = variable							
Cell	**C,C,C**	**V,C,C**	**C,V,C**	**V,V,C**	**C,C,V**	**V,C,V**	**C,V,V**	**V,V,V**
1	5.05E-03	1.47E-02	0	0	1.63E-04	2.55E-03	5.47E-05	1.10E-04
2	5.55E-17	0	0	0	1.08E-04	2.43E-04	4.79E-05	8.20E-05
3	0	0	0	0	8.39E-05	1.39E-04	4.48E-05	7.21E-05
4	0	0	0	0	6.66E-05	9.19E-05	4.20E-05	6.41E-05
5	0	0	0	0	5.27E-05	6.41E-05	3.93E-05	5.70E-05
6	0	0	0	0	4.13E-05	4.57E-05	3.66E-05	5.06E-05
7	0	0	0	0	6.76E-06	6.76E-06	3.39E-05	4.51E-05
8	0	0	0	0	6.76E-06	0	6.76E-06	6.76E-06
9	0	0	0	0	0	0	6.76E-06	6.76E-06
10	0	0	0	0	0	0	6.76E-06	6.76E-06

Subsurface Outflow and Return Flow

During the 240 hours of drainage for the 'hot-start' on the S-shaped hillslope, only two scenarios exhibit unique subsurface outflow patterns out of cell 10 as seen in

Figure 37. The variable K_{sat}-variable θ profile scenarios (*C,V,V* & *V,V,V*) both show a decrease in flow over time, with the variable ϕ profile having less flow at the end of drainage. The maximum subsurface outflow is 0.0023 m^3/hr, when cell 9 & 10 are both saturated. The remaining six scenarios show a constant subsurface outflow, indicating that they will have less storage at the start of rainfall than the *C,V,V* and *V,V,V,* scenarios as confirmed in $\overline{\phi_a}$ previous results.

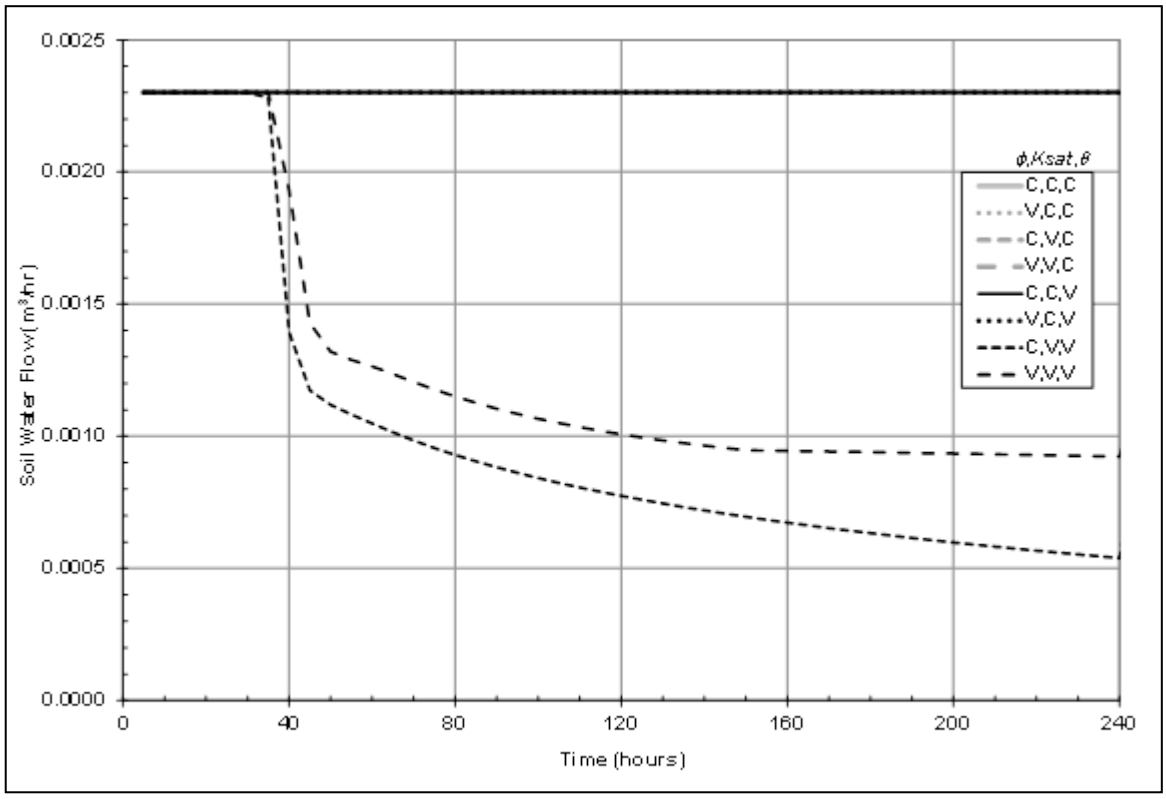

Figure 37: S-shaped hillslope subsurface outflow during drainage from saturation.

Lateral subsurface stormflow out of cell 10 is shown in Figure 38 for the wetting period during the applied rainfall. It is approximately two orders of magnitude less than peak surface runoff on the S-shaped hillslope. Only scenarios *C,V,V, and V,V,V* show any variance in subsurface outflow during rainfall as cell 10 in the other six scenarios remains saturated. The difference in subsurface hydrograph peaks appears to be mostly

associated with the starting conditions but the constant ϕ scenario *C,V,V* does peak about five hours before the variable ϕ scenario *V,V,V* and has made up most of the difference from the conditions at the start of rainfall. After rainfall stops, drainage continues in a similar manner as before.

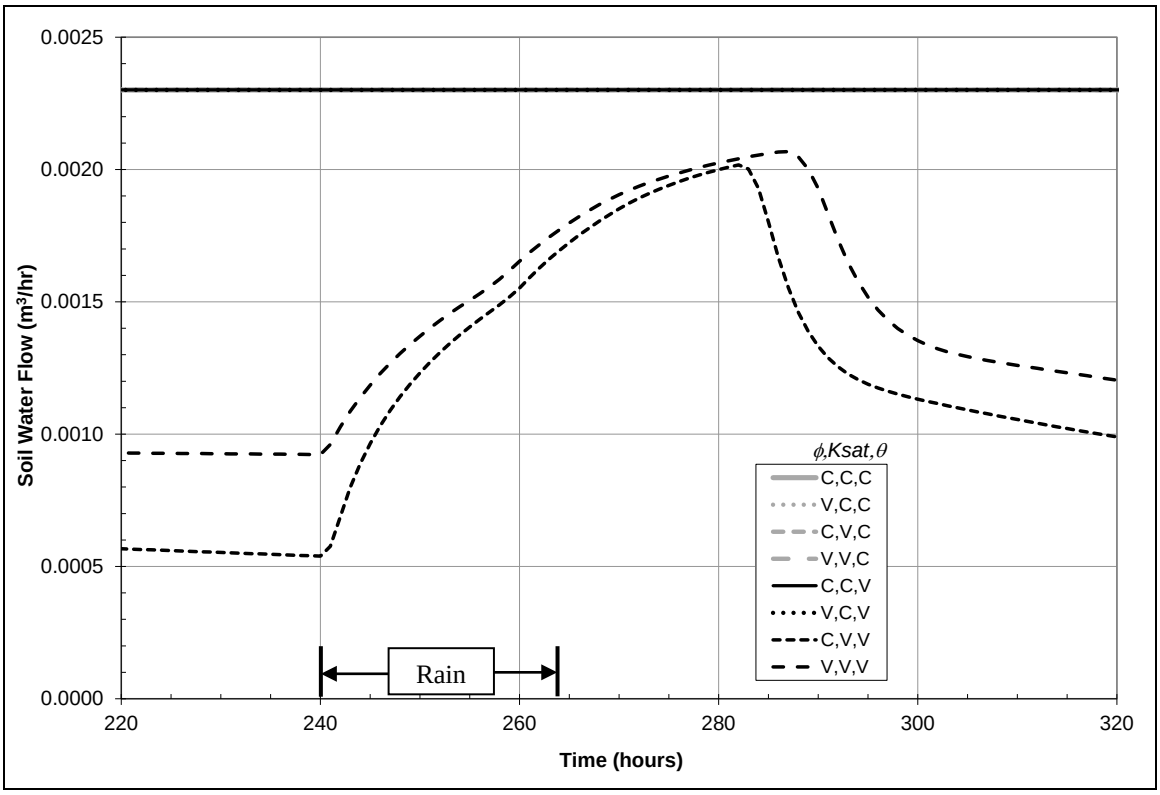

Figure 38: S-shaped hillslope subsurface outflow from cell 10 during rainfall.

Return Flow

Return flow (or exfiltration) occurs on the S-shaped hillslope due to increasingly smaller water table slopes from the concave portion of the hillslope from cell 6 to cell 10. This causes greater subsurface flow from the steeper cells to return to the surface when there is no room for it in the downhill cells. Cells 1-5 does not have return flow due to the increase in slope of each downhill cell allowing more sub-surface flow to leave than enter.

Figure 39 shows a variance in the return flow hydrographs during drainage. Return flow adds to surface runoff, but is about three orders of magnitude less than runoff from direct precipitation and four times less than soil water flow out of cell 10 at saturation. Return flow from variable θ scenarios is consistently lower than the corresponding constant θ scenarios. Return flow from variable ϕ scenarios is higher than the corresponding constant ϕ scenarios. Return flow in the four variable K_{sat} scenarios is lower than in the constant K_{sat} scenarios.

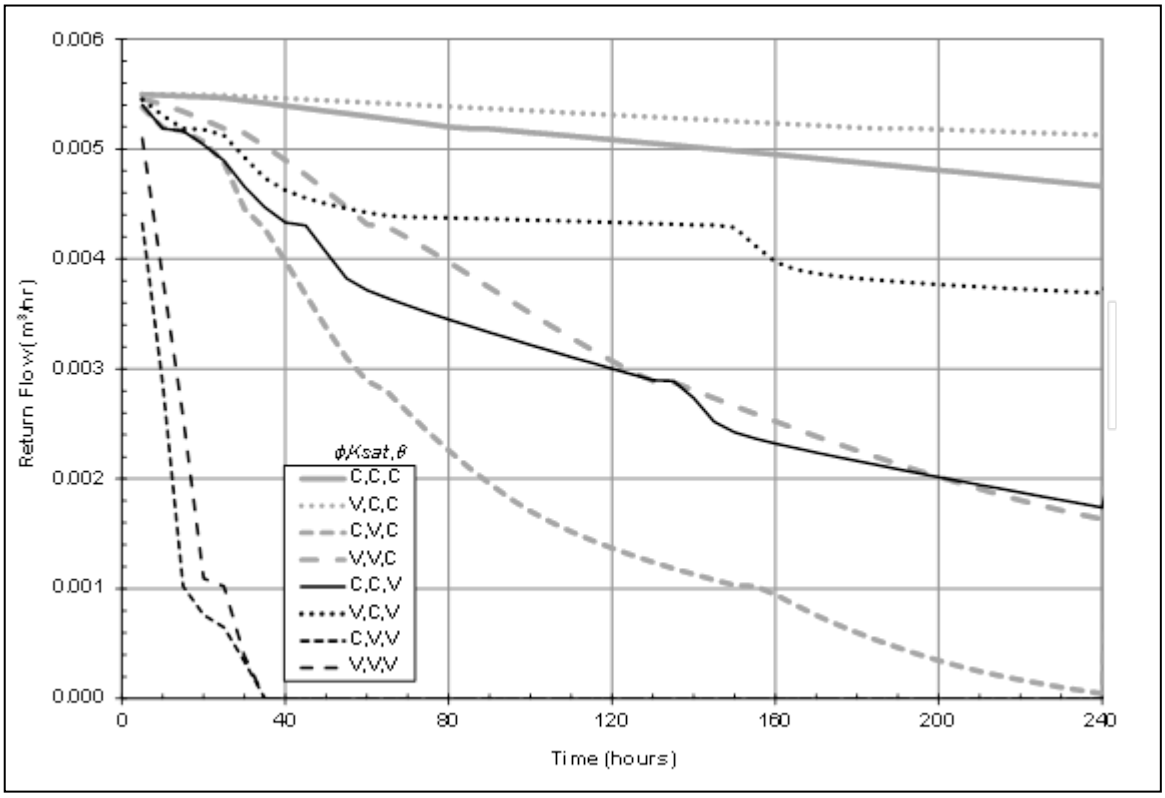

Figure 39: S-shaped hillslope return flow during drainage.

Figure 40 shows similar groupings of return flow behavior during rainfall. All four constant θ scenarios reach a steady state, indicating that cells 6-10 are all saturated during drainage, while the variable θ scenarios each have a different level of saturation.

Among variable θ scenarios, there is more within-storm return flow for the variable ϕ scenarios and constant K_{sat} scenarios.

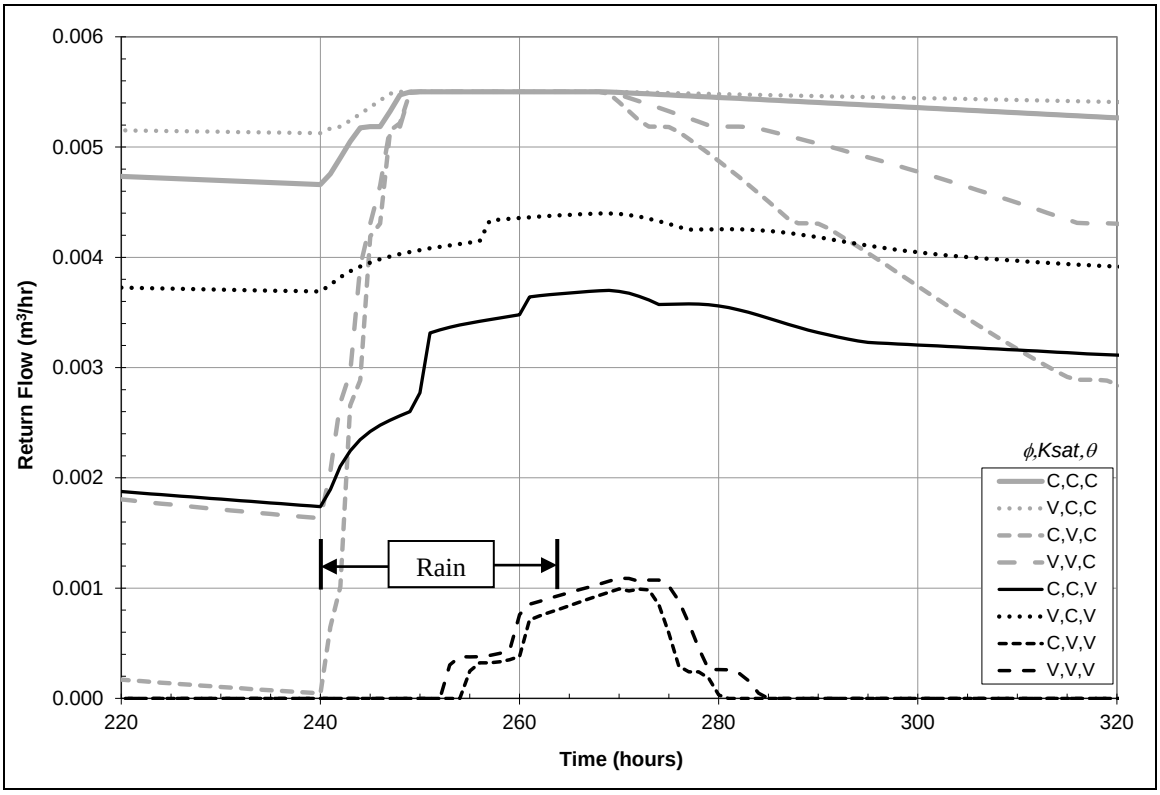

Figure 40: S-shaped hillslope return flow during rainfall.

Surface Runoff

The total cumulative surface runoff that occurs during rainfall is summarized in Figure 41. There is a difference of about 12% between the maximum and minimum across all scenarios, similar to the straight hillslope. There is no clear correlation between changing any of the three soil variables and more or less total surface runoff. The difference could be in either direction.

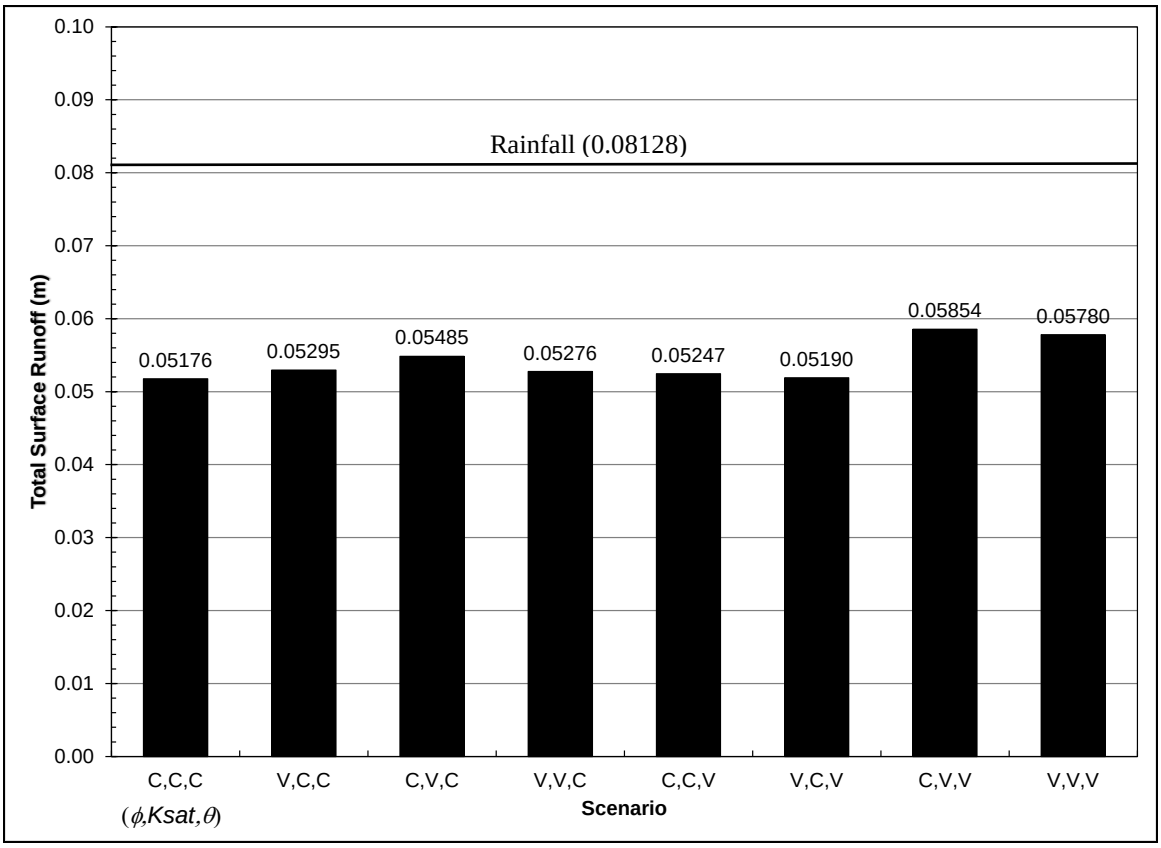

Figure 41: Total surface runoff (meters) for S-shaped hillslope.

A significant amount of surface runoff continues to accumulate after rainfall ends, between about 4% to 26% of the surface runoff total at hour 480. Figure 42 shows that surface runoff continues until hour 480, when the model ends, except for in two scenarios. For the *C,V,V* and *V,V,V* scenarios, it stops at hour 282.0 (18 hours after rainfall ends) and hour 286.4 (about 22 hours after rainfall ends) respectively. Most of this runoff is from return flow. The totals in this figure do not include surface from the run-in period prior to the start of rainfall.

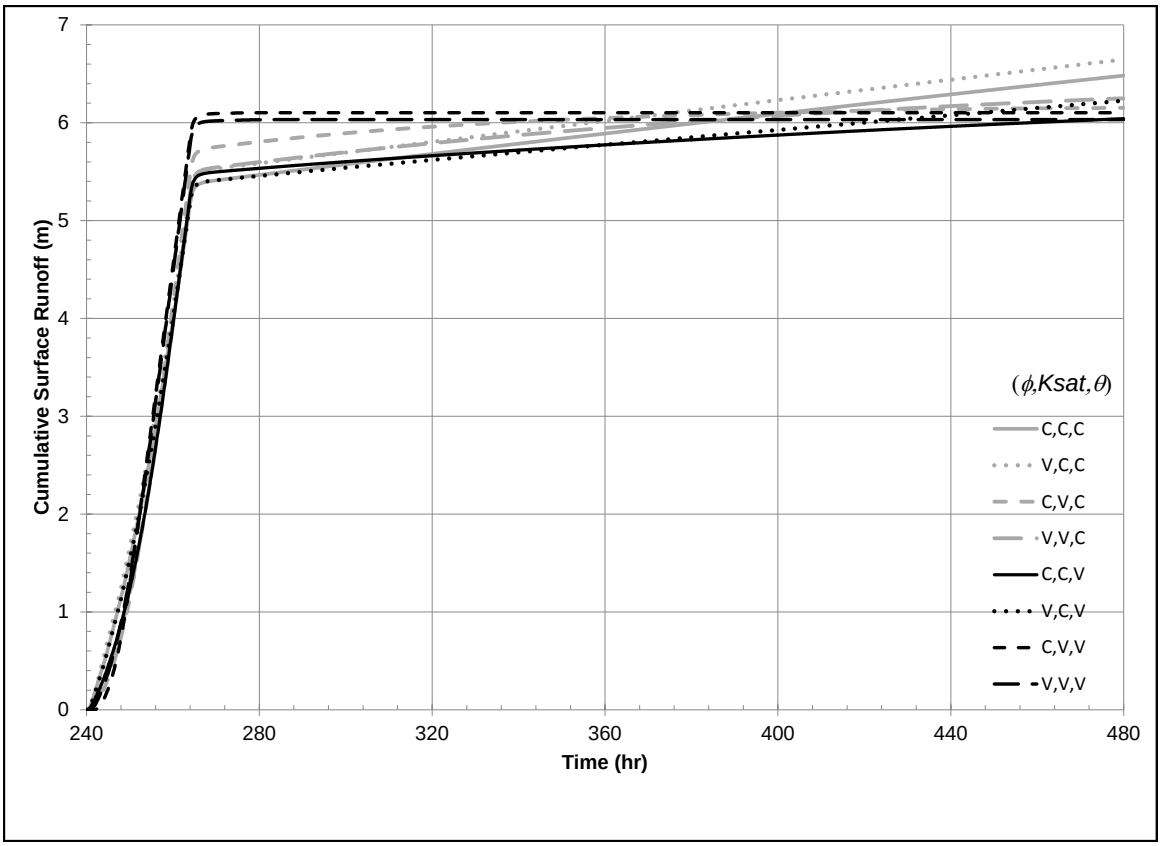

Figure 42: Surface runoff accumulation from the S-shaped hillslope.

Surface runoff hydrographs from the S-shaped hillslope are shown in Figure 43. The hydrographs exhibit a crossing pattern with the scenarios producing the most runoff early on reaching their peaks later, and the ones producing runoff the latest having steeper hydrograph slopes. The reasons for this crossing pattern may be related to the distribution of available pore space (ϕ_a) throughout the hillslope for each scenario. For cells with low initial ϕ_a, runoff increases rapidly as cells saturate as opposed to cells that have greater initial ϕ_a and thus more water holding capacity.

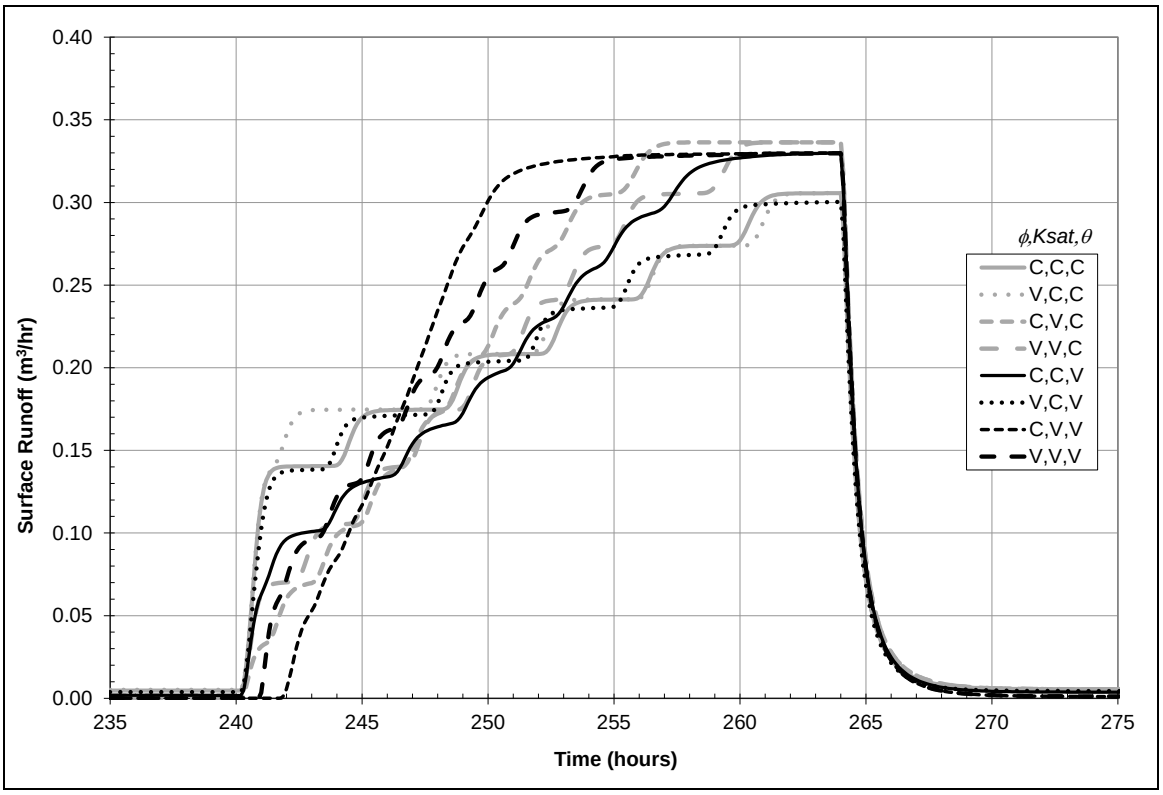

Figure 43: Surface runoff from S-shaped hillslope.

Runoff from individual parameter profile changes are shown as three sets of four figures for the purpose of isolating the effects of each parameter change. The first set (Figure 44 through Figure 47) shows the effects of changing the K_{sat} profile from constant to variable for each combination of secondary parameters. All four figures show a distinct crossing pattern where the variable K_{sat} profile hydrographs rise slower at the start of rainfall, but approach their peak flow quicker than the constant K_{sat} hydrographs. This is the expected result based on observations of the θ_a distribution at the beginning of rainfall as previously discussed.

Actual runoff peaks occur at the end of rainfall but are preceded by long flat or near-flat portions that occur when runoff producing cells are approaching equilibrium with the rainfall rate. True equilibrium is only reached in two of the scenarios (*C,V,C* &

V,V,C). All ten cells are producing runoff in all of the variable K_{sat} profiles but only in one constant K_{sat} profile (*C,V,V* in Figure 46). This causes a distinctly larger peak between hydrograph pairs in all figures except Figure 46, where there is a small increase in runoff for the constant K_{sat} profile hydrograph.

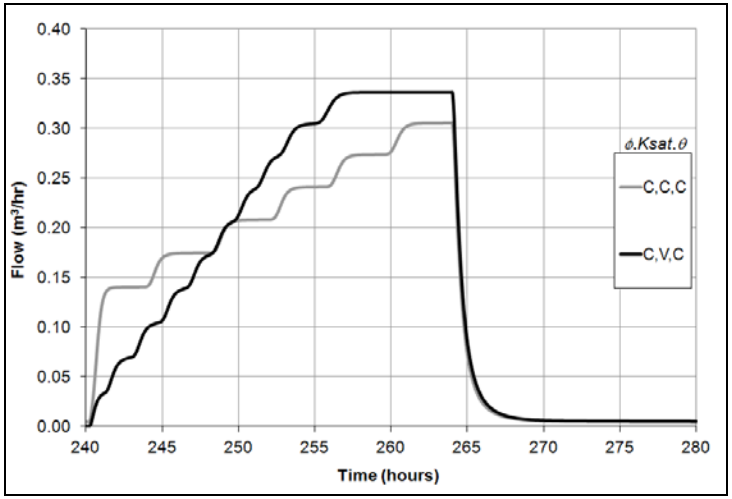

Figure 44: S-shaped hillslope surface runoff: changing K_{sat}, constant ϕ and θ.

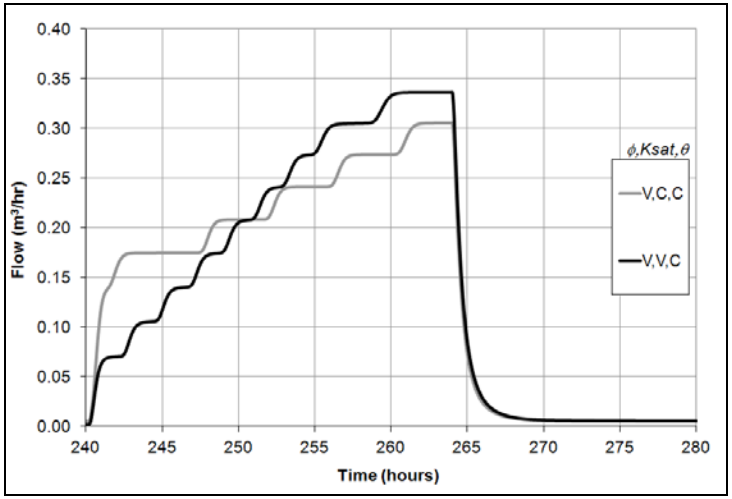

Figure 45: S-shaped hillslope surface runoff: changing K_{sat}, variable ϕ, constant θ.

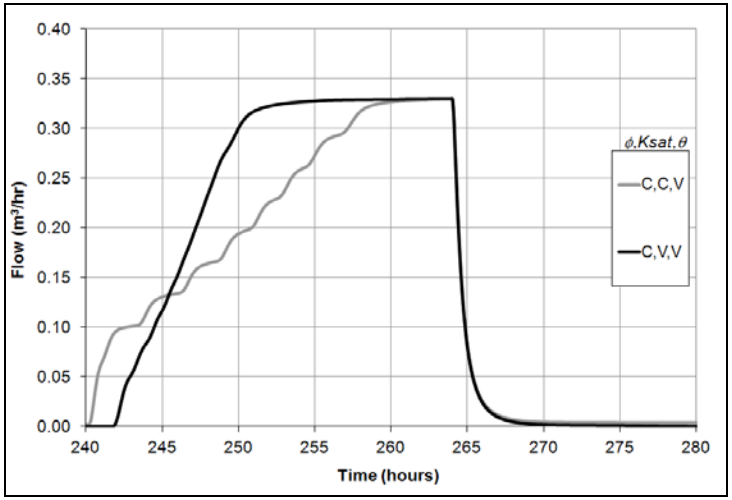

Figure 46: S-shaped hillslope surface runoff: changing K_{sat}, constant ϕ, variable θ.

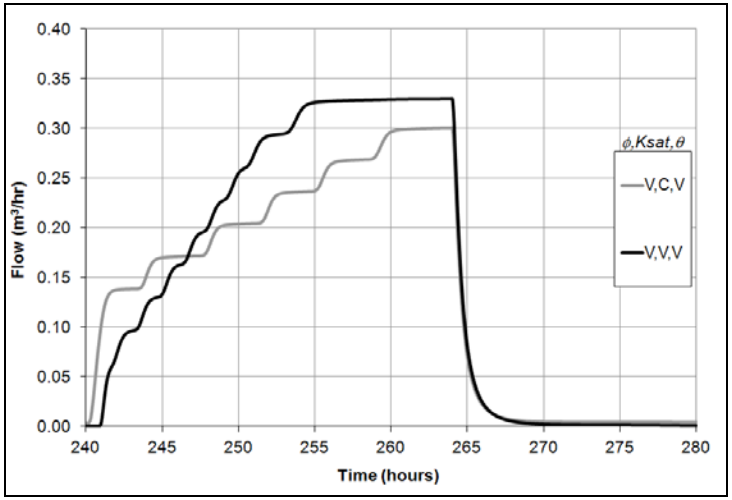

Figure 47: S-shaped hillslope surface runoff: changing K_{sat}, variable ϕ and θ.

Figure 48 through Figure 51 show the effects of using constant vs. variable ϕ profiles. Each of the four figures has different K_{sat} and θ secondary variable profile combinations. Similar to K_{sat}, all the ϕ profile hydrograph pairs exhibit a crossing pattern but it is the constant ϕ profiles that begin to produce runoff slowly at first and then begin to approach equilibrium earlier than their variable ϕ counterparts. The effect is much less pronounced than the previous K_{sat} profile comparisons with all peaks except in Figure 50 being similar in magnitude.

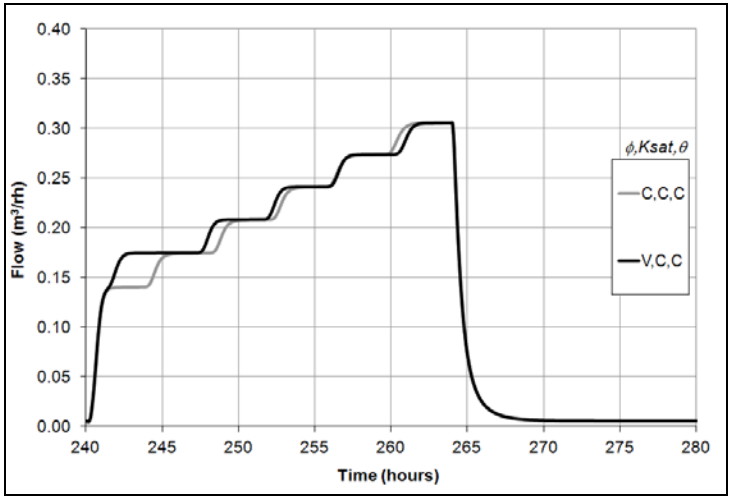

Figure 48: S-shaped hillslope surface runoff: changing ϕ, constant K_{sat} and θ.

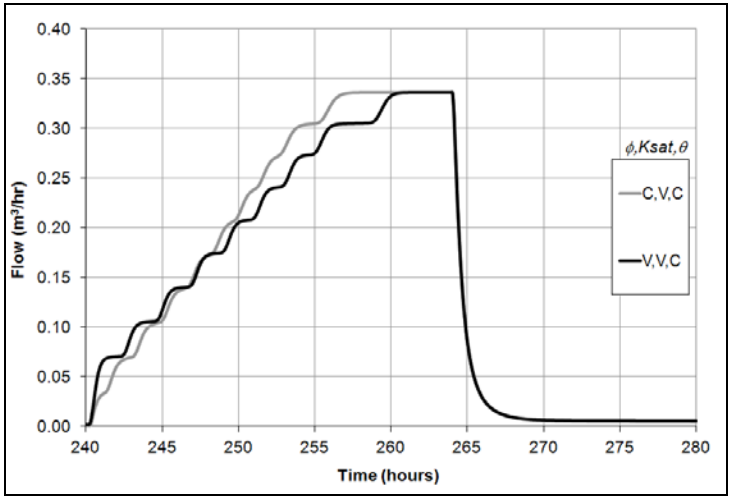

Figure 49: S-shaped hillslope surface runoff: changing ϕ, variable K_{sat}, constant θ.

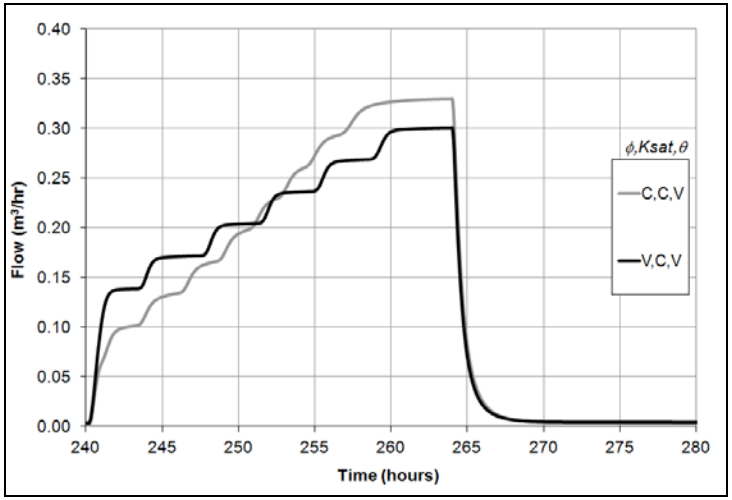

Figure 50: S-shaped hillslope surface runoff: changing ϕ, constant K_{sat}, variable θ.

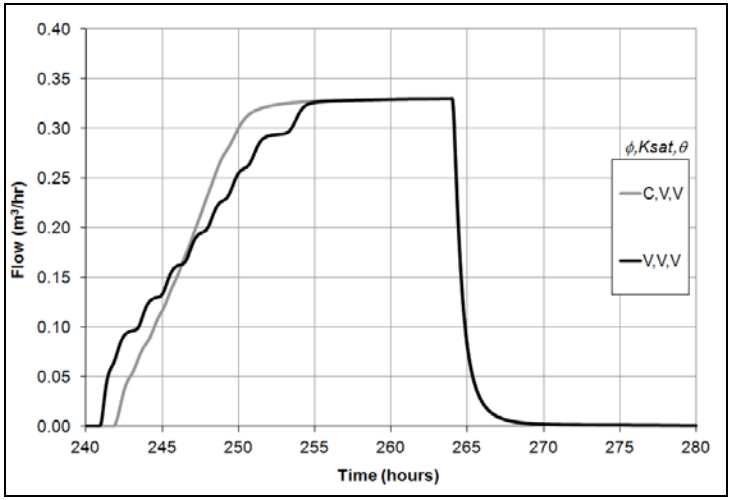

Figure 51: S-shaped hillslope surface runoff: changing ϕ, variable K_{sat}, and θ.

87

Figure 52 through Figure 55 show the effects of constant vs. variable θ scenarios on runoff. Each of the four figures has different ϕ and K_{sat} secondary profile combinations. Similar to the K_{sat} graphs, all of the hydrograph pairs cross, with the variable θ hydrographs starting off slower but approaching equilibrium much faster than the corresponding constant θ hydrographs. Hydrograph peaks are approximately equal in all pairs except Figure 52, where an additional cell is producing runoff for the variable θ scenario. For the remaining figures, the constant θ scenarios produce a slightly higher amount of runoff than their corresponding variable θ scenarios. This may be related to the sub-surface water behavior previously discussed where additional subsurface outflow for the variable θ scenarios will reduce the amount of runoff from direct precipitation at equilibrium.

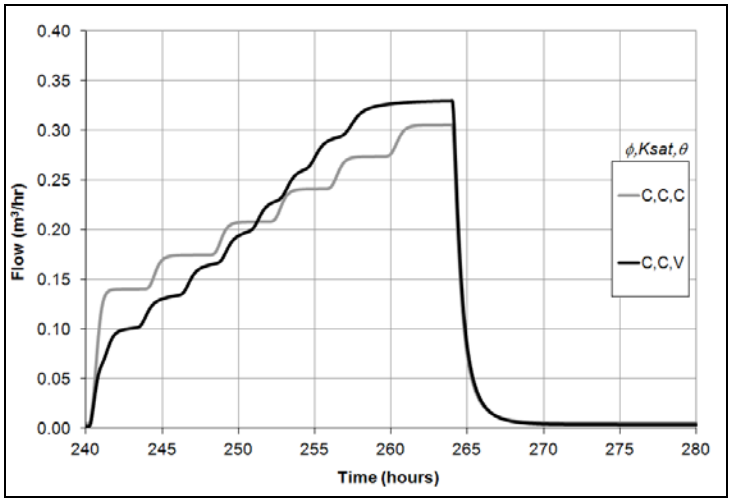

Figure 52: S-shaped hillslope surface runoff: changing θ, constant ϕ and K_{sat}.

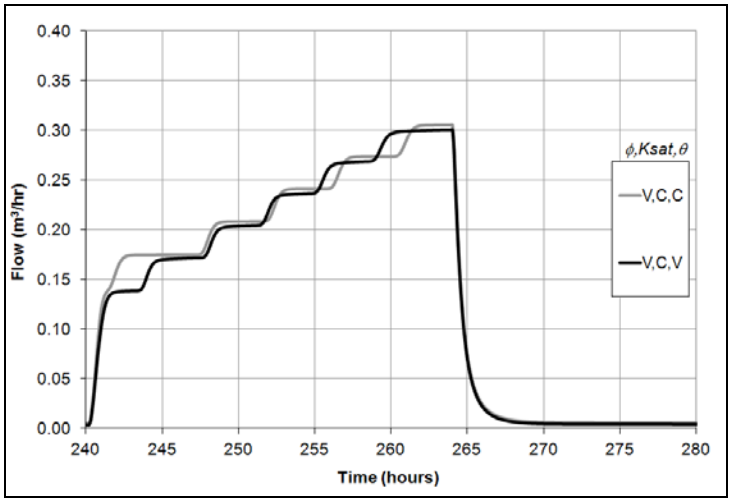

Figure 53: S-shaped hillslope surface runoff: changing θ, variable ϕ, constant K_{sat}.

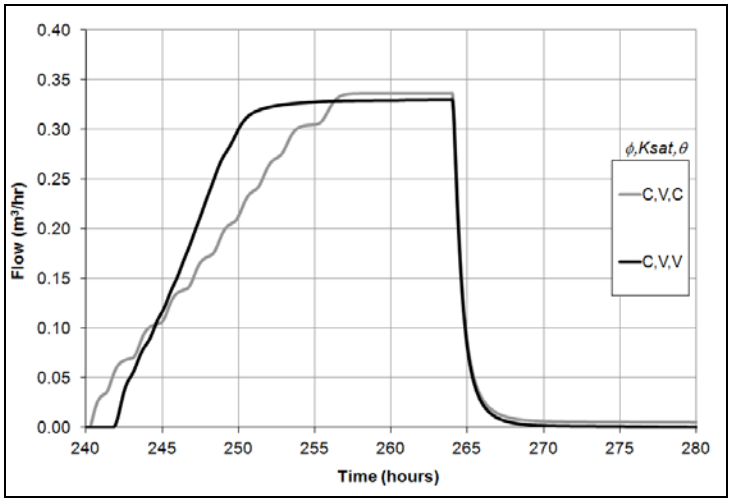

Figure 54: S-shaped hillslope surface runoff: changing θ, constant ϕ, and variable K_{sat}.

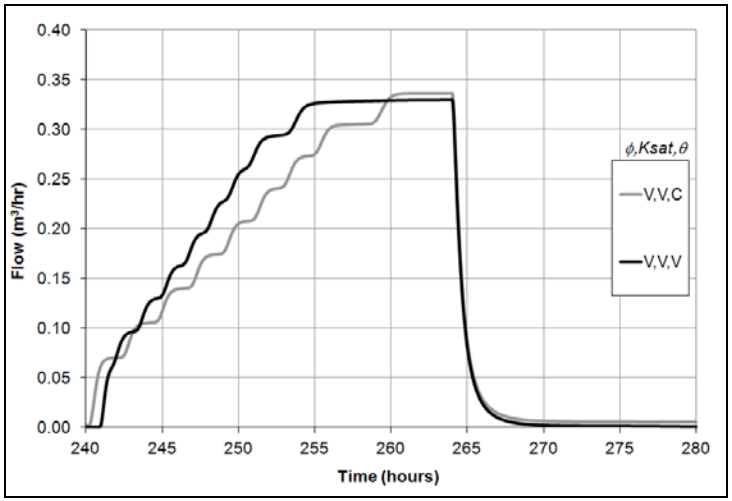

Figure 55: S-shaped hillslope surface runoff: changing θ, variable ϕ, and K_{sat}.

89

Total Hillslope Discharge

The total discharge rate from the S-shaped hillslope includes both surface runoff and groundwater flow out of Cell 10. The peak occurs at the end of rainfall (hour 264.0), coincident with the peak surface runoff time. Peak groundwater discharge out occurs either at that time or afterwards. Table 11 shows the total hillslope discharge and the percent of rainfall rate converted to 0.338667 m^3/hr. 100% equals equilibrium. Total runoff for the *C,V,C* and *V,V,C* scenarios reach equilibrium with the rainfall rate for the entire hillslope.

Table 11: Total hillslope discharge at end of rainfall for S-shaped hillslope.

Scenario (ϕ, K_{sat}, θ)	**C,C,C**	**V,C,C**	**C,V,C**	**V,V,C**	**C,C,V**	**V,C,V**	**C,V,V**	**V,V,V**
Total Hillslope Discharge (m^3/hr)	0.307924	0.307956	0.338667	0.338667	0.332267	0.302669	0.331634	0.331436
Percent of Rainfall Rate	90.9%	90.9%	100.0%	100.0%	98.1%	89.4%	97.9%	97.9%

Figure 58 and Figure 57 show the stormflow runoff components; direct precipitation runoff, return flow, and groundwater discharge out of cell 10 for the *C,C,C* and *V,V,V* scenarios respectively. The runoff from direct precipitation is approximate and measured by subtracting return flow from total surface runoff. These two figures show that the runoff components are highly variable among scenarios.

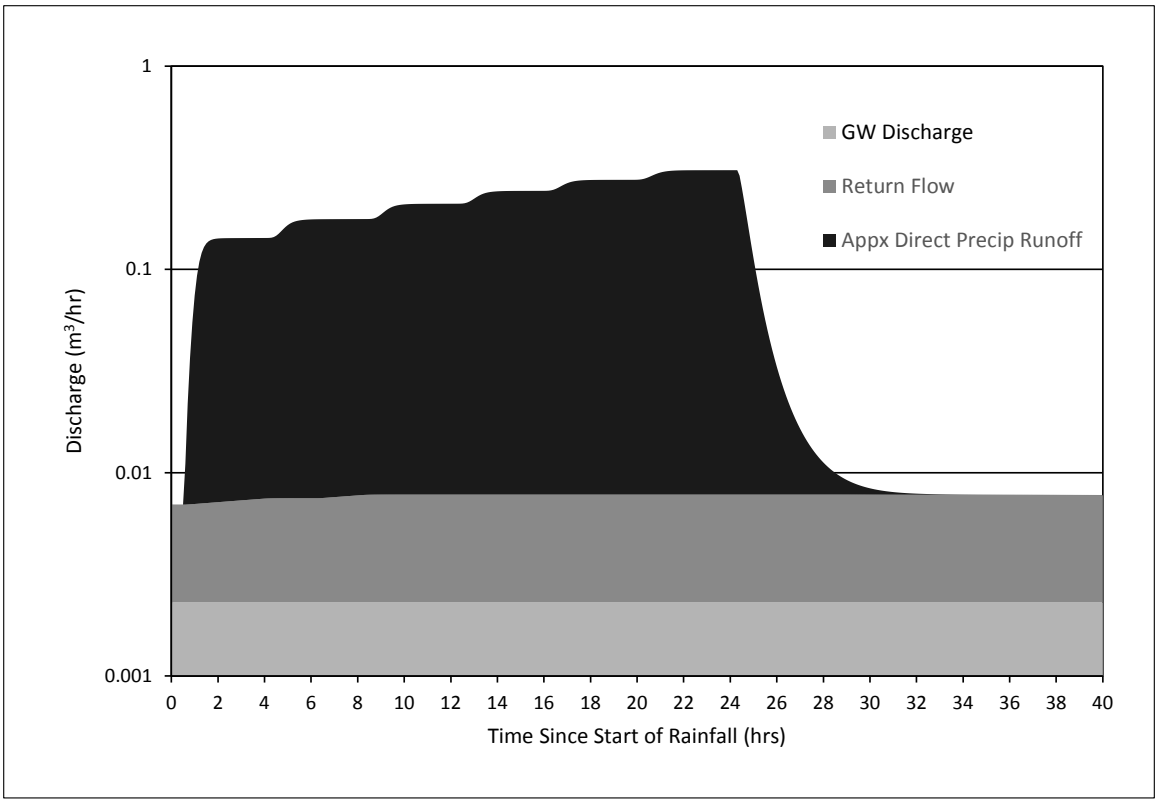

Figure 56: Stormflow components for the S-shaped Hillslope *C,C,C* Scenario.

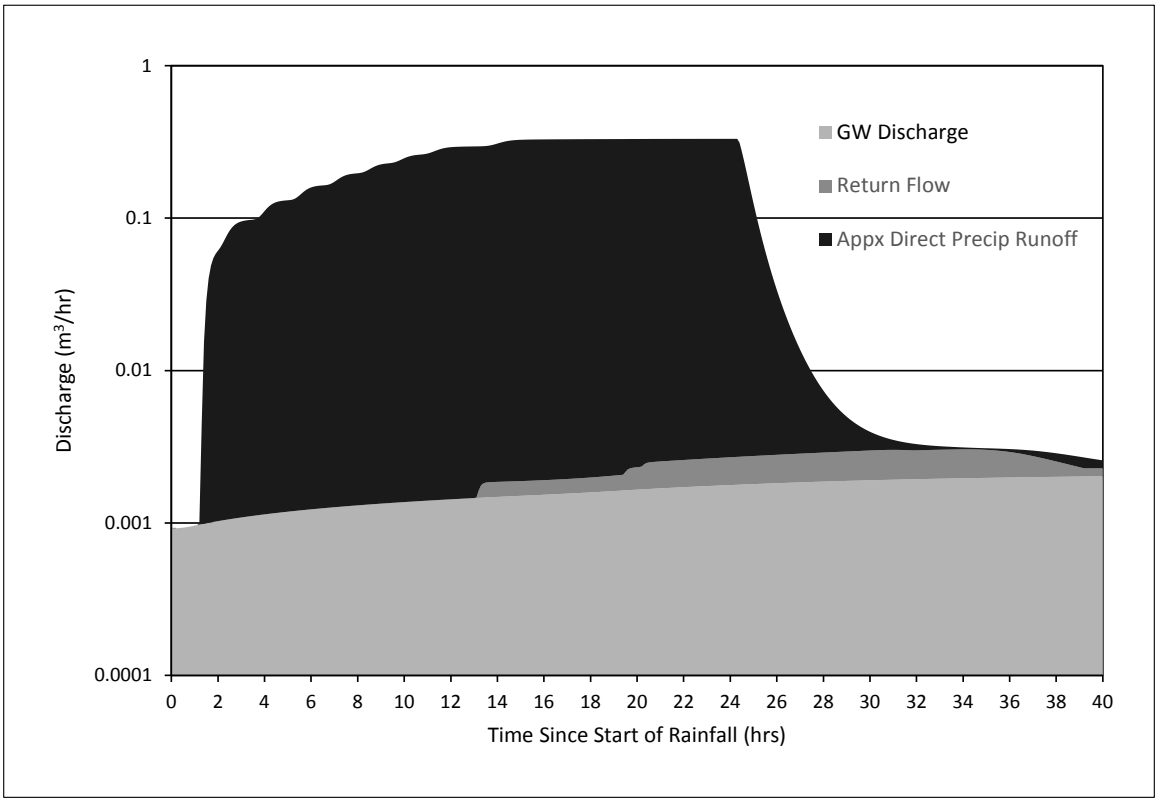

Figure 57: Stormflow components for the S-shaped Hillslope *V,V,V* Scenario.

Effects of Hillslope Shape

Available Pore Space and Saturated Extents

Figure 58 shows that there are different amounts of hillslope average available pore space ($\overline{\phi_a}$) at the time of rainfall start among scenarios for the S-shaped hillslope when using the 'hot-start'. In all scenarios $\overline{\phi_a}$ is less for the S-shaped hillslope than the straight hillslope. This difference in available storage indicates that there will likely be more saturation excess runoff production for the S-shaped hillslope than for the straight hill slope.

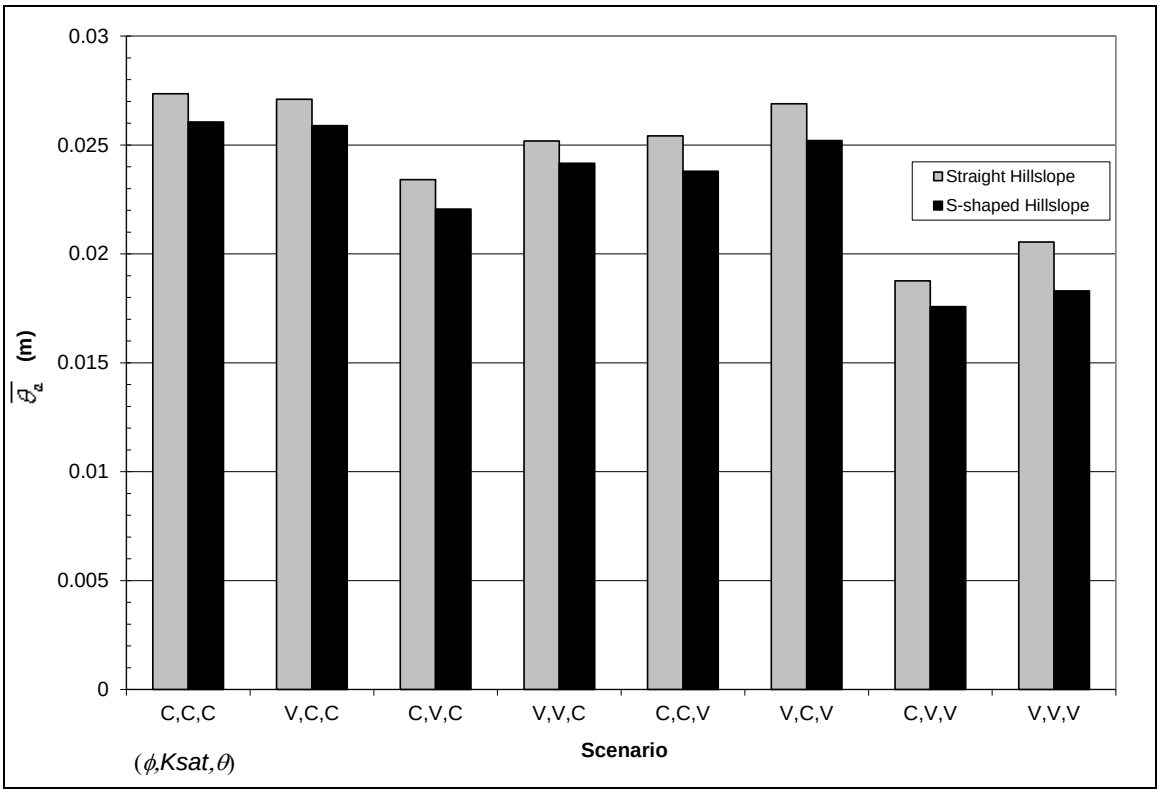

Figure 58: Straight vs. S-shaped hillslope - ($\overline{\phi_a}$) at rainfall start.

The hillslope shape also leads to different patterns of ϕ_a and saturated extents at the start, during, and end of rainfall. Figure 59 shows the different ϕ_a distributions at the

start of rainfall for the *C,C,C, and V,V,V* scenarios between hillslope. For the both scenarios, there is less ϕ_a in the flatter top (cell # 1) and concave bottom of the S-shaped hillslope than on the straight hillslope, but more ϕ_a in the convex portion from cells 2-5. The only cells that are saturated when rainfall begins are at the bottom of the S-shaped hillslope as previously seen in Figure 36.

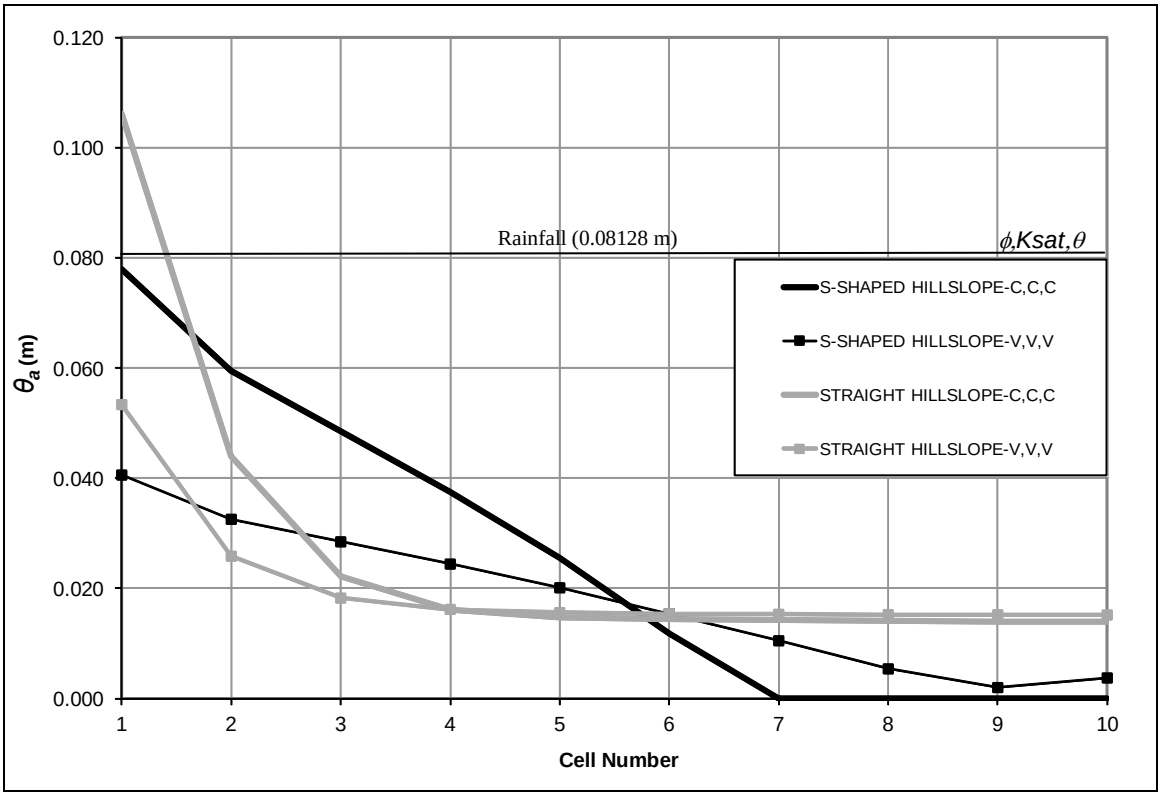

Figure 59: θ_a at start of rainfall between hillslope shapes for two scenarios.

At the end of rainfall, most cells are saturated ($\phi_a = 0$) for both hillslope forms in the constant θ scenarios. The corresponding variable θ scenarios have some cells with very small ϕ_a indicating that they should saturate within a single 0.1 hr time step. Figure 60 shows the differences for the *V,V,V* scenario only.

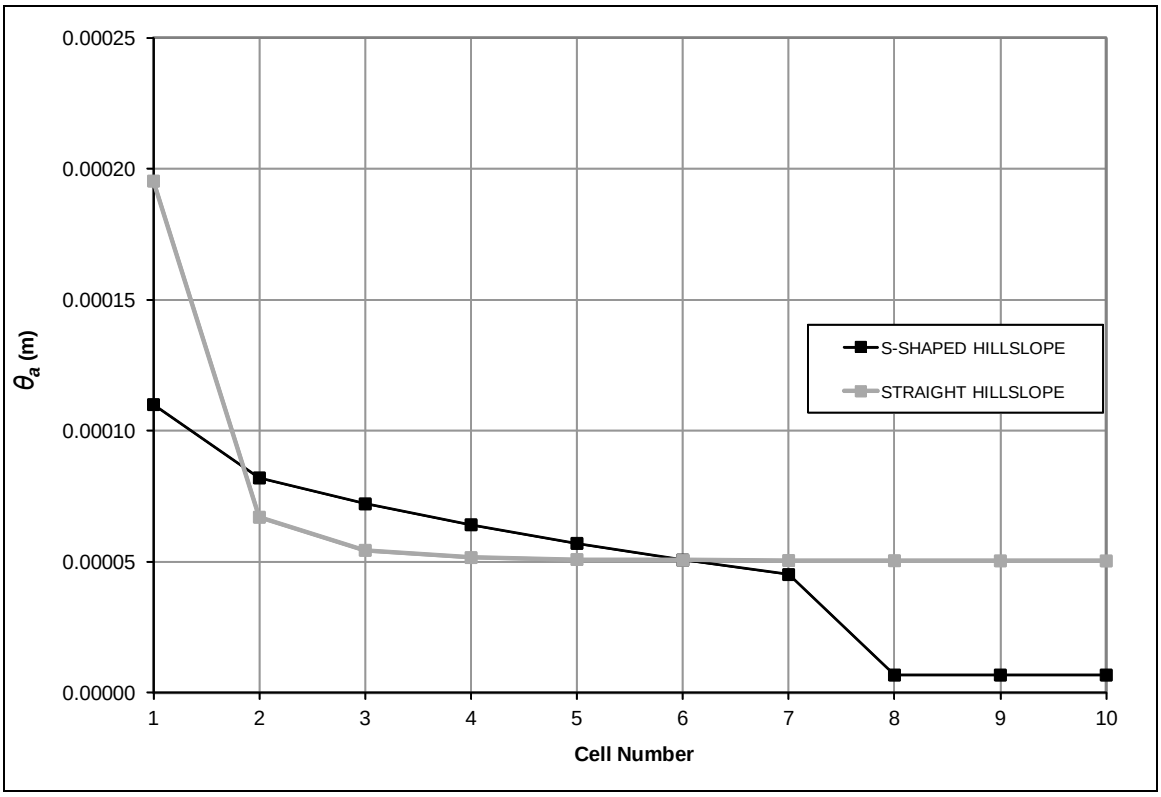

Figure 60: θ_a at end of rainfall between hillslope shapes for *V,V,V* scenario.

Subsurface Outflow

Subsurface outflow is highly variable between the straight and S-shaped hillslope forms. Figure 61 shows the subsurface outflow from cell 10 for the *C,C,C, and V,V,V* scenarios through drainage from the 'hot-start' and the subsequent applied rainfall period.

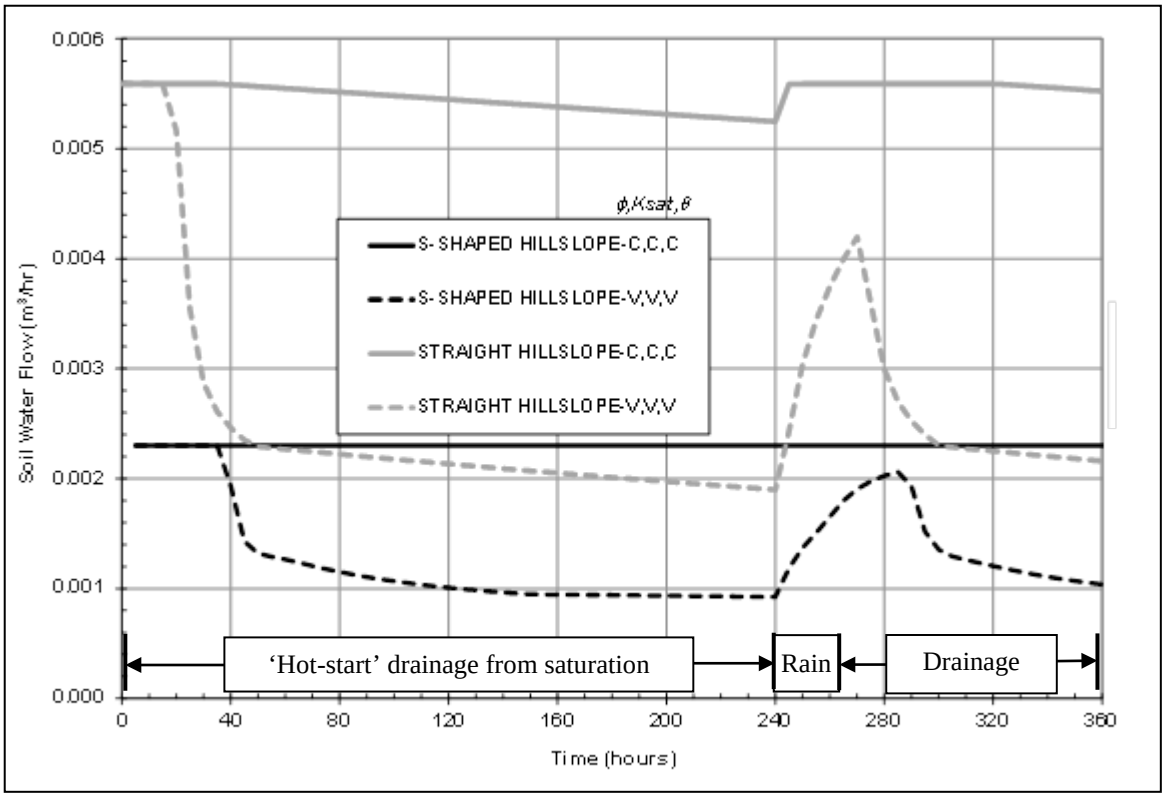

Figure 61: Cell 10 subsurface outflow between hillslope shapes for two scenarios.

The differences in subsurface outflow are greater due to hillslope form at first, when the cells are near saturation, but as water tables drop the differences are actually greater due to the combined soil parameter profile forms. The reason for these differences is that the slope between cells 9 and 10 is different between hillslope forms and thus will likely have different water table slopes between cells. At saturation subsurface outflow from cell 10 is about twice as much for the straight hillslope due to the steeper slope, 20% vs. 12%.

Return Flow

The different hillslope forms also have an effect on return flow. There is no return flow (exfiltration) for the straight hillslope, however return flow is observed in the

bottom concave portion of the S-shaped hillslope, where the steeper water table gradients of the each uphill cell causes an unbalanced subsurface outflow (more flow in than out).

Surface Runoff

Cumulative surface runoff during rainfall is summarized in Figure 62. There is between 3.7% less and 4.6% more cumulative surface runoff during rainfall for the S-shaped hillslope than the straight hillslope among scenarios. This is not the expected result as return flow (present only on the S-shaped hillslope) should add to surface runoff from the current rainfall input and previous drainage from the 'hot-start'. However, after a prolonged 10-day period of drainage, there is between 3% and 18% more surface runoff for the S-shaped hillslope.

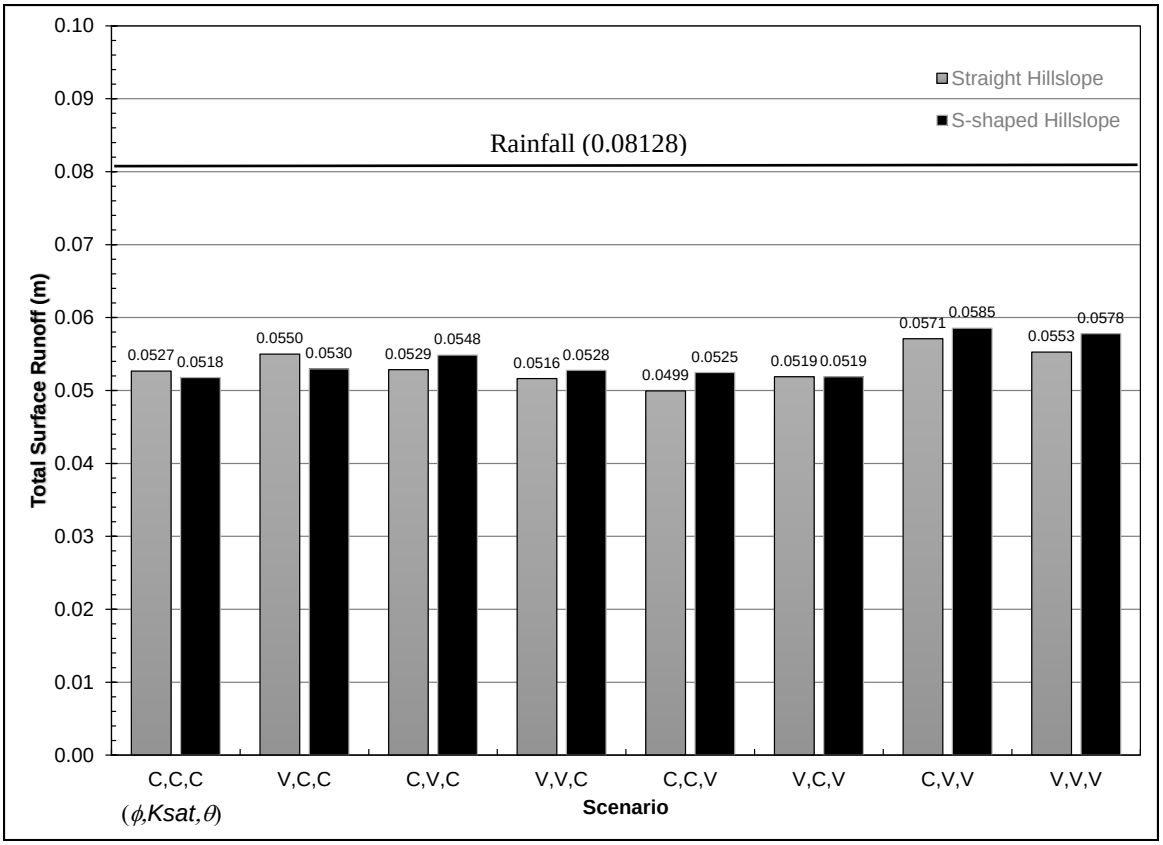

Figure 62: Total surface runoff between hillslopes.

Figure 63 shows the effects on surface runoff due to changing hillslope form for two scenarios (*C,C,C* and *V,V,V*). For both scenarios, the hydrographs begin to rise first on the S-shaped hillslope. Both sets of hydrographs cross after about 5 hours of rainfall, and the straight slope runoff become larger than the S-shaped slope runoff. This difference in timing is most likely due to time needed to fill the lower cells of the straight hillslope with rainfall and subsurface flow. At the start of rainfall, these cells are less saturated than the S-shaped hillslope lower cells so they take longer to fill.

Further along the hydrograph, the *V,V,V* hydrographs cross twice more and both scenarios end with the straight hillslope having slightly more runoff at the end of rainfall. The maximum runoff is 3.387×10^5 m^3/hr on the straight hillslope, and 3.364×10^5 m^3/hr on the variable hillslope showing that neither hillslope form reaches equilibrium with the rainfall rate in these two scenarios.

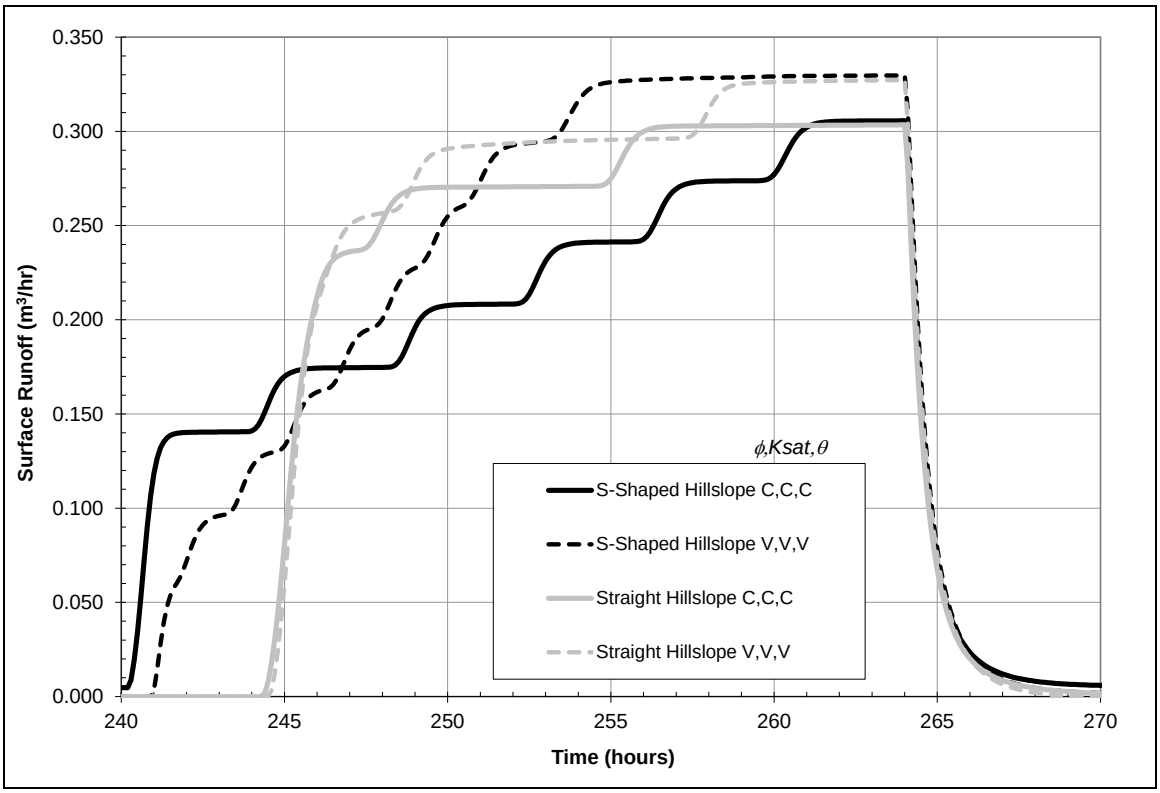

Figure 63: Surface runoff between hillslope shapes for *C,C,C* & *V,V,V* scenarios.

Other scenarios (not shown) behave similarly, with all straight hillslope hydrographs beginning to rapidly rise around hour 245 and all S-shaped hillslope hydrographs beginning to rapidly rise between hours 240 and 242.5.

The boundary condition for surface runoff is different between the two hillslope forms. Velocity, and thus runoff is based on the cell 10 surface slope, 20.0 % for the straight hillslope and 8.1% for the S-shaped hillslope. However, the different cell 10 slopes do not create more or less total runoff at equilibrium. The only real differences are the proportions flowing out of the surface vs. flowing out through groundwater. For the surface runoff out, velocity and depth are different, with the straight hillslope having faster velocity but lower ponding depth. Among all the scenarios, the maximum surface ponding depth of cell 10 is 0.0038 m for the constant hillslope and 0.0050 m for the S-

shaped hillslope. The corresponding surface velocities of cell 10 are 87.33 m/hr for the constant hillslope and 66.85 m/hr for the S-shaped hillslope.

Total Hillslope Discharge

Total discharge from the S-shaped hillslope includes both surface runoff and groundwater flow out of Cell 10. The peak occurs at the end of rainfall (hour 264.0), coincident with the peak surface runoff time. Peak groundwater discharge out either occurs at that time or afterwards. Table 12 shows total hillslope discharge percent of equilibrium rainfall for the two hillslope shapes. The *V,V,*C and C,*C,*V scenarios have both increased more than 0.7%. The other percentages are essentially the same as for the straight hillslope, with the rates being equal or slightly lower on the S-shaped hillslope for the three constant K_{sat} - constant θ scenarios and equal or slightly higher on the S-shaped hillslope for the remaining three variable θ scenarios.

Table 12: Total hillslope discharge at end of rainfall as percent of rainfall rate.

Scenario (ϕ, K_{sat}, θ)	**C,C,C**	**V,C,C**	**C,V,C**	**V,V,C**	**C,C,V**	**V,C,V**	**C,V,V**	**V,V,V**
Percent of Rainfall Rate (S-Shaped Hillslope)	90.9%	90.9%	100.0%	100.0%	98.1%	89.4%	97.9%	97.9%
Percent of Rainfall Rate (Straight Hillslope)	91.3%	91.4%	100.0%	91.3%	97.3%	89.3%	97.9%	97.8%
Difference	-0.4%	-0.5%	0.0%	+0.7%	+0.8%	+0.1%	0.0%	+0.1%

Unsteady Rainfall Results

Application of unsteady rainfall is not analyzed in detail in this study. The general trend of the results is that that the peak runoff occurs within one time step of the peak rainfall and therefore is associated with direct precipitation onto saturated areas, the dominant hydrograph component. Therefore it would be very difficult to find meaningful results for unsteady rainfall in this study. At the hillslope scale, the overland routing time is small relative to the length of slope traveled within one time step (0.1 hours) and does not greatly delay runoff. At longer distances overland travel time should have greater effects on the peak runoff.

Sensitivity Analysis

A limited sensitivity analysis is conducted to evaluate several key parameters including K_{sat}, and combined pore size distribution index (b) and ψ_{ae}. It is impossible to test every parameter or combination for sensitivity in this study but these key parameters are determined to be the most important to test. Mean available pore space ($\overline{\phi_a}$) at the time of rainfall start and at peak runoff, and the Q_p are evaluated for several parameter combinations. All results here are for the S-shaped hillslope with constant ϕ vertical profile and variable θ profile scenarios (*C,C,V*, & *C,V,V*).

K_{sat} values of 1/2, and 2 times the constant and vertically distributed values are tested with results shown in Table 13. Note that the minimum $\overline{\phi_a}$ does not necessarily occur at peak time (Q_p) but may be delayed as surface water continues to infiltrate.

Table 13: K_{sat} Sensitivity for S-shaped hillslope.

K_{sat} Profile	Multiplier	$\overline{\phi_a}$ at rain start (240 hours) (m)	$\overline{\phi_a}$ at Q_p (m)	Q_p (m^3/hr)
Constant	1	0.0238	0.00005365	0.332267
"	0.5	0.0173	0.00003662	0.332796
"	2	0.0354	0.00018517	0.320558
Variable	1	0.0176	0.00003224	0.331634
"	0.5	0.0160	0.00003659	0.331575
"	2	0.0211	0.00003695	0.331635

*Numbers are rounded below STELLA output precision for clarity.

At the beginning of rainfall, $\overline{\phi_a}$ changes positively with increasing K_{sat} and negatively with decreasing K_{sat} for both the *C,C,V* and *C,V,V* scenarios. This is the expected result as increasing or decreasing K_{sat} should increase or decrease drainage rates respectively. For the constant K_{sat} profile, halving K_{sat} has a minor effect on peak runoff (Q_p) while doubling K_{sat} slightly decreases (Q_p). For the variable K_{sat} profile, the differences in (Q_p) are negligible for either condition. At peak runoff time, $\overline{\phi_a}$ is highly variable but most values are approximately 2 orders of magnitude less than the amount of rain in a single time step. The one exception is for the 2x constant K_{sat} model run, in which $\overline{\phi_a}$ at peak runoff time is approximately one third the amount of rain in a single time step. In all cases presented, the overall effect on runoff from $\overline{\phi_a}$ at peak time is minimal. Most of the runoff differences can be attributed to the direct effect of K_{sat} on subsurface outflow.

The pore size distribution index (b) and ψ_{ae} combinations are examined for the fine sandy loam as described before, the mean values of a sand, and a sandy clay loam. (Clapp & Hornberger, 1978) These parameters are chosen as they are the main components of the θ equation besides ϕ and because ϕ does not very greatly among soil

textural classes (Warner, 2008). These tests use a constant vertical K_{sat} profile. Table 14 and Table 15 show the results for the *C,C,V* and *C,V,C* scenarios respectively

Table 14: b & ψ_{ae} Sensitivity for S-shaped hillslope and *C,C,V* scenario.

Soil Texture	b	ψ_{ae}	$\overline{\phi_a}$ at rain start (240 hours) (m)	$\overline{\phi_a}$ at Q_p (m)	Q_p (m^3/hr)
Sand	4.38	12.1	0.0245	0.00004236	0.332100
Sandy Loam	4.90	20.0	0.0238	0.00005365	0.332267
Sandy Clay Loam	7.12	29.9	0.0225	0.00008427	0.331381

B & ψ_{ae} values from Clapp & Hornberger, 1978

Table 15: b & ψ_{ae} Sensitivity for S-shaped hillslope and *C,V,V* scenario.

Soil Texture	b	ψ_{ae}	$\overline{\phi_a}$ at rain start (240 hours) (m)	$\overline{\phi_a}$ at Q_p (m)	Q_p (m^3/hr)
Sand	4.38	12.1	0.0180	0.00002055	0.331755
Sandy Loam	4.90	20.0	0.0176	0.00003224	0.331634
Sandy Clay Loam	7.12	29.9	0.0171	0.00007110	0.331252

B & ψ_{ae} values from Clapp & Hornberger, 1978

Limitations of Model/Methods

The use of the power and exponential curves to fit field data may not be suitable for all soil types or for prediction of unmeasured soils. Other options would be to replicate the soil column by horizon and use an average value for each, like in SWAT, or to try other equations such as linear or polynomial functions. However, it is necessary to use equations without an intercept for this model. By avoiding the use of an intercept the integral of the equation can be rearranged so that the upper limit may become the unknown variable and can be solved from a known amount of water. This convenient feature is used to calculate the depth of the saturated zone of the soil profile.

Some limitations of the STELLA® version 8 software affect the model. The inability to use variables in reference to a cell's position within the array means that some equations have to be manually input for each cell which limits practically the number of

cells that can be along the slope and leads to the “stair-step” results for surface water runoff from the hillslope.

Conclusions/Recommendations

Conclusions

Comparison of the model results with field observations and other modeling applications for the Coweeta sloping slab drainage shows that the soil water drainage from the hillslope model in STELLA reacts similarly to other physical and analytical soil drainage models near saturation and for a period of time suitable to the single storm analysis in this study. The STELLA model developed in this study conserved mass for all runs.

Both hillslope shape and distribution of soil hydraulic parameter values in the soil profile affect the timing and peak flow rates of outflow from the hillslope tested in this study under a steady rainfall. Resulting hydrographs exhibited differences among all combinations of slope shape and soil hydraulic parameters. Specific results include:

- Changes in the vertical distribution of hydraulic parameters had a greater influence on surface runoff for the S-shaped hillslope than for the straight hillslope.
- Surface runoff on the S-shaped hillslope began earlier than on the straight hillslope.
- The surface runoff hydrographs had steeper rates of rise for the straight hillslope than for the S-shaped slope.
- The depth-variable soil parameters resulted in a higher peak discharge for both the straight and S-shaped hillslopes compared to using the depth-constant parameters.

- Transmissivity is always less in the variable K_{sat} scenarios except when it is equal at full profile drainage and full saturation.
- Pore space is always less in the variable ϕ scenarios except when it is equal at full profile drainage and full saturation.
- Changing the K_{sat} profile from constant to variable had a greater influence on surface runoff than changing either porosity or soil water content profiles, apparently due to the range of K_{sat} values being larger than the range of the other parameters.
- Recession curves of the surface runoff hydrographs were similar for each slope and did not change with varied vs. constant with depth parameters.
- Direct precipitation onto saturated areas is the dominant component of runoff for both the straight and S-shaped hillslopes, with subsurface outflow and return flow producing much less discharge for both hillslope forms.

Initial conditions, i.e. water content and water table elevation along the slope at the start of rainfall, affect model results for both hillslope shapes, especially for the rising limbs of the hydrographs. The use of a 'hot-start', i.e. allowing a set period of 10 days drainage time before start of rainfall resulted in a reasonable approach to compare the slope shapes that mimics natural processes.

Hillslope shape affected the magnitude and relative importance of subsurface stormflow (interflow) vs. surface/overland flow from the bottom-most cell. The lower boundary conditions at the bottom-most cell affect subsurface stormflow out of the model. There is no return flow contribution to surface runoff on the straight hillslope due in part to the combination slope of the cell and the horizontally uniform rainfall rate. The

S-shaped slope did produce return flow in the bottom-most cells due to the decreasing water table slopes in the downhill direction.

Recommendations

While the model used in this study provided useful comparisons and satisfied the initial objectives of the study, additional experiments should be conducted to determine if the observations in this study are similar in other situations. The model structure should be further refined and analyzed. Expansion of the model's capabilities would also make it more flexible to apply to other experiments.

With the limited number of scenarios used in this study it is difficult to make a positive correlation that changing one soil parameter profile form will always result in the same relative outcome. Further testing should be conducted with different hillslope sizes and shapes\slopes, rainfall amounts and rates, and initial conditions.

The impacts of initial wetness conditions could be assessed by varying the time of drainage between rainfall events. The degree and spatial variability of initial soil water along the different slope shapes may be an important factor in the frequency and amount of runoff. The seasonally dependent factors; frequency, and typical time between rainfall events are expected to be important factors not addressed in this single event exercise. As further discussed below, ET during the drainage period between rainfall events is expected to be important in assessing initial wetness, especially when comparing seasonal variations in runoff.

The model was used to test one steady rainfall rate for a 24 hour storm. Further analyses are recommended to test different intensities and durations, including varying within-storm intensities. Running the model for higher rainfall rates or durations could

allow analysis at full saturation or true equilibrium. Running at lesser rainfall rates or shorter durations could be done to analyze subsurface flow in more detail. Comparisons of an "Advanced" to a "Delayed" precipitation intensity pattern for varying initial wetness and type of slope could be a future consideration given that the variation of wetness by slope position is apparently an important factor, and especially since "Direct Precipitation" is by far the largest source of surface runoff.

Further testing of the model structure is warranted, including the impact of cell resolution on the amount and timing of surface runoff for both hillslope forms. The model structure could be modified to increase the number of hillslope cells and decrease their size, to obtain smoother hydrographs. On a real hillslope the saturated source area producing the stair-step hydrographs would most likely move up the hillslopes in a smoother fashion. This may be easier to do if the model was rewritten in another programming language instead of using STELLA®.

Currently the model includes saturation overland flow and return flow as the only surface water runoff methods and there is no delay in infiltration or percolating water. An option to allow for infiltration excess overland flow could be added in the future to handle high rainfall rates or to infiltrate ponded water over unsaturated soil. A simple method to account for the timing of percolation and infiltration of water is to use a delay function to represent a soil with no identifiable wetting front. A more robust method for infiltration excess runoff modeling is to use the Green & Ampt (1911) infiltration method with redistribution (Ogden & Saghafian, 1997). Under the Green & Ampt theory of infiltration, a saturated wetting front moves through the soil as a single unit and does not reach the water table until the soil becomes saturated. Redistribution of the Green &

Ampt wetting front, as described by Ogden & Saghafian, can account for situations in which the rainfall rate is slower than the percolation rate. Inclusion of a Green-Ampt infiltration mechanism would also permit comparisons of changes in land use, and disturbance (e.g. compaction or tillage) at different slope positions. Yet another future improvement would be the ability to have a dual infiltration/percolation system which would allow separate rates for preferential flow paths (i.e. macropores) and the soil matrix.

To be properly used over longer periods of time the model may need to apply unsaturated soil water flow, but other factors such as ET and deep groundwater losses may be as important as unsaturated flow to include for longer periods. For more accurate evapotranspiration estimates, diurnal and seasonal fluxes could be added or calculated based on soil moisture, rather than just an applied constant rate. To do this, the root zone may have to be separated from other unsaturated water. Deep groundwater is currently lost from the system when this component is turned on. In real hillslopes it is thought that deep groundwater may return at the bottom of the slope and help keep the soil wet in these areas. This could be added to the model as a deeper set of stocks with a very slow flow path, with some groundwater flow allowed to return at the hillslope bottom.

Once the conceptual model design is updated, it might be advantageous to switch from using STELLA to another programming environment/language. A different environment may make it easier to handle 2-D and 3-D arrays and larger number of cells alternatively some of these analyses may be applied in an existing model framework.

The development and inclusion of additional model components is needed to apply this model to a wider range of conditions. Adding land use / land cover to the

model can apply horizontally distributed parameters such as Manning's *n* and functions such as, interception, and evapotranspiration. It may be possible to link a 3-D version of the model to GIS data such as LULC grids or digital elevation models, from which surface elevations and slopes could be derived. Interception of rainfall is partially included in the model but is turned off for this study. It might be possible to expand this model beyond its single event usage to continuous usage. This may require using a variable time step for wetting (rainfall) vs. drainage (non-rainfall) periods.

References

Ambroise, B., Beven, K., and Freer J. (1996a). Toward a generalization of the TOPMODEL concepts: Topographic indices of hydrological similarity, *Water Resour. Res., 32*(7), 2135-2145.

Ambroise, B., Beven, K. and Freer J. (1996b). Application of a generalized TOPMODEL to the small Ringelbach catchment, Vosges, France, *Water Resour. Res., 32*(7), 2147-2159.

Arnold, J.G., R. Srinivasan, R.S. Muttiah and Williams, J.R. (1998). Large-area hydrologic modelling and assessment: Part I. Model development, *J. American Water Resources Assoc., 34*(1), 73-89.

Beven, K. (1982). On Subsurface Stormflow: Predictions With Simple Kinematic Theory for Saturated and Unsaturated Flows, *Water Resour. Res., 18*(6), 1627-1633.

Beven, K. (1984). Infiltration Into a Class of Non-Uniform Soils, *Hydrological Sciences Journal, 29*(4): 425-434

Beven, K., Lamb, R., Quinn, P., Romanawicz, R., and Freer, J. (1995). TOPMODEL, in *Computer Models of Watershed Hydrology*, edited by V.P. Singh, 627-668, Water Resour. Publ., Highlands Ranch, Colo.

Bevin, K.J. and Kirkby, M.J. (1979). A physically based, variable contributing area model of basin hydrology, *Hydrological Sciences Bulletin, 24*(1), 43-69.

Boll, J., Brooks, E.S., Campbell, C.R., Stockle, C.O., Young, S.K., Hammel, J.E., and McDaniel, P.A. (1998). *Progress Toward Development of a GIS-based Water Quality Management Tool for Small Rural Watersheds: Modification and Application of a Distributed Model. Paper No. 982230,* American Society of Agricultural Engineers, St. Joseph, MI.

Brooks, E.S., J. Boll, and McDaniel, P.A. (2004). A hillslope-scale experiment to measure lateral saturated hydraulic conductivity, *Water Resour. Res., 40,* W04208, doi:10.1029/2003WR002858.

Carr, Jerry E.; Chase, Edith B.; Paulson, Richard W.; Moody, David W. (1990). *National Water Summary 1987: hydrologic events and water supply and use*. USGS Water Supply Paper 2350.

Clapp, R.B. and Hornberger, G.M. (1978). Empirical Equations for Some Soil Hydraulic Properties. *Water Resour. Res., 14*(4), 601-604.

Cloke, H.L., Renaud, J.-P., Claxton, A.J., McDonnell, J.J., Anderson, M.G., Blake, J.R., and Bates, P.D. (2003). The effect of model configuration on modelled hillslope-riparian interactions, *J. Hydrol 279*, 167-181

Cronshey, Roger C. and Woodward, Donald E. (1989) Derivation of Type III Rainfall Distributions, *International Conference on Channel Flow and Catchment Runoff, May 22-26.* University of Virginia, Charlottesville, VA.

Dest, William. (2006). Personal communication of unpublished data from Bill Dest, Professor Emeritus, University of Connecticut, Plant Science Department, Storrs, CT.

Dingman, L.S. (1994). Physical Hydrography. Prentice Hall, Upper Saddle River, NJ.

Downer C.W. and Ogden F.L. (2003). GSSHA User's Manual, Gridded Surface Subsurface Hydrologic Analysis, Version 1.43 for WMS 6.1, Engineer Research and Development Center Technical Report, in press.

Duan, J. and Miller, N.L (1997). A generalized power function of the subsurface transmissivity profile in TOPMODEL. *Water Resour. Res., 33*(11), 2559-2562.

Dunne, T. and Black, R.D. (1970). Partial Area Contributions to Storm Rainfall in a Small New England Watershed, *Water Resour. Res., 6*(5), 1296-1311.

Dunne T. and Leopold, L.B. (1978). Water in Environmental Planning. W.H. Freeman and Company, NY.

Dunne, T., Moore, T.R., and Taylor, C.H. (1975). Recognition and Prediction of Runoff-Producing Zones in Humid Regions, *Hydrological Sciences Bulletin*, *20*(3), 305-327.

Elsenbeer, H., Cassel, K., and Castro, J. (1992). Spatial Analysis of Soil Hydraulic Conductivity in a Tropical Rain Forest Catchment, *Water Resour. Res.*, *28*(12), 3201-3214.

Engman, E.T. (1086). Roughness coefficients for routing surface runoff, *Journal of Irrigation and Drainage Engineering 112*(1), 39-53.

Green, W.H. and Ampt, G.A. (1911). Studies on Soil Physics: 1. Flow of air and water through soils. *J. Agric. Sci., 4*, 1-24.

Hewlett, J.D. (1961). Watershed Management, *Report for 1961 Southeastern Forest Experiment Station.* U.S. Forest Service, Asheville, NC.

Hewlett, J.D. and Hibbert, A.R. (1963). Moisture and Energy Conditions within a Sloping Soil Mass during Drainage, *Journal of Geophysical Research 68*(4), 1081-1087.

Hilberts, A.J.D., van Loon, E.E., Troch, P.A. and Paniconi, C. (2004). The hillslope-storage Boussinesq model for non-constant bedrock slope. *J. Hydrol. 291*, 160-173.

Holtan, H.N., England, C.B., Lawless, G.P. and Schumaker, G.A. (1968). Moisture Tension Data for Selected Soils on Experimental Watersheds. USDA, ARS Publ. RS 41-44.

Horton, R.E. (1933). The role of infiltration in the hydrologic cycle, *Trans. Amer. Geophys. Un. 14*, 446-460.

Huang, C. Gascuel-Odux, C., and Cros-Cayot, S. (2001). Hillslope topographic and hydrologic effects on overland flow and erosion. *Catena* 46(2001) 177-188.

Iorgulescu, I. and Musy, A. (1997). Generalization of TOPMODEL for a Power Law Transmissivity Profile, *Hydrol. Process*., *11*, 1353-1355.

Jury, W.A., Gardner, R., and Gardner, W.H. (1991). Soil Physics, 5th edition. New York: John Wiley. Page 30.

Ksat Inc. (1994). Compact Head Permeameter – User's Manual, Ksat Inc., Raleigh, NC.

Matonse, A.H. and C. Kroll (2009). Simulating low streamflows with hillslope storage models, *Water Resour. Res.*, *45*, W01407 doi:10.1029/2007WR006529.

McVey, Shawn (2002). (Natural Resources Conservation Service), Use of Amoozemeter to Measure Saturated Hydraulic Conductivity and Comparison to Estimated Permeability in Connecticut and Rhode Island Soil Survey Data, *New England Chapter SWCS Storm Water Infiltration & Groundwater Recharge Conference*, Worcester, MA, 05/21/2002.

Melvin, R.L., B.D. Stone, J.R. Stone, and N.J. Trask. (1992). Hydrogeology of thick till deposits in Connecticut. U.S. Geological Survey, Open-File Report 92-43. Hartford, CT.

Musgrave, G.W. and Holtan, H.N. (1964). Infiltration; Section 12 in *Handbook of Applied Hydrology* (ed. Ven te Chow), McGraw-Hill, New York.

Nieber, John L. and Walter, Michael F. (1981). Two-Dimensional Soil Moisture Flow in a Sloping Rectangular Region: Experimental and Numerical Studies, *Water Resour. Res. 17*(6), 1722-1730.

NRCS (1999), Soil Survey Staff, United States Department of Agriculture, Natural Resources Conservation Service. Official Soil Series Descriptions [Online WWW]. Available URL: [Accessed 10 February 2004].

NRCS (2000), Soil Survey Staff, United States Department of Agriculture, Natural Resources Conservation Service. National Soil Survey Characterization Data, Soil Survey Laboratory, National Soil Survey Center, USDA-NRCS - Lincoln, NE., Monday, November 07, 2005 http://soils.usda.gov/technical/classification/osd/index.html

Ogden, F.L. and Saghafian, B. (1997). Green and Ampt infiltration with redistribution. *Journal of Irrigation and Drainage Engineering 123*, 386-393.

Pelletier, Mary Lou (1982). Characterization of Three Well-Drained Upland Soils in Eastern Connecticut, and Their Relationship to the Regional till Stratigraphy, B.S., University of Connecticut

Renn, Philip (2005). Personal communication from Phil Renn, Water Resources Coordinator, U.S. Department of Agriculture, Natural Resources Conservation Service, Tolland, CT.

Rupp, D.E., and J.S. Selker (2005). Drainage of a horizontal Boussinesq aquifer with a power law hydraulic conductivity profile, *Water Resour. Res., 41*, W11422, doi:10.1029/2005WR0044241.

Rupp, D.E., and J.S. Selker (2006). On the use of the Boussinesq equation for interpreting recession hydrographs from sloping aquifers, *Water Resour. Res., 42*, W12421, doi:10.1029/2006WR005080.

Šimůnek, J., M. Th. van Genuchten, and M. Šejna, Development and applications of the HYDRUS and STANMOD software packages and related codes, *Vadose Zone Journal*, doi:10.2136/VZJ2007.0077, Special Issue "Vadose Zone Modeling", *7*(2), 587-600, 2008.

Sloan, Patrick G. and Moore, Ian D. (1984). Modeling Subsurface Stormflow on Steeply Sloping Forested Watersheds, *Water Resour. Res., 20*(12), 1815-1822.

Steenhuis, T.S. and W.H. Van der Molen. (1986). The Thornthwaite-Mather procedure as a simple engineering method to predict recharge. *J. Hydrol. 84*, 221-229.

U.S. Department of Commerce, Weather Bureau. Washington, D.C. May 1961. *Rainfall Frequency Atlas of the United States for duration from 30 minutes to 24 hours and return periods from 1 to 100 years. Technical paper no. 40*.

Warner, Glenn (2005). Personal Communication. University of Connecticut, Natural Resources Management and Engineering Department, Storrs, CT.

Warner, Glenn (2008). Personal Communication. University of Connecticut, Natural Resources Management and Engineering Department, Storrs, CT.

Wigmosta, Mark S., Vail, Lance W., and Lettenmaier, Dennis P. (1994). A Distributed Hydrology-Vegetation model for complex terrain, *Water Resour. Res., 30*(6), 1665-1679.

Wigmosta, Mark S., and Lettenmaier, Dennis P. (1999). A Comparison of Simplified Methods for Routing Topographically Driven Subsurface Flow, *Water Resour. Res., 35*(1), 255-264.

Appendixes

Appendix 1 STELLA List of Variables

Sector	Variable	Type	Units	Description
Main Model		(blank = standard converter)		
	T multiplier	Slider	none	used to change the value of transmissivity
	Ponding H		m	height of water ponded on the surface
	Surface Water	stock	m^3	Volume of water on the surface
	Unsaturated	stock	m^3	Volume of soil water in the unsaturated zone(above capillary fringe
	Saturated 5a	stock	m^3	Volume of soil water in the saturated zone(below capillary fringe)
	Throughfall b	Flow	m^3/hr	Volume of precip in each time step that actually passes through interception and reaches the ground
	Runoff In	Flow	m^3/hr	Surface flow from above
	Runoff Out	Flow	m^3/hr	Surface flow to next cell below
	Infiltration	Flow	m^3/hr	Amount of surface water entering the soil column below
	Exfiltration	Flow	m^3/hr	Amount of water returning to the surface if it gets forced out by extra groundwater from above
	d_Unsat	biflow	m^3/hr	Flow between unsaturated & saturated zones to correct unsaturated equilibrium based on height
	GW Flow Out Right	Flow	m^3/hr	
	GW Flow Out Left	Flow	m^3/hr	
	GW Flow In Right	Flow	m^3/hr	GW Flow Out Left
	GW Flow In Left	Flow	m^3/hr	GW Flow Out Right
	Deep Perc	Flow	m^3/hr	Percolation lost from upper m of soil column, not to return to model
Precip 1				
	Precip_Duration	Slider	hr	Length of Precipitation
	Precip_Total	Slider	m	total depth of precipitation
	NRCS_Type_III_24h_Rainfall	Graph	m/m	rainfall distribution
	Constant_Rate		m/hr	total/duration
	Precip_Rate		m/hr	either precip or variable depending on switch
	Variable_Rate		m/hr	NRCS distribution*total
Landscape Parameters 2				
	Width_Array		m	needed because can't have slider for array
	Width	Slider	m	width perpendicular to flow path
	Area		m^2	surface area length X width of each cell
	Length_Array		m	needed because can't have slider for array
	Length	Slider	m	length along flow path
	Dist_L_Edge_Array		m	distance from the very left to each left edge of each cell in array
	Variable_Slope_Elev	Graph	m	graph of left edges of surface
	Surface_E_L		m	surface elevation of left edge of cell
	Surface_E_R		m	surface elevation of right edge of cell
	Constant_Slope	Slider	m/m	the slope to use from cell to cell of the hillslope array
	Land Cover	Categorical	none	The land cover category, can be used for surface roughness and interception processes.

Hydrologic Parameters 3				
	Z_f_min_p		m/m	Shallowest depth to use the porosity power function. Shallower depths use a constant based on the value at this point
	W_p		m/m	multiplier in porosity power equation
	N_p		none	exponent in porosity power equation
	PSI_ae	Slider	m	thickness of capillary fringe
	Z_wti_Start	Slider	m	depth at which to start water table
	Z_b		m	depth of bottom of model
	Z_f_min_Ksat		m	Shallowest depth to use the Ksat power function. Shallower depths use a constant based on the value at this point
	W_Ksat		m/m	multiplier in Ksat power equation
	N_Ksat		none	exponent in Ksat power equation
	b	Slider	m/m	pore size distribution index(ratio of flow path to straight line path)
	Ponding_Hi		m	initial ponding height
Modify Hydrologic Properties 4				
	Z_wti		m	Depth of initial water table(after starting)
	Z_fi		m	depth of initial saturated divide
Integrate Below Fringe 5&7				
	Integral_Porosity_i		m	initial depth of saturated water in soil
	Total Pore Space		m	total depth of voids in soil
	Average Porosity		m/m	total pore space/depth of soil
	Transmissivity		m^2/hr	integral of Ksat(multiply by aquifer width to get flow)
WT&Fringe Depth EQ 6				
	Th_f		m	Thickness of the saturated zone
	Z_wt		m	Depth to water table at any time
	Z_f		m	Depth to saturated divide at any time
Point Calculations 8				
	Ksat_b		m/hr	Saturated hydraulic conductivity at the bottom of the system
	Avg_Ksat		m/hr	Average Saturated hydraulic conductivity of whole profile
	Porosity_Zb		m/m	Porosity at the bottom of the system
	Porosity_f		m/m	Porosity at depth of saturated divide
Theta Calculations 9				
	Constant Theta		m	a constant volumetric water content based on the value at the bottom of the profile
	d Theta		m	the difference between the expected Theta at that depth and the actual theta
	Theta Equilibrium		m	The amount(thickness) of water that should be in the saturated zone based on the depth to the saturated interface
AWC Calcs 10				
	AWC		m	the available water capacity (depth) not counting inflows and outflows which will occur at the next time step

GW Flow Calcs 11				
	d_GW_Flow		m^3/hr	Amount of groundwater entering a cell - the amount leaving, used for infiltration & exfiltration calcs
	GW_Slope_Left		m/m	Slope of the groundwater table from a cell to the cell to its right
	GW_Slope_Right		m/m	Slope of the groundwater table from a cell to the cell to its left
	E_wt		m	Elevation of the water table, used for slope calcs
Surface Processes 12				
	Surface Slope		m/m	Slope of the surface of each cell
	Surface E M		m	Surface elevation of the middle of a cell, used for weir flow
	H Weir		m	height of the broad crested weir to be used for reverse surface slopes
	Surface Velocity		m/hr	based on manning's equation for sheet flow
	Manning's n	Graph		manning's n variable with height
	runoff		m^3/hr	Runoff rate calculated in sector to clean up model
Interception & Throughfall				
	Intercepted	Stock	m^3	volume of intercepted water
	Interception	Flow	m^3/hr	rate at which water is intercepted from precip
	Max Interception	graph	m	The maximum depth of rainfall that can be intercepted (can be land use dependent)
	Throughfall a		m^3/hr	Precip not intercepted, calculated separately from main model for clarity
Switches				
	Switch Porosity	Switch		
	Switch Theta	Switch		
	Switch Ksat	Switch		
	Switch Deep Perc	Switch		
	Switch Precip	Switch		
	Switch Slope	Switch		
	Switch Interception	Switch		
Other Variables				
	dt		hr	length of time interval in between calculations (certain time integration methods are actually smaller than dt, ex Runge Kutta 4 = avg(dt/4))

Appendix 2 Woodbridge Soil Description (USDA)

LOCATION WOODBRIDGE CT+MA NH NY RI
Established Series
Rev. MFF-SMF
06/1999
WOODBRIDGE SERIES

The Woodbridge series consists of moderately well drained loamy soils formed in subglacial till. They are very deep to bedrock and moderately deep to a densic contact. They are nearly level to moderately steep soils on till plains, hills, and drumlins. Slope ranges from 0 to 25 percent. Permeability is moderate in the surface layer and subsoil and slow or very slow in the dense substratum. Mean annual temperature is about 48 degrees F., and mean annual precipitation is about 46 inches.
TAXONOMIC CLASS: Coarse-loamy, mixed, active, mesic Aquic Dystrudepts
TYPICAL PEDON: Woodbridge fine sandy loam - grass field. (Colors are for moist soil unless otherwise noted.)
Ap--0 to 7 inches; very dark grayish brown (10YR 3/2) fine sandy loam, light brownish gray (10YR 6/2) dry; moderate medium granular structure; friable; many fine and medium roots; few very dark brown (10YR 2/2) earthworm casts; 5 percent gravel; moderately acid; abrupt wavy boundary. (4 to 10 inches thick)
Bw1--7 to 18 inches; dark yellowish brown (10YR 4/4) fine sandy loam; weak medium subangular blocky structure; friable; common fine roots; few very dark brown (10YR 2/2) earthworm casts; 10 percent gravel; moderately acid; gradual wavy boundary.
Bw2--18 to 26 inches; dark yellowish brown (10YR 4/4) fine sandy loam; weak medium subangular blocky structure; friable; common fine roots; few very dark brown (10YR 2/2) earthworm casts; 10 percent gravel; few medium prominent strong brown (7.5YR 5/6) masses of iron accumulation and light brownish gray (10YR 6/2) iron depletions; moderately acid; gradual wavy boundary.
Bw3--26 to 30 inches; light olive brown (2.5Y 5/4) fine sandy loam; weak medium subangular blocky structure; friable; few fine roots; 10 percent gravel; common medium prominent strong brown (7.5YR 5/6) masses of iron accumulation and light brownish gray (10YR 6/2) iron depletions; moderately acid; clear wavy boundary. (Combined thickness of the Bw horizons is 12 to 37 inches.)
Cd1--30 to 43 inches; light olive brown (2.5Y 5/4) gravelly fine sandy loam; weak thick platy structure; very firm, brittle; 20 percent gravel; many medium prominent strong brown (7.5YR 5/8) masses of iron accumulation and light brownish gray (10YR 6/2) iron depletions; moderately acid; gradual wavy boundary. (3 to 25 inches thick)
Cd2--43 to 65 inches; light olive brown (2.5Y 5/4) gravelly fine sandy loam; weak thick platy structure; very firm, brittle; few fine prominent very dark brown (10YR 2/2) coatings on plates; 25 percent gravel; common fine prominent strong brown (7.5YR 5/8) masses of iron accumulation; moderately acid.

TYPE LOCATION: Tolland County, Connecticut; town of Mansfield, 0.75 mile south of the intersection of Connecticut Routes 275 and 195, and 0.25 mile east on the University of Connecticut Agronomy Farm, 800 feet north of the greenhouses near the corner of a brushy field. USGS Spring Hill topographic quadrangle, latitude 41 degrees 47 minutes 53 seconds N., longitude 72 degrees 13 minutes 48 seconds W., NAD 27.

RANGE IN CHARACTERISTICS: Thickness of the solum ranges from 18 to 40 inches. Depth to densic materials commonly is 20 to 40 inches but the range currently includes 18 to 40 inches. Depth to bedrock is commonly more than 6 feet. Rock fragments range from 5 to 35 percent by volume. Except where the surface is stony, the fragments are mostly subrounded gravel and typically make up 60 percent or more of the total rock fragments. Unless limed, reaction ranges from very strongly acid to moderately acid.

The Ap horizon has hue of 10YR, value of 3 or 4, and chroma of 2 to 4. Dry value is 6 or more. Undisturbed pedons have a thin A horizon with value of 2 or 3 and chroma of 1 or 2. The Ap or A horizon is loam, fine sandy loam, or sandy loam in the fine-earth fraction. It has weak or moderate granular structure and is friable or very friable.

Some pedons have a thin E horizon below the A horizon. It has hue of 10YR or 2.5Y, value of 4 to 6, and chroma of 1 to 3. Texture, structure, and consistence are like the A horizon.

The upper part of the Bw horizon has hue of 7.5YR to 2.5Y, value of 3 to 6, and chroma of 3 to 8. The lower part of the Bw horizon has hue of 10YR or 2.5Y, value of 4 to 6, and chroma of 3 to 6. Iron depletions are within a 24 inch depth. The Bw horizon is loam, fine sandy loam, or sandy loam with less than 65 percent silt plus very fine sand. It has weak granular or subangular blocky structure, or it is massive. Consistence is friable or very friable.

Some pedons have a thin BC horizon with value and chroma like the lower part of the B horizon, but is typically one hue yellower. The BC horizon has texture, structure, and consistence like the B horizon.

Some pedons have an E or E' horizon up to 3 inches thick below the B horizon. It has hue of 10YR to 5Y, value of 5 or 6, chroma of 2 or 3, and has redoximorphic features. Typically, it is coarser-textured than the overlying horizon.

The Cd horizon has hue of 10YR to 5Y, value of 4 to 6, and chroma of 1 to 4. It commonly has redoximorphic features. Texture is loam, fine sandy loam, sandy loam, or coarse sandy loam in the fine-earth fraction. The horizon has weak medium to very thick plates, or it is massive. Consistence is firm or very firm.

COMPETING SERIES: The Rainbow, Sutton, and Wilbraham series are currently in the same family. Wapping and Watchaug are soils in similar families. Sutton, Wapping, and Watchaug soils do not have a dense substratum. Rainbow soils have more than 65 percent silt plus very fine sand in the solum. Wilbraham soils are wetter and have iron depletions throughout the B horizon.

GEOGRAPHIC SETTING: Woodbridge soils are nearly level to moderately steep and are on till plains, hills and drumlins. Slope commonly is less than 8 percent, but the range includes 0 to 25 percent. The soils formed in acid till derived mostly from schist, gneiss, and granite. Mean annual temperature ranges from 45 to 52 degrees F., mean annual precipitation ranges from 37 to 49 inches, and the growing season ranges from 115 to 180 days.

GEOGRAPHICALLY ASSOCIATED SOILS: These are the competing Rainbow and Sutton soils and the Bernardston, Broadbrook, Canton, Charlton, Chatfield, Georgia, Hollis, Leicester, Montauk, Paxton, Ridgebury, Scituate, Wapping, and Whitman soils on nearby landscapes. The well drained Paxton, poorly drained Ridgebury, and the very poorly drained Whitman soils are associated in a drainage sequence. Bernardston and Broadbrook soils are well drained and are finer textured. Canton and Charlton soils are well drained and do not have a dense substratum. Chatfield and Hollis soils have bedrock within depths of 20 to 40 and 10 to 20 inches respectively. Georgia soils are calcareous within 80 inches. Leicester soils are poorly drained and do not have a dense substratum. Montauk soils are well drained and are coarser textured. Scituate soils have a loamy sand substratum.

DRAINAGE AND PERMEABILITY: Moderately well drained. Surface runoff is slow to rapid. Permeability is moderate in the solum and slow to very slow in the substratum. Woodbridge soils have a seasonal high water table.

USE AND VEGETATION: Many areas are cleared and used for cultivated crops, hay, or pasture. Scattered areas are used for community development. Some areas are wooded. Common trees are red, white, and black oak, hickory, white ash, sugar maple, red maple, hemlock, and white pine.

DISTRIBUTION AND EXTENT: Glaciated uplands of Connecticut, Massachusetts, New Hampshire, eastern New York, and Rhode Island; MLRAs 144A, 145, and 149B. The series is of large extent. Woodbridge soils were previously used in Maine. Soil temperature studies in Maine have resulted in the use of the frigid soil temperature regime for soils in areas formerly identified as mesic.

MLRA OFFICE RESPONSIBLE: Amherst, Massachusetts

SERIES ESTABLISHED: Essex County, Massachusetts, 1925.

REMARKS: This revision reflects update in soil taxonomy and general updating. Cation exchange activity class placement determined from a review of limited lab data and similar or associated soils.

Woodbridge soils were previously classified as Aquic Dystrochrepts and before that as Typic Fragiochrepts.

Diagnostic horizons and features recognized in this pedon are:

1. Ochric epipedon - the zone from 0 to 7 inches (Ap horizon).
2. Cambic horizon - the zone from 7 to 30 inches (Bw horizons).
3. Aquic feature - low chroma iron depletions within a 24 inch depth (Bw2 horizon).
4. Densic materials - the zone from 30 to 65 inches (Cd1 and Cd2 horizons).

National Cooperative Soil Survey
U.S.A.

*** Primary Characterization Data ***

Pedon ID: 00CT013003 (Tolland, Connecticut) Print Date: Nov 7 2005 4:47PM

Sampled as : Woodbridge ; Coarse-loamy, mixed, active, mesic Aquic Dystrudept
Revised to :

SSL - Project CP00CT199 CONNECTICUT AND RHODE ISLAND
- Site ID 00CT013003 Lat: 41° 47' 38.00" north Long: 72° 13' 30.00" west MLRA: 144A
- Pedon No. 00P1227
- General Methods 1B1A, 2A1, 2B

United States Department of Agriculture
Natural Resources Conservation Service
National Soil Survey Center
Soil Survey Laboratory
Lincoln, Nebraska 68508-3866

Layer	Horizon	Orig Hzn	Depth (cm)	Field Label 1	Field Label 2	Field Label 3	Field Texture	Lab Texture
00P07115	Ap	Ap	0-20				FSL	L
00P07116	Bw1	Bw1	20-33				FSL	FSL
00P07117	Bw2	Bw2	33-43				FSL	L
00P07118	BC	BC	43-61				FSL	FSL
00P07119	Cd1	Cd1	61-99				FSL	FSL
00P07120	Cd2	Cd2	99-132				FSL	FSL
00P07121	Cd3	Cd3	132-203				FSL	FSL

Pedon Calculations

Calculation Name	Result	Units of Measure
CEC Activity, CEC7/Clay, Weighted Average	0.99	(NA)
Clay, carbonate free, Weighted Average	7	% wt
Weighted Particles, 0.1-75mm, 75 mm Base	43	% wt
Volume, >2mm, Weighted Average	8	% vol
Clay, total, Weighted Average	7	% wt
LE, Whole Soil, Summed to 1m	1	cm/m

Weighted averages based on control section: 25-61 cm

PSDA & Rock Fragments

				-1-	-2-	-3-	-4-	-5-	-6-	-7-	-8-	-9-	-10-	-11-	-12-	-13-	-14-	-15-	-16-	-17-
				(- - - - - Total - - - - -)			(- - Clay - - -)		(- - - - Silt - - -)		(- - - - - - - - - - - - - Sand - - - - - - - -)					(Rock Fragments (mm))				
				Clay	Silt	Sand	Fine	CO_3	Fine	Coarse	VF	F	M	C	VC	(- - - - - - - - Weight - - - - - - - -)				>2 mm
				<	.002	.05	<	<	.002	.02	.05	.10	.25	.5	1	2	5	20	.1-	wt %
	Depth			.002	-.05	-2	.0002	.002	-.02	-.05	-.10	-.25	-.50	-1	-2	-5	-20	-75	75	whole
Layer	(cm)	Horz	Prep	(- % of <2mm Mineral Soil -)												(- - - - - - - % of <75mm - -- - -)				soil
				3A1	3A1	3A1			3A1	3A1	3A1	3A1	3A1	3A1	3A1	3B1	3B1	3B1		
00P07115	0-20	Ap	S	12.0	42.5	45.5			20.2	22.3	14.7	16.6	8.7	3.8	1.7	1	2	3	35	6
00P07116	20-33	Bw1	S	5.9	49.8	44.3			22.8	27.0	12.8	14.9	8.2	5.2	3.2	3	7	5	42	15
00P07117	33-43	Bw2	S	9.4	45.3	45.3			21.9	23.4	13.3	15.7	7.8	5.4	3.1	4	8	1	41	15
00P07118	43-61	BC	S	6.5	37.9	55.6			16.4	21.5	16.9	21.1	9.8	5.1	2.7	4	3	1	44	11
00P07119	61-99	Cd1	S	9.5	27.6	62.9			14.0	13.6	17.7	22.6	12.5	7.0	3.1	5	7	7	56	24
00P07120	99-132	Cd2	S	10.0	28.4	61.6			14.5	13.9	15.5	21.5	13.9	7.0	3.7	5	8	3	55	18
00P07121	132-203	Cd3	S	10.0	28.1	61.9			14.0	14.1	17.0	22.0	12.3	8.2	2.4	5	8	3	54	26

Bulk Density & Moisture				-1-	-2-	-3-	-4-	-5-	-6-	-7-	-8-	-9-	-10-	-11-	-12-	-13-
				(Bulk Density)		Cole	(- - - - - - - - - - - Water Content - - - - - - - - - - - -)						WRD	Aggst		
				33	Oven	Whole	6	10	33	1500	1500 kPa	Ratio	Whole	Stabl	(- - Ratio/Clay - -)	
	Depth			kPa	Dry	Soil	kPa	kPa	kPa	kPa	Moist	AD/OD	Soil	2-0.5mm	CEC7	1500 kPa
Layer	(cm)	Horz	Prep	(- - - g cm^{-3} - - -)			(- - - - - - - - - - - - % of < 2mm - - - - - - - - - - - -)						cm^3 cm^{-3}	%		
				4A1d	4A1h			4B1c	4B1c	4B2a		4B5	4C1		8D1	8D1
00P07115	0-20	Ap	S	0.91	1.06	0.051		44.8	43.9	22.9		1.025	0.19		1.65	1.91
00P07116	20-33	Bw1	S	1.25	1.29	0.010		32.1	30.9	9.9		1.018	0.24		1.44	1.68
00P07117	33-43	Bw2	S	1.51	1.55	0.008		20.9	20.2	7.6		1.015	0.17		0.87	0.81
00P07118	43-61	BC	S	1.78	1.80	0.003		15.7	15.1	4.7		1.008	0.17		0.85	0.72
00P07119	61-99	Cd1	S	1.93	1.96	0.004		11.8	11.5	6.5		1.009	0.08		0.57	0.68
00P07120	99-132	Cd2	S	2.04	2.06	0.003		9.6	9.3	5.0		1.006	0.08		0.48	0.50
00P07121	132-203	Cd3	S	2.02	2.05	0.004		10.5	10.0	4.5		1.005	0.09		0.39	0.45

Carbon & Extractions

				-1-	-2-	-3-	-4-	-5-	-6-	-7-	-8-	-9-	-10-	-11-	-12-	-13-	-14-	-15-	-16-	-17-	-18-
				(- - - - - Total - - - - -)			Org	C/N	(- - - Dith-Cit Ext - - -)			(- - - - - - - Acid Oxalate Extraction - - - - - -)						(- -- Na Pyro-Phosphate -- -)			
	Depth			C	N	S	C	Ratio	Fe	Al	Mn	Al+½Fe	ODOE	Fe	Al	Mn	Si	C	Fe	Al	Mn
Layer	(cm)	Horz	Prep	(- - - -- - % of <2 mm - - - - -)					(- - - - - - - - - - - - - - - - % of < 2mm - - - - - - - - - - - - - -)				mg kg^{-1}	(- - - - - -- - % of < 2mm - - -- - - - -)							
				6A2f	6B4b	6R3d			6C2h	6G7g	6D2g		8J1c	6C9b	6G12b	6D5b	6V2b				
00P07115	0-20	Ap	S	5.58	0.468	tr		12	1.3	0.7	tr	1.24	0.31	0.55	0.97	160.0	0.17				
00P07116	20-33	Bw1	S	1.40	0.130	tr		11	1.3	0.6	--	1.26	0.15	0.57	0.98	32.0	0.27				
00P07117	33-43	Bw2	S	0.72	0.070	tr			1.2	0.4	--	0.79	0.09	0.48	0.55	--	0.13				
00P07118	43-61	BC	S	0.18	0.024	--			1.0	0.1	--	0.28	0.05	0.30	0.12	53.0	0.04				
00P07119	61-99	Cd1	S	0.13	0.004	tr			1.2	0.1	tr	0.28	0.05	0.33	0.11	127.0	0.04				
00P07120	99-132	Cd2	S	0.12	0.019	--			1.2	0.1	tr	0.21	0.05	0.27	0.07	127.0	0.04				
00P07121	132-203	Cd3	S	0.12	--	--			1.1	0.1	tr	0.15	0.03	0.19	0.06	106.0	0.04				

CEC & Bases

				-1-	-2-	-3-	-4-	-5-	-6-	-7-	-8-	-9-	-10-	-11-	-12-	-13-	-14-
				(- - - NH_4OAC Extractable Bases -- - -)								CEC8	CEC7	ECEC		(- - - Base - - -)	
								Sum	Acid-	Extr	KCl	Sum	NH_4	Bases	Al	(- Saturation -)	
	Depth			Ca	Mg	Na	K	Bases	ity	Al	Mn	Cats	OAC	+Al	Sat	Sum	NH_4OAC
Layer	(cm)	Horz	Prep	(- - - - - - - - - - - - - - - - cmol(+) kg^{-1} - - --- - - - - - - - - - - - -)							mg kg^{-1}	(- - - - cmol(+) kg^{-1} - - -)				(- - - - - - - % - - - - - - -)	
				6N2i	6O2h	6P2f	6Q2f		6H5a	6G9c	6D3b	5A3a	5A8b	5A3b	5G1	5C3	5C1
00P07115	0-20	Ap	S	5.2	1.1	0.3	tr	6.6	26.6	1.0	1.1	33.2	19.8	7.6	13	20	33
00P07116	20-33	Bw1	S	0.9	0.2	0.2	--	1.3	14.1	0.7	--	15.4	8.5	2.0	35	8	15
00P07117	33-43	Bw2	S	1.2	0.4	0.3	tr	1.9	9.9	1.0	--	11.8	8.2	2.9	34	16	23
00P07118	43-61	BC	S	1.3	0.5	0.3	0.1	2.2	4.4	0.4	--	6.6	5.5	2.6	15	33	40
00P07119	61-99	Cd1	S	3.2	0.9	0.3	0.2	4.6	4.2			8.8	5.4			52	85
00P07120	99-132	Cd2	S	3.1	0.9	0.3	0.2	4.5	3.2			7.7	4.8			58	94
00P07121	132-203	Cd3	S	2.6	0.8	0.3	--	3.7	2.2			5.9	3.9			63	95

Salt				-1-	-2-	-3-	-4-	-5-	-6-	-7-	-8-	-9-	-10-	-11-	-12-	-13-	-14-	-15-	-16-	-17-	-18-	-19-	-20-
				(- - - - - - - - - - - - - - - - - - - Water Extracted From Saturated Paste - - - - - - - - - - - - - - - - - - -)																	Pred		
																			Total	Elec	Elec	Exch	
	Depth			Ca	Mg	Na	K	CO_3	HCO_3	F	Cl	PO_4	Br	OAC	SO_4	NO_2	NO_3	H_2O	Salts	Cond	Cond	Na	SAR
Layer	(cm)	Horz	Prep	(- - - - mmol(+) L^{-1} - - - -)				(- mmol(-) L^{-1} - - - - - - - - - - - - - - - - -)											(- - - % - - -)	(- dS m^{-1} - -)		%	
																						5D2	
00P07115	0-20	Ap	S																			2	
00P07116	20-33	Bw1	S																			2	
00P07117	33-43	Bw2	S																			4	
00P07118	43-61	BC	S																			5	
00P07119	61-99	Cd1	S																			6	
00P07120	99-132	Cd2	S																			6	
00P07121	132-203	Cd3	S																			8	

pH & Carbonates

Layer	Depth (cm)	Horz	Prep	KCl	$CaCl_2$ 0.01M 1:2 4C1a2a	H_2O 1:1 4C1a2a	Sat Paste	Sulf	NaF 8C1d	As $CaCO_3$ <2mm	As $CaCO_3$ <20mm	As $CaSO_4*2H_2O$ <2mm	As $CaSO_4*2H_2O$ <20mm	Resist ohms cm^{-1}
				-1-	-2-	-3-	-4-	-5-	-6-	-7-	-8-	-9-	-10-	-11-
				(- - - - - - - - - - - - - - - - pH - - - - - - - - - - - - -)						(- Carbonate -)		(- - Gypsum - -)		
										(- - - - - - - - - - % - - - - - - - - - -)				
00P07115	0-20	Ap	S		4.8	5.0			10.5					
00P07116	20-33	Bw1	S		5.0	5.4			10.9					
00P07117	33-43	Bw2	S		4.9	5.4			10.4					
00P07118	43-61	BC	S		4.9	5.5			8.9					
00P07119	61-99	Cd1	S		5.1	5.9			8.7					
00P07120	99-132	Cd2	S		5.5	6.2			8.4					
00P07121	132-203	Cd3	S		5.7	6.4			8.3					

Phosphorous

				-1-	-2-	-3-	-4-	-5-	-6-	-7-	-8-	-9-	-10-

Layer	Depth (cm)	Horz	Prep	Melanic Index	NZ	Acid Oxal	Bray 1	Bray 2	Olsen	H_2O	Citric Acid	Mehlich III	Extr NO_3
					(- - - - - - - - - - - - - - - - - - Phosphorous - - - - - - - - - - - - - - - - -)								
					%	(- -mg kg^{-1} - - - - - - - - - - - - - - - - - -)							mg kg^{-1}
						6S8a	6S3e						
00P07115	0-20	Ap	S			502.0	1.0						
00P07116	20-33	Bw1	S			236.0	tr						
00P07117	33-43	Bw2	S			138.0							
00P07118	43-61	BC	S			96.0							
00P07119	61-99	Cd1	S			127.0							
00P07120	99-132	Cd2	S			159.0							
00P07121	132-203	Cd3	S			116.0							